HYDROGEOLOGIC RESPONSES TO SEISMIC EVENTS: THREE CASE STUDIES IN ITALY

Tutor: prof. Massimo Mattei

Co-tutors: prof. Marco Tallini and dott. Francesco La Vigna

TABLE OF CONTENTS

TABLES

1 INTRODUCTION TO THE "WATER AND EARTHQUAKE TOPIC"

All along the humanity have desired to control the natural events, in particular the catastrophic ones such as earthquakes, volcanic eruptions or floods, and it's just from this desire that the curiosity for the "earthquake hydrology" was born.

The stress-fluid interaction, and in particular the relationship between water and earthquake, has been documented since more than two thousand years (Manga, 2001). Examples include the formation of new springs, disappearance of previously active springs, variation in discharge in streams and springs which can be permanent or transient (even few hours), fluctuations in water levels in wells, permanent changes in water levels in wells coincident with earthquakes located thousands of kilometers away, hydrothermal events, variation in chemical and physical parameters of water, turbidity. Moreover liquefaction phenomena, occurrence of mud volcanoes and well eruption are documented. But, these are only few examples.

In the recent past, there was a rapid increase in the number and the quality of quantitative observations documenting hydrological changes during, following and sometimes before earthquakes, especially due to the implementation of hydrological, seismological and geodetic monitoring system around the world.

It will be helpful when discussing responses to distinguish hydrologic responses by the spatial relationship between the observation and the earthquake. It will be used the terms near-field, intermediate-field, and far-field, for distances within one fault length, more than one fault length away from the earthquake source but within a radius of 10 ruptured fault lengths, and more than 10 ruptured fault lengths, respectively.

In general it is possible to assume that earthquakes change the static stress (i.e., the offset of the fault generates a static change in stress in the crust) and also cause dynamic stresses (from the seismic waves). Both stresses increase as the seismic moment of the earthquake, but they decay very differently with distance *r.* Static stresses decrease as $1/r^3$. By comparison, dynamic stresses, which are proportional to the seismic wave amplitude, decrease more gradually. A standard empirical relationship between surface-wave amplitude and magnitude has dynamic stress decreasing as $1/r^{1.66}$(Manga, Wang, 2007).

In the near-field, changes in the properties of the fault zone itself may be responsible for hydrologic responses. Examples include the formation of new springs along ruptured faults or changes in groundwater flow paths because of changes in the permeability near the fault zone (Gudmundsson, 2012). In both the near- and intermediate-fields, dynamic and static strains are large enough that they might cause a measurable hydrologic response. In the far-field, however, only dynamic strains are sufficiently large to cause responses.

This phd thesis is focused on hydrologic responses outside the fault zone.

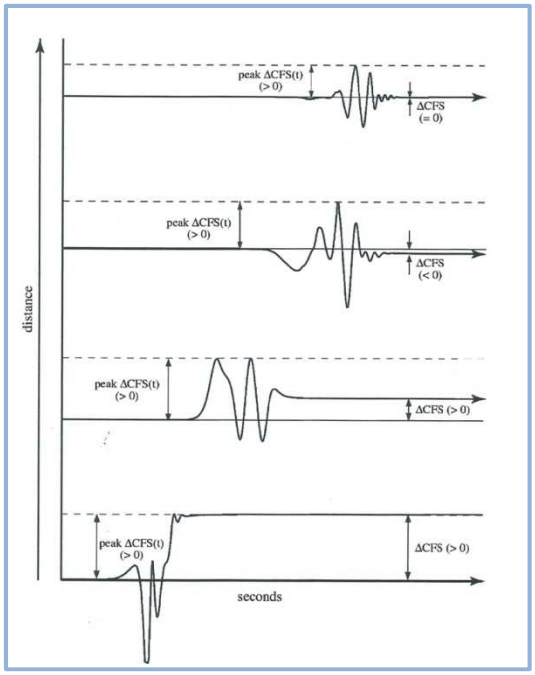

Figure 1: from (C.-Y. Wang & M Manga, 2010)Cartoon illustrating the peack dynamic Coulomb stress change (ΔCFS(t)) and Static Coulomb stress change (ΔCFS), and their variation with distance from the ruptured fault.

The **Figure 1** illustrates how static and dynamic stress change with increasing distance from the epicentre. The dynamic component of the Coulomb stress change (ΔCFS(t))is the time dependent change in the Coulomb failure stress resolved onto a possible failure plane.

$$\Delta CFS(t) = \Delta\tau(t) - \mu[\![\Delta\sigma_n\ (t) - \Delta P(t)]\!] \qquad 1$$

Where:

τ = shear stress on the fault

σ_n = stress normal to the fault

P = pore pressure

M = coefficient of friction

The static stress change, denoted ΔCFS, diminishes much more rapidly with distance than the transient, dynamic change. Thus at close distances the ratio is approximately proportional to the source-receiver distance, *r*, and at larger distances proportional to r^2. In the near and intermediate field, the static and the peak dynamic changes are comparable in magnitude while in the far field the peak dynamic change is much greater than the static change. The relative magnitude of the static and dynamic stresses is reflected in the hydrogeologic responses to earthquakes and is critical to understanding the origin of hydrological changes.

Explaining the hydrologic responses to earthquakes should in principle be simple because they reflect the strain caused by earthquakes. The great variety of hydrologic responses,

however, highlights the complexity of deformation and structure of geological materials and the interaction between processes. Effectively other factors such as directivity, radiation pattern, and crustal structure will also influence the amplitude of ground shaking. However, the significant difference in the dependence on distance is a robust feature distinguishing static and dynamic stresses.

In any case, it is possible to give some simple explanations (but not sufficient) for the hydrologic responses: earthquakes cause strain, and strain changes fluid pressure and alters hydrogeologic properties such as permeability, which controls the rate of fluid flow, as in **Figure 2** is schematized.

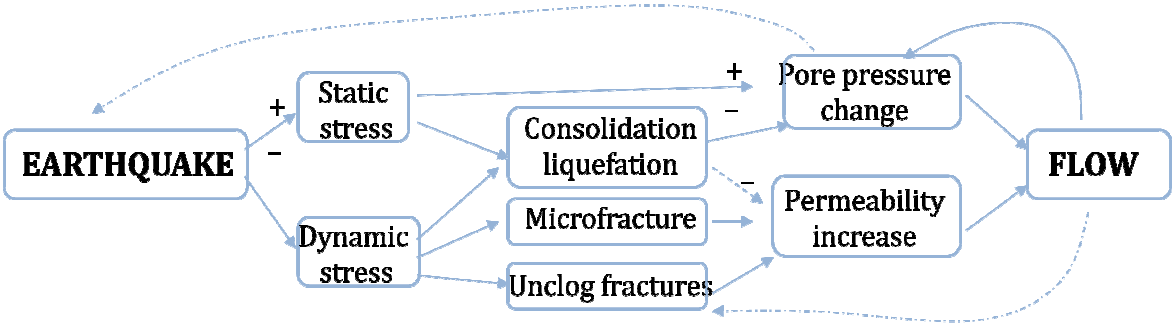

Figure 2: from Montgomery & Manga, 2003, schematic description of hydrologic responses to earthquakes.

1.1 Proposed Mechanisms

Over the last decade there has been a trend toward developing quantitative physically based models to explain hydrogeological responses to earthquakes with an emphasis on explaining phenomena that cannot be explained by linear poroelastic models alone but, sometimes, is needed to appeal at the permanent deformation concept. In particular, below are treated models proposed to explain increased stream discharge or groundwater level changes, because concerning the three case studies of this thesis.

1.1.1 Increased stream discharge

1.1.1.1 Coseismic elastic strain

A first model is proposed by Muir-Wood & King (1993), it consists in expulsion of deep crustal fluids resulting from coseismic elastic strain. The Autors noted that changes in the static elastic strain in the crust produced by earthquake faulting cause rocks to dilate or contract and thus saturated cracks in rocks to open or close, resulting in a decrease or increase in the groundwater discharge into streams and springs.

In **Figure 3** the simplified model proposed by these Autors is reported:

a) For extensional faulting, the preseismic period is associated with crack opening and increase of effective porosity;

b) At the time of the earthquake, cracks close and water is expelled;

c) For compressional faulting, the preseismic period is associated with crack closure and the expulsion of water;

d) At the time of the earthquake, cracks will open and water will be drawn in.

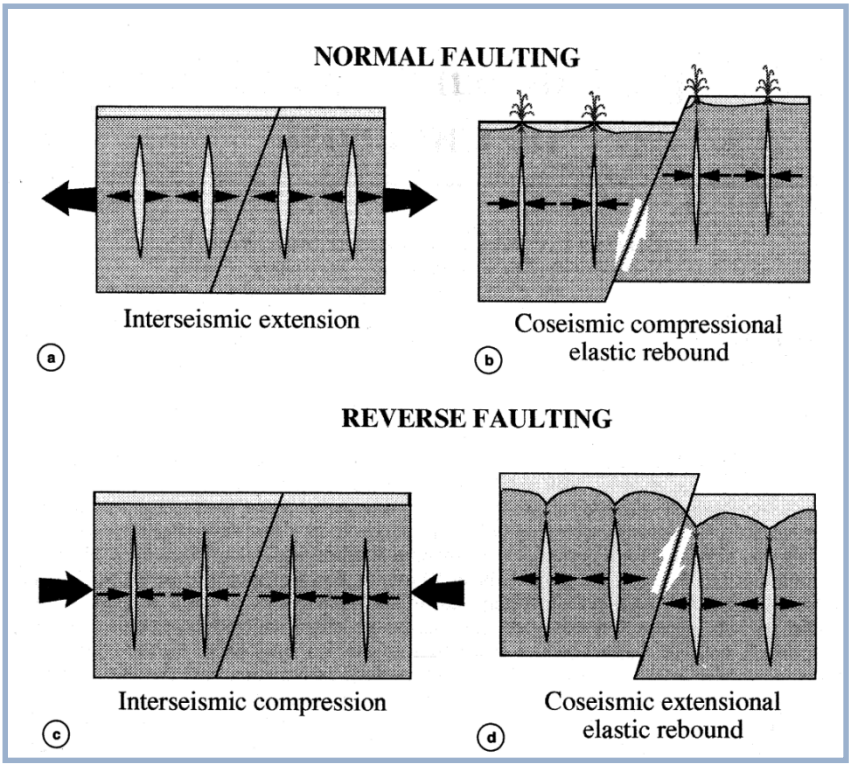

Figure 3: (Muir-Wood R. & King G. C. P., 1993)Simplified model for the interseismic accumulation and coseismic release of strain in extensional and compressional tectonic contests.

1.1.1.2 Enhanced permeability

Several Autors (Briggs, 1991; Rojstaczer & Wolf, 1992; Rojstaczer, Wolf, & Michel, 1995; Sato, Sakai, Furuja, & Kodama, 2000) proposed the enhance in near-surface permeability resulting from seismically induced craks and fractures and the cleaning of fractured filled by sediments to explain the increased discharge in streams. This model can be applied on solid rocks. In **Figure 4** is reported a simplified model to show deformation mechanisms in solid rocks: a) opening of new cracks and fractures, b) cleansing fractures.

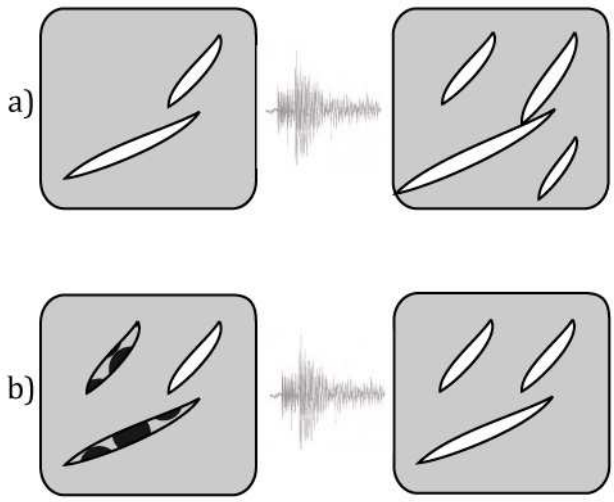

Figure 4: deformation mechanisms in solid rocks.

1.1.1.3 Coseismic consolidation and liquefaction

With an earthquake occurrence, in response to stresses, porous solid deform, the pressure of fluids within pores changes, and pore fluids can flow, so a redistribution of pore pressure is proposed as a mechanism to explain consolidation in loose sediments.

Under undrained conditions, permanent deformation can be associated with significant changes in pore pressure and groundwater flow. During permanent deformation, the cohesion among the grains of sediments and soils is disrupted and the grains tend to move to reach a new state of equilibrium. The basic characteristic of deformation, however, depend on the consolidation state of sediments and soils.

For loose deposits, shear deformation causes grains to move into pre-existing pores. This reduces the original porosity, and thus the volume of sediments decreases, this process is commonly known as consolidation.

Shear deformation of dense deposits, in contrast, will cause sediment grains to roll over each other and create new porosity, thus the volume of sediments increases, this process is commonly known as dilatancy.

Since it undrained consolidation of saturated soils can increase pore pressure in saturated soils and cause liquefaction, (Manga, 2001; Manga, 2003; Montgomery & Manga, 2003) suggested that coseismic liquefaction of loose sediments of floodplains may provide the water for the increases in stream discharge following earthquakes.

In **Figure 5** is reported a simplified model to represent the deformation mechanisms in loose sediments: a) compaction, b) dilatancy.

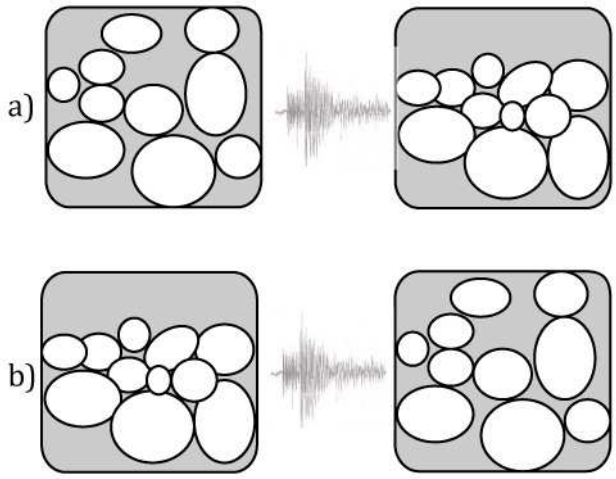

Figure 5: deformation mechanisms in loose sediments

1.1.2 Groundwater level changes

To study groundwater level changes in literature have been followed two different approaches: one relies on data from a single well that responds to many earthquakes (Roeloffs, 2009; Matsumoto & Roeloffs, 2003a; Brodsky, 2003); the other examines data from many wells that respond to a single earthquake (Chia et al., 2001; Chia et al., 2007; Wang et al., 2001; Wang et al., 2004; Wang & Chia, 2008).

The two different approaches applied in different part of the world, have led to consistent results and provides conclusions generally valid:

a) In the near field groundwater level shows step-like changes;

b) In the intermediate field groundwater level changes are more gradual and can persist for hours to weeks;

c) In the far field only transient oscillations of the water level were documented.

1.1.2.1 Groundwater well level changes in the near field

Both the sign and amplitude of coseismic water level changes can be compared with those predicted from models to provide insight into the causal mechanisms. In some cases the coseismic static strain and pore pressure change predicted by poroelastic theory, in particular the well level rise in zones of contraction, and fall in regions of dilation.

In other instances this observation was contradicted, the water level rose in most wells where the coseismic change of volumetric strain is positive (dilatation), and fell in other wells where the volumetric strain change is negative (contraction), thus the observed

responses is just the opposite from the pattern predicted from the hypothesis of coseismic static volumetric strain.

A mechanism proposed to explain step-like groundwater level increase is the undrained consolidation hypothesis, it consist in the fact that ground shaking causes sediments around a well to consolidate or dilate independently from the tectonic stresses.

1.1.2.2 Groundwater well level changes in the intermediate field

In the intermediate field, groundwater level changes are usually characterized by a more gradual onset and can last for hours to week.

The hypothesis of static poroelastic volumetric strain induced by earthquakes and the mechanisms of undrained consolidation was also used to interpret changes in intermediate field. Several Authors suggested that seismic waves may enhance rock permeability by removing precipitates and colloidal particles from clogged fractures, which in turn may lead to redistribution of pore pressure and changes of water level in areas near a local pressure source (Matsumoto & Roeloffs, 2003b; Matsumoto & Roeloffs, 2003a; Brodsky, 2003; Wang & Chia, 2008).

1.1.2.3 Groundwater well level changes in the far field

Groundwater level in wells can amplify ground motions, and when recorded at high enough frequencies, often shows oscillations associated with long-period Rayleigh waves.

This behavior has been documented since the early days of seismometer use and groundwater level fluctuations as large as 6 m (peak to peak amplitude) were recorded in Florida, thousand of kilometers away from the epicenter, during the 1964 Alaska earthquake (Wang & Manga, 2010).

Large water-level oscillations such as these at great distances occur when the geometric (water depth in the well, well radius, aquifer thickness) and the hydrogeologic (trasmissivity) properties have the right combination. The commonly accepted mechanisms is that seismic waves may cause aquifer to expand and contract which in turn may cause pore pressure to oscillate. If the aquifer has high enough trasmissivity, the pore pressure oscillation may induce fluid flow into and out of the well, which in turn may set up resonant motions in the water column.

1.2 Global case history

In the past has been studied countless hydrological changes caused by earthquakes, is impossible to list all studied cases in literature but following some important cases are argued. These are only a few examples of water-earthquake interaction which are recorded in instrument epoch. Many of them regard effects co and post seismic. Very infrequent the precursor phenomena.

The first documented groundwater change due to earthquake is represented by the mysterious abandonment of palaces on Crete during the Late Minoan period. This was always a challenging problem for archeologists and geologists, it is interpreted as the result of depletion of groundwater supply caused by persistent earthquake activity that took place during the Bronze Age (Gorokhovich, 2005). This explanation is supported by field observations and numerous studies of similar phenomena in other locations.

Earthquake activity could potentially influence the decline of water supply in palaces, which are usually located on high elevations. Earthquakes could break aqueduct systems and increase permeability of the rocks on higher elevations.

Significant hydrologic changes were observed after the M_w 7.3 **central Idaho earthquake** that occurred on October 28, 1983. Groundwater levels rose by as much as 3 meters near the epicenter. Discharge in many streams and springs increased, in some instances by more than 100%. One warm spring ceased flowing for several days; the flow then resumed and peaked at about nine times its original rate (Whitehead, Harper, & Sisco, 1985) The most prominent changes in the hydrologic system occurred near the epicenter. Some changes were noted in wells in other parts of Idaho, and also in Montana and Wyoming as far away as 700 kilometers.

The 1989 M_w 7.1 **Loma Prieta earthquake** (California) caused significant changes in hydrogeology of San Lorenzo and Pescadero drainage basin, located northwest of the epicenter. Streamflow increased at most gauging stations within 15 minutes after the earthquake. Ionic concentration and the calcite saturation index of the stream water also increased. Streamflow and solute concentrations decayed significantly over a period of several months following the earthquake. The spatial and temporal character of the hydrogeologic response suggests that the earthquake increased rock permeability and temporarily enhanced ground water flow rates in the region (Suart Rojstaczer & Stephen Wolf, 1992).

Changes of groundwater level induced by the 1999 M_w 7.6 **Chi-Chi earthquake** in Taiwan were observed at 158 monitoring wells in the Choshui River alluvial fan at the time of the mainshock (Chia et al, 2002; Lai et al., 2004; Manga &. Wang, 2007). This alluvial fan is characterized by 4 superimposed aquifers, that pass from unconfined shallow aquifer to

confined deep, the aquifer is also divided into the upper-fan, middle-fan and lower-fan areas based on the difference of the hydrological and geological settings.

The water well level changes magnitude, ranging from a rise of 7,42 m to a fall of 11,09 m on hourly records, tends to vary not only with distance from the epicenter or the fault but with well depth, implying that the impact of stress change by fault thrusting is three-dimensional. In the uppermost, partially confined aquifer, the coseismic changes are generally small except in an area on the northeastern edge of the alluvial fan where positive changes occurred, this area is closely associated with the occurrence of liquefaction (Manga & Wang, 2007).

It was also observed that the water level changes show both steplike and oscillatory patterns. The oscillatory changes happen mostly in the shallow unconfined aquifers. In the deeper aquifers, the changes show a step-like pattern. (Lai et al., 2004).

The differences are observed also in the changes duration. For the shallow unconfined aquifers, the groundwater level rose back to the original level in a duration of 1 to 2 hours. But for the deeper aquifers or partially confined shallow aquifers, the duration ranges from 1 to 6 months. Some of the wells had permanent changes in the groundwater level of about several meters. This may probably depends on the properties of the aquifers. For example, the short recovery time for the unconfined aquifers is considered to show easier flow occurrence or quicker diffusion in the unconfined aquifer than that in the confined.

All authors agree that these coseismic changes could have been induced by stress redistribution due to fault movement or mechanical response to seismic shaking.

Jonsson et al. (2003) describe the water level variation in response to M_w 6.5 17 and 21 June 2000 **earthquake** in the **south Iceland seismic zone** (SISZ), characterized by a left-lateral transform zone connecting two sections of the mid-Atlantic plate boundary.

The authors superimposed the satellite radar interferograms (InSAR) of the SISZ to the groundwater variation observations. As shown in **Figure 6** the wells show a characteristic pattern of positive and negative changes of groundwater level similar to that of coseismic and post-seismic static strain change. The authors affirm that large earthquakes cause pore-pressure increase in areas of compression and decrease in areas of dilation.

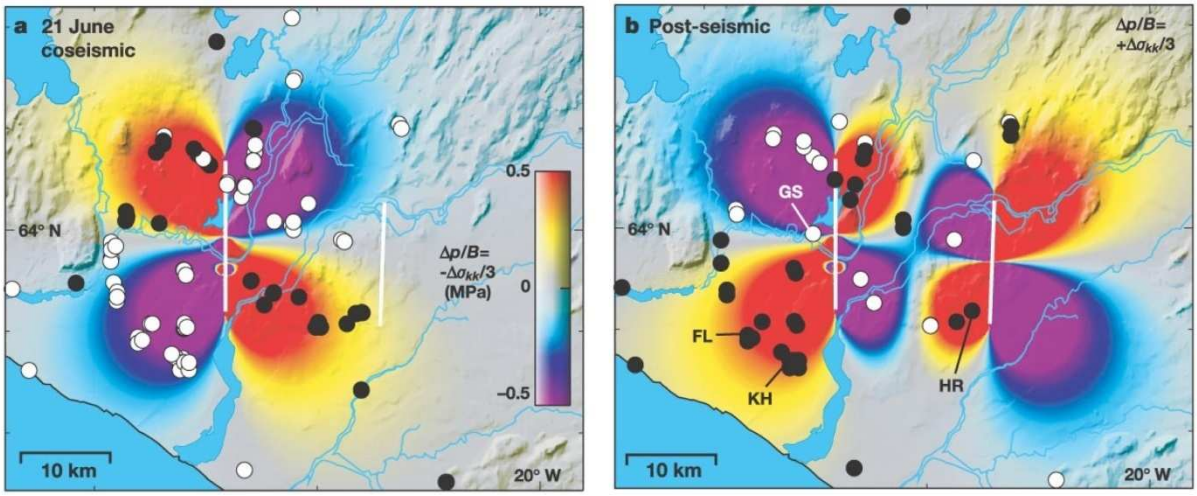

Figure 6: Coseismic and post-seismic water-level changes in geothermal wells in south Iceland. a) The 21 June coseismic water-level increase (black dots) and decrease (white dots) as well as the predicted coseismic pore-pressure change at 0.5 km depth (normalized by $B\,\Delta p/B = -\Delta\sigma_{kk}/3$). B) Post-seismic water-level changes after 21 June and predicted post-seismic pore-pressure changes (Dp/B¼þDjkk /3).

Following the M_w 6.**5 San Simeon earthquake**, California, on December 22, 2003, USGS stream gauges documented two consecutive increases in streamflow in the Salinas River and Lopez Creek in the central Coast Ranges. The first increase occurred within 15 minutes after the earthquake and lasted about an hour; the second one occurred a few hours later and lasted much longer. Evidence and simulation suggest that these increases were caused by earthquake-induced rupturing of pressurized hydrothermal reservoirs (C.-Y. Wang et al., 2004). Thus the source for the increased discharge was most likely a subsurface hydrothermal reservoir.

Associated with the Mw 9.0 2004 off the west coast of northern **Sumatra earthquake**, changes in groundwater levels or pressures were observed at many observation stations in Japan which are more than 5000 km from the hypocenter. At 38 of the 45 observation stations, there were changes in groundwater levels or pressures. At the 10 observation stations in which the Ishii-type borehole strain instruments were established, changes in crustal strains were also observed.

A major part of the changes in crustal strains and groundwater levels or pressures were dynamic oscillations due to a seismic wave. At some stations, coseismic or postseismic rises or drops were also observed. At five stations where both crustal stain and groundwater levels or pressures were observed, postseismic changes in groundwater levels or pressures were consistent with coseismic static steps in crustal strains. At the other five stations, postseismic changes in groundwater levels or pressures did not agree with the coseismic static steps At two of these five stations, it is presumed that the cause of postseismic changes in groundwater levels is a diffusion of abrupt coseismic pore water pressure changes near a well. At another station, postseismic changes in groundwater level possessed the same characteristics as a model removing the temporary deposition.

However this interpreting is poorly supported by observation results and theories at the present time.

The 2011 off the Pacific Coast of **Tohoku earthquake** (M_w 9.0) occurred on March 2011, just after the earthquake, a giant tsunami attacked the coasts facing the Pacific and caused severe damages. Geological Survey of Japan, AIST has many groundwater observatories in Tokai, Kinki and Shikoku. At many of the observatories, coseismic and/or postseismic changes in groundwater level, groundwater pressure or discharge rate were observed (Kitagawa & Koizumi, 2011). The depths of screens of the wells range from 10 to 1200 meters, and the wells distances from the epicenter range from 300 to 1100 km.

At many of the wells persistent changes in the groundwater level and the rest were observed during or after the dynamic oscillations. Unconfined groundwater, which is usually shallower than 50 m, is not sensitive to the volumetric strain changes. At some of the wells in coastal areas, the fluctuations of the groundwater level and the rest due to the tsunami were observed. 45 postseismic drops and one postseismic rise are explained by the static volumetric strain changes due to the fault slip of the earthquake. However 16 postseismic rises cannot be explained by it. Probably ground shaking caused the 16 postseismic rises.

Keskin (2010) contributes to research on **earthquake prediction**. Between 2007 and 2009, changes were observed in two geothermal and mineral springs located in Eskipazar (~3–5km to the north of the North Anatolian Fault Zone) in Turkey, in relation to small magnitude earthquakes. During pre-seismic and post- seismic activities, variations were observed in the hydrogeological parameters of the spring waters. Temperature increases of 0.4–1°C were measured in one of the springs prior to three different earthquakes. There was a slight increase in the spring discharge with respect to the first earthquake, which occurred closest to the spring. This led to a reduction in electrical conductivity (EC), total dissolved solids (TDS), Ca, HCO3, δ13C, Al, Mn, and Fe concentrations in the spring water, whereas tritium and Se values increased. Several days before the third earthquake, which occurred at a shallower depth, a decrease was observed in the discharge, which led to a reduction in tritium, δ13C and Si concentrations.

The author explained these variations by changes in the mixing ratio of different genesis water (probably shallower and deeper groundwater) in relation to the changes of aquifer boundary conditions, permeability, pore pressure, and flow path due to regional stress changes. The aquifer rock of Akkaya Hamamı Spring consists of highly faulted and fissured limestone with calcite and silica filling and clay bands from place to place, and the cover rock has claystone-sandstone levels. This structure would be expected to display the observed hydrogeological changes associated with the aquifer permeability changes under stress conditions. Hydrogeological factors include the formation of new microcracks and/or blockage of the gaps throughout the flow path due to filling of materials and clay

fragmented under various stresses (the stress increase before the earthquake, and the stress decrease after the earthquake).

2 CASE STUDY ONE: NEAR FIELD HYDROGEOLOGIC RESPONSE TO IRPINIA EARTHQUAKE 23TH NOVEMBER 1980 (M_W 6.9)

2.1 Southern Appennine geological setting

The Southern Apennines is a Neogene east-verging thrust belt resulting from the west-dipping subduction of the Apulian continental lithosphere (Doglioni et al., 1996). The belt is associated with the Tyrrhenian back-arc basin to the west and with the Bradano foredeep to the east (**Figure 7**). From Late Tortonian to Lower–Middle Pleistocene, the basin–thrust belt– foredeep system migrated eastward, as a response to the flexure-hinge retreat of the subducting foreland lithosphere (Malinverno & Ryan, 1986; Patacca & Scandone, 1989; Patacca et al., 1990) and progressively involved both basinal and carbonate platform paleogeographic domains (D'Argenio et al. 1974)

The Southern Apennines may be subdivided into two major arcs, the NNW–SSE-trending Molise–Sannio arc to the north and the WNW–ESE-trending Campania–Lucania arc to the south, which join in the Irpinia region (**Figure 7**). Starting from Early–Middle Pleistocene times, the axial zone of the chain underwent NE–SW extensional tectonics (Cinque et al., 1993; Hippolyte et al., 1994). This change in the tectonic regime was responsible for the development of large extensional and transtensional structures, which crosscut the preexisting compressional structure, thus further complicating the internal geometry of the thrust belt.

The intense hydrocarbon exploration in the Southern Apennines has provided a great deal of seismic reflection and well data, which have favoured the definition of structural models of the Southern Apennines (Mostardini & Merlini, 1986; Patacca & Scandone, 1989, 2001; Casero et al., 1991; Roure et al., 1991; Menardi & Rea, 2000).

These data reveal a considerable thickening of the thrust sheet stacks moving towards the innermost areas, the sole thrust of the duplex system being more than 20 km deep beneath the Southern Apennines inner zone. The foreland is represented by the Apulia Carbonate Platform (ACP), consisting of 7–8-km-thick Mesocenozoic carbonate sequence, which overlies Permotriassic clastic deposits (Verrucano Fm., Roure et al., 1991)(**Figure 8**). In the eastern margin of the Bradano Trough, Plio–Pleistocene terrigenous deposits stratigraphically cover the flexed ACP (Casnadei, 1988). Proceeding westward to the external zone of the belt, the ACP (that is covered by unconformable Upper Messinian carbonates and anhydrites) progressively dips below the rootless nappes and is in turn involved in the folds and thrusts of the thrust belt (**Figure 8**). According to Patacca et al., 1992 the thrust sheet stacks overlying the ACP are derived from the deformation of three main paleogeographic domains:

- The Lagonegro Basin (LB) located between the ACP and the Western Carbonate Platforms. The Lagonegro unit can be differentiated in two complementary lithostratigraphic sequences: (i) a Triassic– Lower Cretaceous sequence consisting of siliciclastic deposits and dolomites, cherty limestones, radiolarites and siliceous claystones with limestones, (ii) Upper Cretaceous –Lower Miocene plastic successions mainly composed of carbonate resediments, arenaceous turbidites, variegated clays and quartzarenites, followed by Upper Miocene flysch deposits and calcareous turbidites.
- The Western Carbonate Platform (WCP), consisting of Mesozoic and Paleogene carbonate sequences followed by Upper Miocene siliciclastic flysch deposits; the latter accumulated above the WCP during its foredeep phase.
- More internal basinal domains, which are related to the Sannio and Sicilide Complexes (SAC and SIC, respectively). These complexes, which consist of variegated clays, arenaceous turbidites and carbonate resediments, appear often as chaotic tectonic melanges. They have been incorporated in the thrust belt before the opening of the Tyrrhenian Basin and correspond to the geometrically highest structural units in the Southern Apennines. Syntectonic terrigenous sequences, representing the infill of satellite basins of Late Tortonian to Early Pleistocene age, unconformably cover the thrust sheet stacks (Patacca & Scandone, 2001).

The axial and internal sectors of the chain toward the Tyrrhenian side are characterized by the development of widespread low angle faults that omit hundreds of meters to kilometers of structural section. The low-angle normal faults are distributed along a northwest southeast trending belt lying within the internal zone of the orogen. These low-angle faults were first described by Ietto, 1965 in the Picentini Mountains, located east of Naples, along the western flank of the orogenic belt (**Figure 9**). For many years the faults were interpreted in a compressional context as gravity-drive (Ietto, 1965) or out-of-sequence (Roure et al.,1991) thrusts. Reinterpretation of the tectonic setting of the Picentini Mountains led D'Argenio et al., 1987 to argue that these faults formed in extension. Regional and structural investigations throughout the Southern Apennines belt, from the Matese Mountains in the northwest to the Pollino Mountains in the southeast document the existence of substantial and previously unrecognized extensional displacement parallel to the axis of the orogen (D'Argenio et al., 1993, Oldow et al., 1993; Ferranti et al.,1995). The areas of greatest extension form discrete domains bound by breakaway faults, transcurrent displacemet transfer systems, and extensional allochthonous.

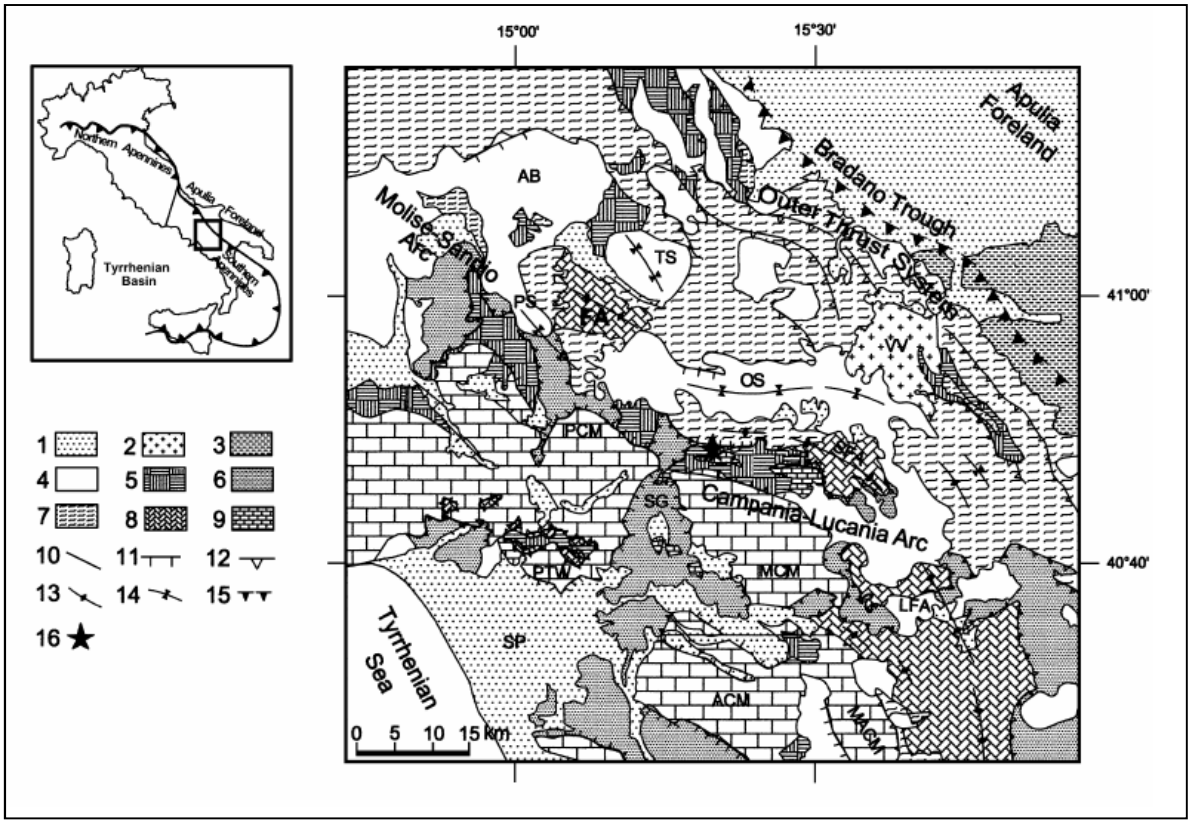

Figure 7: from Improta et al., 2003. Geological map of the Irpinia region. 1—Middle Pleistocene and Holocene deposits; 2—volcanites of the Vulture Volcano (Middle–Upper Pleistocene); 3—Bradano sedimentary cycle (Lower– Middle Pleistocene); 4—thrust sheet– top syntectonic clastic sequences (Upper Messinian– Early Pleistocene); 5—Upper Miocene siliciclastic flysch deposits (including the thrust sheet –top succession of the S. Bartolomeo Fm., Lower Messinian); 6—Sicilide and Sannio Complexes (Paleogene–Lower Miocene); 7—Tertiary deposits of the Lagonegro Basin; 8—Lagonegro Basin lower sequence (Lower Triassic –Lower Cretaceous); 9—Western Carbonate Platform (Mesozoic–Paleogene); 10—faults; 11—normal faults; 12—thrusts; 13—axis of antiform; 14—axis of synform; 15—buried frontal ramp of the Apennines thrust sheets; 16—epicenter of the 1980, Irpinia earthquake (from Westaway and Jackson, 1987). AB, Ariano Basin; TS, Trevico synform; PS, Paternopoli synform; FA, Frigento antiform; OS, Ofanto synform; SFA, S. Fele antiform; LFA, Lifoi antiform; VV, Vulture Volcano; PCM, Picentini carbonate massif; MCM, Marzano carbonate massif; MACM, Maddalena carbonate massif; ACM, Alburno carbonate massif; PTW, Picentini tectonic windows; SG, Sele River graben; SP, Sele plain.

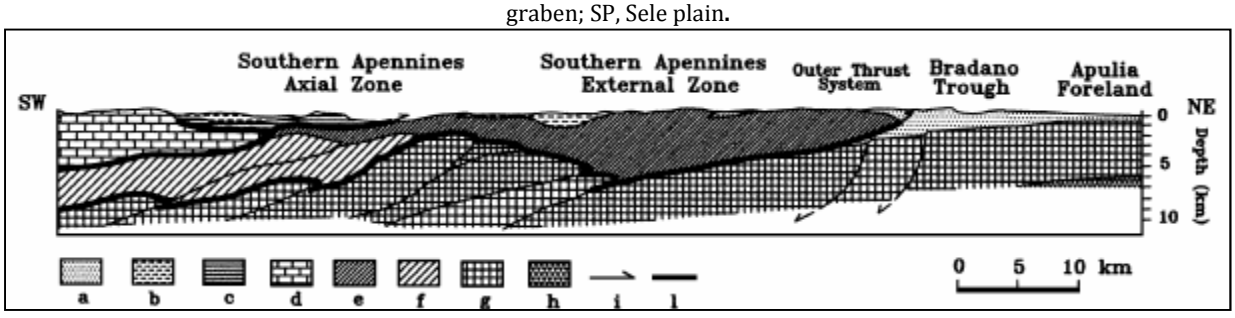

Figure 8: from Improta et al. (2003)Schematic section of the shallow structure of the Southern Apennines across the Irpinia region. (a) Plio– Pleistocene deposits of the Bradano Trough; (b) thrust sheets –top successions (Upper Miocene–Early Pleistocene); (c) Sicilide and Sannio nappes (Paleogene–Lower Miocene); (d) Western Carbonate Platform (Mesozoic– Paleogene) and Upper Miocene flysch deposits associated with the foredeep phase; (e) Lagonegro Basin upper sequence (Upper Cretaceous– Upper Miocene); (f) Lagonegro Basin lower sequence (Lower Triassic–Lower Cretaceous); (g) Apulia Carbonate Platform (Triassic –Upper Miocene); (h) Verrucano Fm. (Permian–Lower Triassic); (i) thrusts and normal faults; (l) boundary of the main tectono-stratigraphic units.

On the basis of crosscutting relations it is established that the low-angle fault systems developed during orogen-parallel extension that preceded inception of high-angle normal faults related to Tyrrhenian rifting. Some of the best exposures of the low-angle normal faults in the Southern Apennines are found in the Picentini Mountains (Mount Cervialto 1809 m), where detailed mapping, structural analysis, and a comprehensive understanding of the Mesozoic stratigraphy of deep-basin and carbonate-platform rocks allow examination of the relationship between earlier contractional and later low-angle extensional structures. Cross-section restoration and forward modeling illustrate the displacement history of extensional low angle decollements and related faults of the hanging wall assemblage. Geometric control afforded by exhumation on younger high-angle faults during Tyrrhenian rifting documents the lack of basement tilt during extension on the basal decollement systems. Displacement on the basal decollement occurred at present-day attitudes and supports the concept of supercrustal extension on shallowly dipping faults.

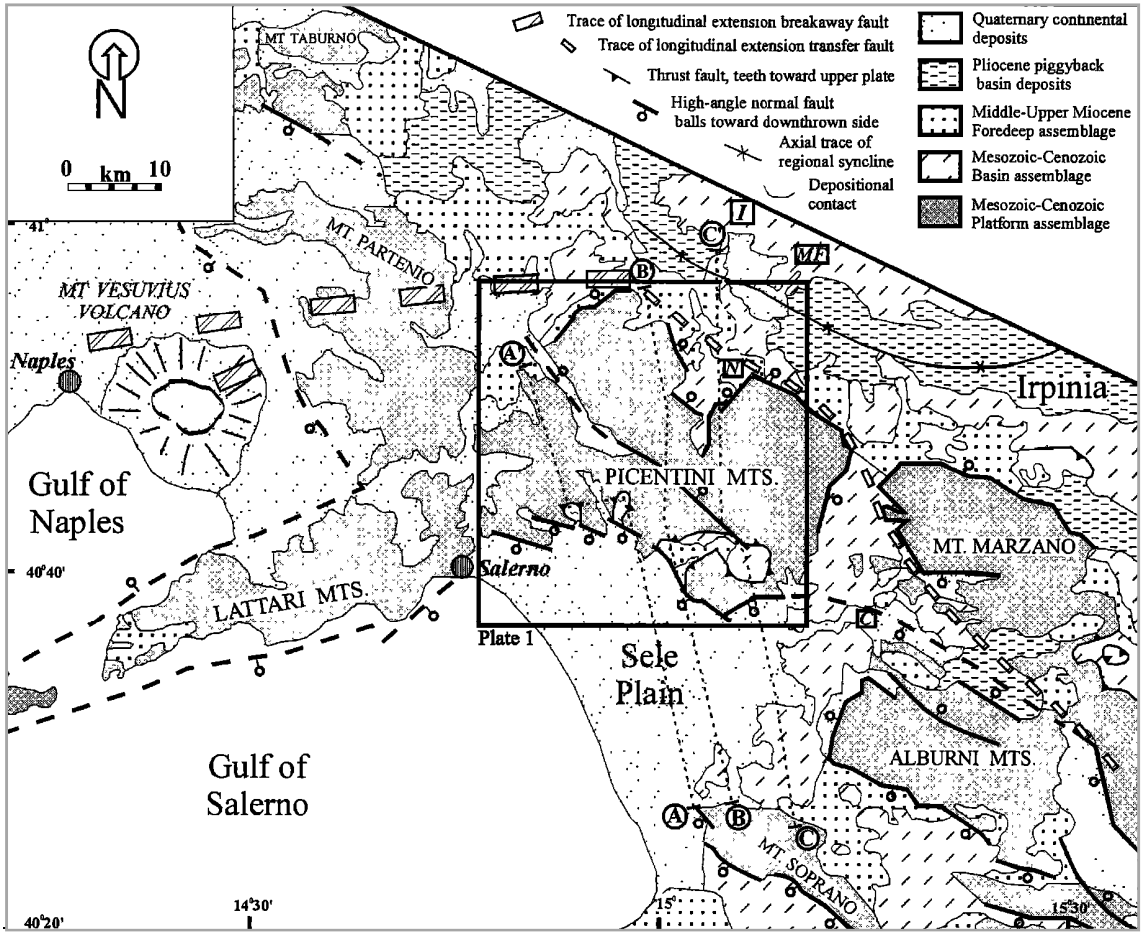

Figure 9: from Ferranti & Oldow, 1999.Semplified geological map of Picentini Mountains. Boxed letters show the location of deep wells: Irpinia 1; MF, Monte Forcuso1; N, Nusco2; C, Conturs1.

2.2 Earthquake kinematics

As indicated by borehole breakouts analysis and by the focal mechanism of large earthquakes, the extensional stress regime is still active at present and is responsible for the present-day crustal seismicity of the Southern Apennines (Amato & Montone, 1997). Earthquakes occur within a seismic belt, at about 20 km thick and 40 km wide, centred on the axis of the Apenninic range and are characterised by predominant normal-faulting focal mechanisms with NW-oriented nodal planes. This seismic belt is also delineated by the isoseismal areas of large historical (IzX MCS) earthquakes, which repeatedly struck the Molise–Sannio and the Campania–Lucania Apennines (Postpischl et al., 1985).

The Irpinia region is one of the most active seismic zones of the Southern Apennines. Large destructive earthquakes occurred both in historical and recent times in this region, which was struck in 1980 by the strongest event (M_w = 6.9) of the past century in the Southern Apennines. Detailed seismological studies on the 1980 Irpinia earthquake have demonstrated the complexity of its source mechanism, which consists of at least three normal-faulting ruptures nucleated in a time range of 40 s on separate fault segments (Pantosti & G. Valensise, 1990; Amato & Selvaggi, 1993) (**Figure 10**). The geometry of the faults, the amount of coseismic slip and the distribution of the aftershocks, appear to be correlated with P-wave velocity variations in the upper crust and with known surface geologic structures, thus suggesting that lithological heterogeneities in the upper crust played an important role in the rupture process (Amato & Selvaggi, 1993).

Although the Irpinia is one of the Italian regions with the highest seismic hazard, so far a thorough study of the upper crust in this sector of the belt is lacking. Two regional structural profiles based on surface and subsurface information, which extend from the Tyrrhenian margin to the Apulia foreland across the Irpinia region, were presented by Mostardini & Merlini (1986) and Casero et al. (1988). However, due to the large distance between the profiles (about 35 km), they do not accurately depict the lateral changes in the architecture of the thrust belt along the strike of the chain. Structural analysis, paleostress reconstruction and seismic reflection data were integrated by Hippolyte et al. (1994b) in order to investigate the tectonic evolution and the shallow crustal structure in a small sector of the Irpinia region (Ofanto Basin).

Improta et al. (2003) provided new information on the upper crustal structure in the Irpinia region by integrating gravity data, seismic reflection lines and subsurface information from many deep wells.

The proposed model by Improta et al. (2003) displayed important lateral density variations (**Figure 11**), clearly evident thanks to the fine profile spacing also moving along the strike of the range. This study suggested a possible relation between lithological heterogeneities found in the upper crust and the aftershock distribution and rupture

propagation of the 1980 Irpinia earthquake. In particular, these correlations suggested that the high-density, high-velocity carbonates of the Apulia Platform can be related to high-strength regions characterized by unstable sliding, and that the geometry of the ACP played an important role in the rupture propagation and in the aftershock distribution.

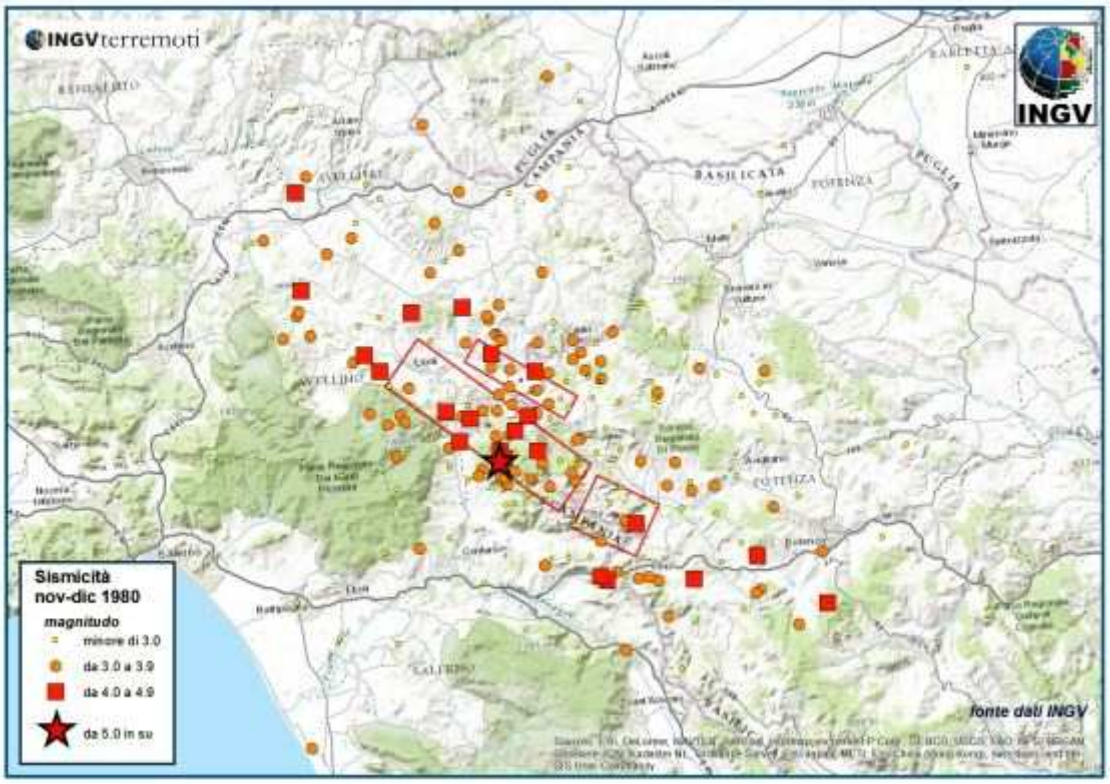

Figure 10: from INGV website. The fault segments and the aftershocks of the 1980, Irpinia earthquake. Note that the earthquake is characterized by the rupturing of three faults in less than one minute

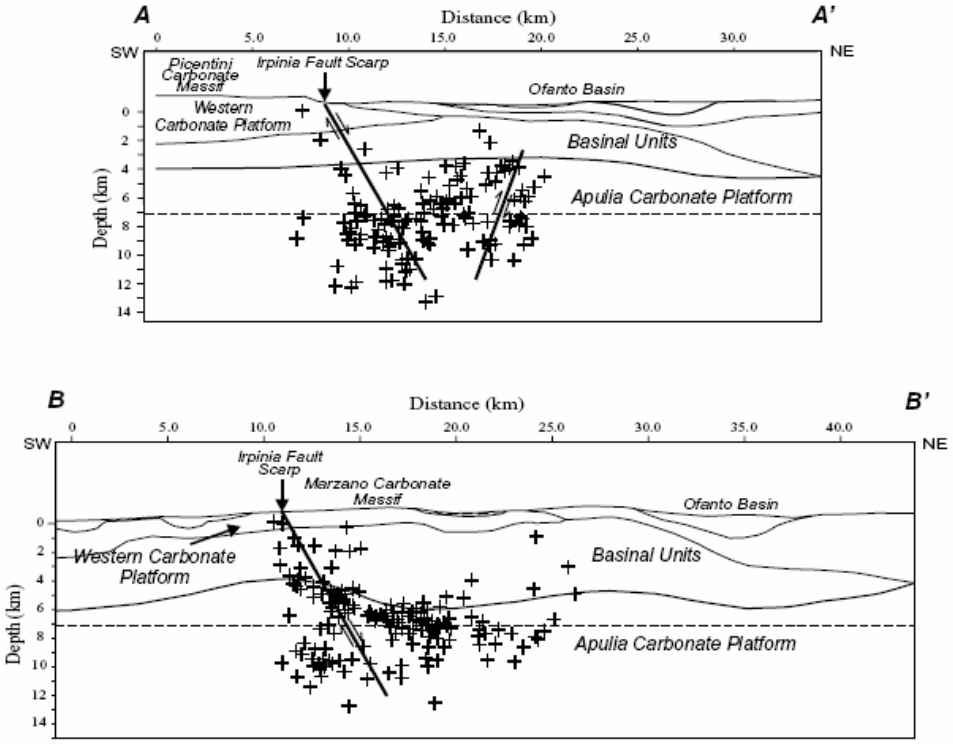

Figure 11: from Improta et al. (2003).The fault segments and the aftershocks of the 1980, Irpinia earthquake. Note that the aftershocks cluster mostly within the Apulia Carbonate Platform.

2.2.1 Documented hydrogeological response to seismic event

The influence of earthquake on springs flow is well documented. In particular in the southern Apennines, it is known that large events can disrupt water flow rate of fresh water springs. Esposito et al. (2001) studied the spring flow variations at Caposele and Cassano Irpino (**Figure 13**), located near the epicenter of the Irpinia earthquake (23 November), by considering the monthly averages in 10 years (Pece et al., 1999). The year 1980 appeared to be hydrologically anomalous.

In **Figure 14** the anomaly consists of the great increase in the flow rate for the thermal spring Acqua Fetente and Pollentina and Bagno Springs, between 17 and 30 November (earthquake was on 23 November) and this increase lasted many months. These increases cannot be imputable to the rainfalls that preceded the seismic event because a consistent lag among rainfalls and increases in the flow rates is recorded (**Figure 14**) (Esposito et al., 2001; Celico, 1981, Cotecchia & Salvemini, 1981).

The data relative to the hydrological variations' distribution versus the distance from the epicenter (**Figure 15**) show that the high concentration of phenomena (75%) lie between 25–80 km, whereas 19% were inside the epicentral area (0– 25 km); only 6% of these

phenomena occurred at greater distances (about 100 km); this distribution is very similar to those reported by Kissin and Grinevsky (1990).

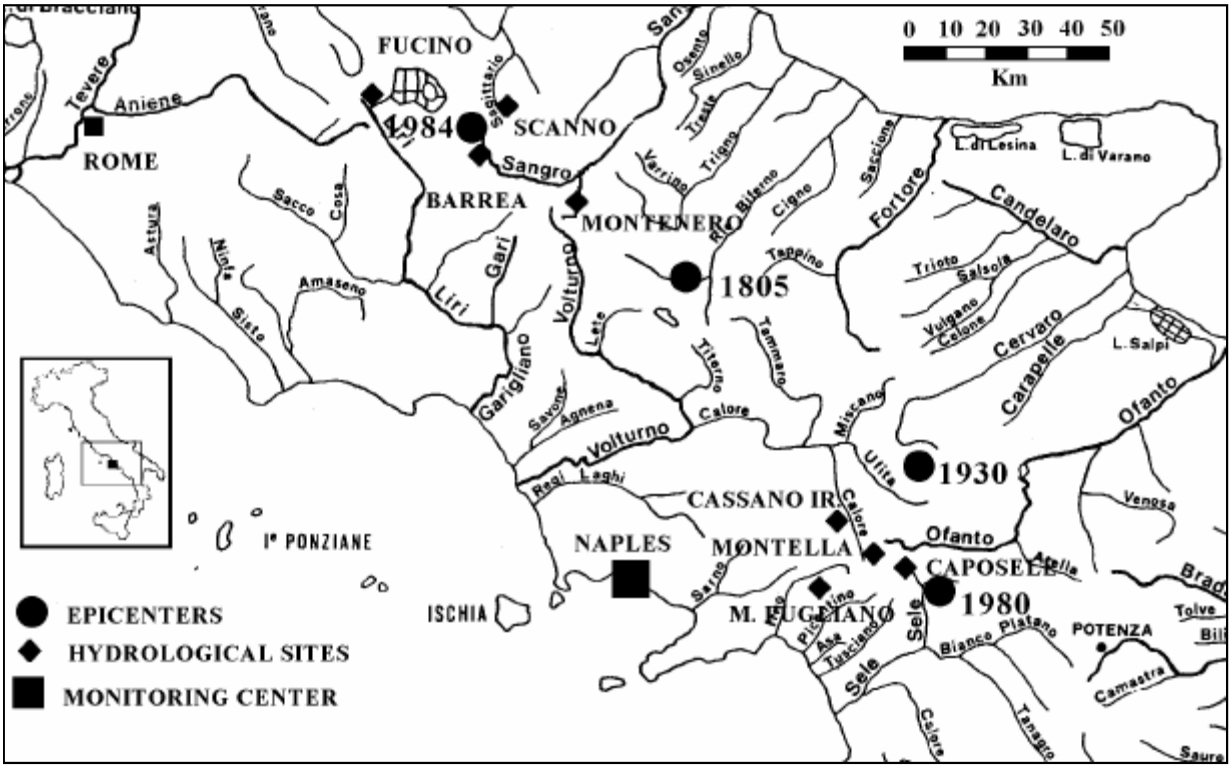

Figure 12: from Esposito et al. (2001) Sketch map of mentioned hydrological sites and the Irpinia epicenter (1980).

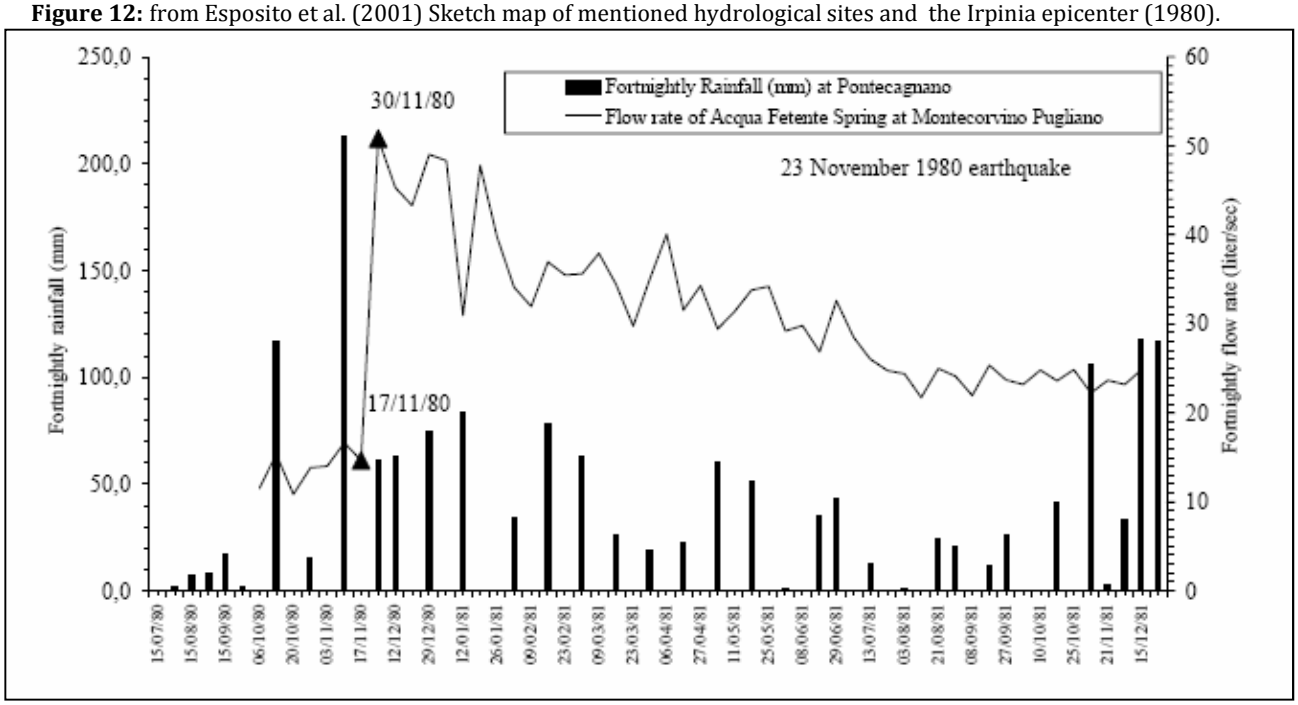

Figure 13: from Esposito et al. (2001). Hydrological anomaly correlated to the 23 November 1980 earthquake, consisting of a great increase in the flow rate of Acqua Fetente Spring at Montecorvino Pugliano from 14.7 to 50.8 l/s. This variation lasted for more than one year.

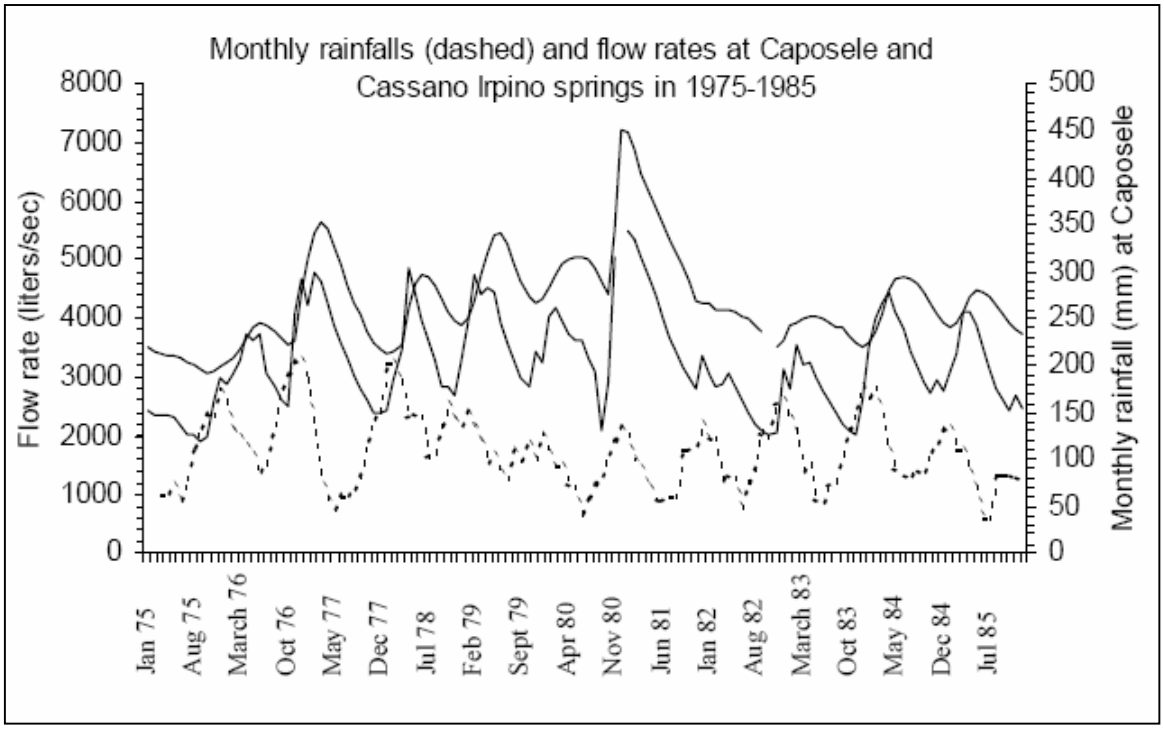

Figure 14: from Esposito et al. (2001). Monthly rainfalls (dashed) and flow rates at Caposele and Cassano Irpino Springs in 1975–1985 showing the lag between rainfalls and subsequent increase in flow rate.

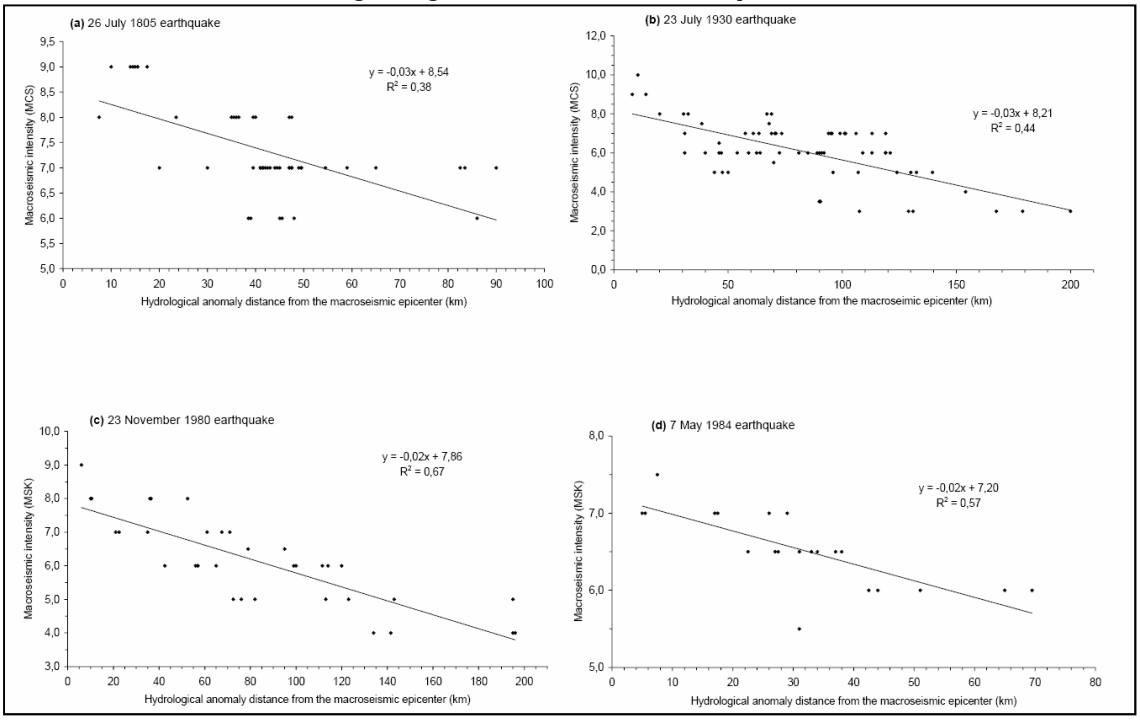

Figure 15: from Esposito et al. (2001). The figure shows for each earthquake the distance from epicenter and intensity (MCS or MSK) of the sites where hydrological anomalies have been observed. A clear negative linear regression is visible. For the 1930 (M = 6.5) and 1980 (M = 6.8) earthquakes the two trends are parallel.

2.3 Hydrogeological setting of the Monte Cervialto aquifer

Cervialto Mountain is part of the Picentini Mountains, that constitute a large karst system in the Campania region of Italy, over 600 km^2 wide (**Figure 16**). In the north-eastern sector, over 70% of the catchment lies above 1.000 m a.s.l., with the highest catchment being located on the top of Mt. Cervialto (1.809 m a.s.l.). In the north-western sector, 30% of the catchment lies above 1,000 m a.s.l., with the highest catchment being located at the top of Mt. Terminio (1,806 m a.s.l.) (Fiorillo & Ventafridda, 2010).

Outcropping rocks in the region primarily belong to the calcareous and calcareous-dolomite series (Late Triassic–Miocene), are 2.500 m thick, heavily fractured and faulted and frequently reduced to breccias. Karstic phenomena have considerably dissolved the rocks, but due to high density of fractures and fissures, no well conduits development has been occurred. These karstic rocks are mantled by pyroclastic deposits of Somma-Vesuvius activity, which play an important role in the infiltration of water into the karst substratum (Fiorillo & Guadagno, 2011).

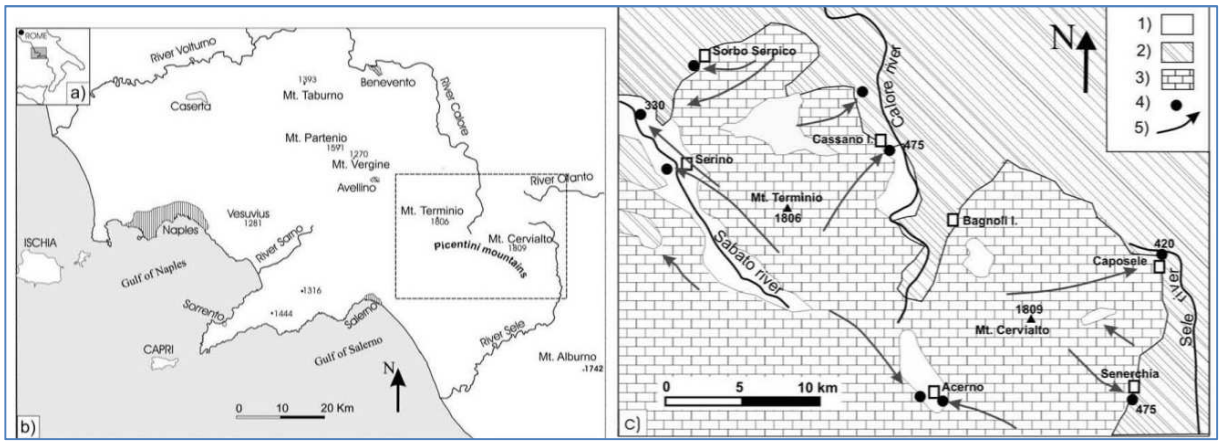

Figure 16: Modified by (Fiorillo, 2009). (a) Southern Italian peninsula. (b) Map of the Western Campania region. (c) Hydrogeological map of the Northern Picentini Mountains (modified from Fiorillo, 2009). (1)Slope breccias and debris, pyroclastic, alluvial and lacustrine deposits (Quaternary); (2) argillaceous complex and Flysch sequences (Paleogene–Miocene); (3) calcareous–dolomite series (Jurassic–Miocene); (4) main spring; (5) groundwater flow direction.

The calcareous-dolomite series are tectonically bounded by terrigenous and impermeable deposits, constituting complex argillaceous (Paleocene) and flysch sequences (Miocene). Quaternary continental deposits, including slope breccias, debris, alluvial and lacustrine deposits, cover the marine substratum (**Figure 16**).

Picentini Mountains has several important springs, that of interest in this thesis are the Caposele and Cassano Irpino groups.

Caposele group is formed by the Sanità spring (420 m a.s.l.), which is located at the head of the Sele river basin along the north-eastern boundary of the Picentini Mountains. This spring, which is primarily fed by the Cervialto Mountain (Celico & Civita, 1976), has a mean annual discharge of 3,96 m^3/s. The spring was tapped in 1920 by the Pugliese aqueduct,

which passes through the Sele-Ofanto divide via a tunnel and supplies the Puglia region with water. The Cassano group, which is located in the Calore river basin along the northern boundary of the Picentini Mountains, is formed by the Bagno della Regina, Peschiera, Pollentina and Prete springs (473–476 m a.s.l.). These springs are primarily fed by the Terminio Massif, with an overall mean annual discharge of 2,65 m^3/s. In 1965, these springs were tapped to supply the Puglia region with water, and a gravity tunnel was joined to the Pugliese aqueduct (Fiorillo, 2009).

In this thesis the focus is on the Cervialto Mountain massif and on the Sanità di Caposele spring.

From the hydrogeological point of view, Cervialto Mountain's boundaries are represented by (Celico & Civita, 1976) (S. Aquino & A. Aquino, 2008):

- NW and NE, by contact with terrigenous deposits belonging to the impermeable Sicilide Unit and to lithostratigraphic units pre-and late Neogene orogen, in particular, along the north-western margin there is a major tectonic discontinuity with transcurrent characters;
- SW, by the outcropping dolomite substratum, often sandy reduced, which hinders any connection between Monte Cervialto and Monte Accellica,
- SE, from the tectonic track Acerno-Calabritto showing clear compressive characters; along this margin is possible to observe the Monte Polveracchio overlapping on Monte Cervialto;
- NE, by the Mt. Cervialto overlapping on impermeable soils.

2.4 Available data and methods

2.4.1 Data

To understand the hydrogeological changes due to the Irpinia earthquake occurrence, discharge data from Caposele and Cassano Irpino spring groups were analyzed. As described in the previous paragraph, Caposele spring is composed by one rising called Sanità di Caposele spring, while Cassano Irpino is characterized by 4 rising called: Prete, Pollentina, Peschiera and Bagno della Regina springs, the last one is the most important for discharge amount.

The two springs are managed by the Acquedotto Pugliese S.p.A., but the data have been provided by the Alto Calore Servizi S.p.A.. The discharge data have been compared with precipitation data to understand how rainfall influences the springs discharge trends.

Caposele spring available data has been daily recorded from 1964 to 1999, and twice data for month from 1920 to 1963. Cassano Irpino springs available data have been recorded every ten days from 1965 to 1991. In **Table 10**, **Table 11** and **Table 12** historic data of the Caposele spring are reported attending the indications by Braca, et al. (2013).

For the first step the data were tabulated and arranged in time series to recognize the discharge variations at the 1980 Irpinia earthquake.

From **Figure 17** to **Figure 21** it is possible to observe that springs show an increase in discharge just after the earthquake occurrence, but it is clear that Caposele spring showed a response greater than Cassano Irpino (Bagno della Regina) spring. Moreover it is possible to observe that the discharge increase of Caposele spring anticipates a few months the maximum peak flow of the spring, usually it occur in april/may but in consequence of the earthquake it is reached at January 6, 44 day after the earthquake. Furthermore until 1985 the spring doesn't recover his normal trend, it maybe happened that the aquifer needed to recover the water lost with the earthquake occurrence.

Another particular observation consist in the amount of discharge increase, Caposele spring has a mean discharge of about 4 m^3/sec, with a pre-earthquake peak of 6,7 m^3/sec. After the earthquake the spring got to a value of 7,2 m^3/sec, never reached before and in only one month. On the contrary Cassano Irpino springs showed an increase, but not so significant as Caposele. A particular observation is possible to do from the **Figure 18**, just before the earthquake the discharge shows an abrupt decrease.

In this thesis the analysis are focused on the Caposele group, because the variation due to Irpinia earthquake observed there was greater than the variation at Cassano Irpino group.

To quantify Monte Cervialto recharge has been important to retrieve rainfall data representative of the area. Available data (Annali Idrografici) have been recorded daily

from 1973 to 1999 for Acerno rain gouge, from 1971 to 1999 for Montella rain gouge, from 1970 to 1999 for Senerchia rain gouge, from 1972 to 1999 for Caposele rain gouge, from 1972 to 1980 for Materdomini rain gouge, from 1974 to 1979 for Laceno raingouge, from 1972 to 1984 for Montemarano rain gouge, from 1972 to 1984 for Cassano Irpino rain gouge, from 1969 to 1999 for Montevergine rain gouge, as reported in tables from **Table 1** to **Table 9**.

As reported in the previous paragraph, over 70% of the catchment lies above 1.000 m a.s.l., the only high-altitude rain gouge lying on the aquifer consist in Laceno rain gouge that unfortunately only worked since 1974 to 1989. To confront discharge with rainfall has been also considered Montevergine rain gouge, in spite of is located about 40 km far away Laceno rain gouge, it lies 1.287 m a.s.l. and it could be considered representative of the rain trend at high-altitude in that geographic area.

In **Figure 17** reported below are graphed daily discharge data and monthly rain data from Caposele spring and Acerno raingouge January 1975 to December 1985.

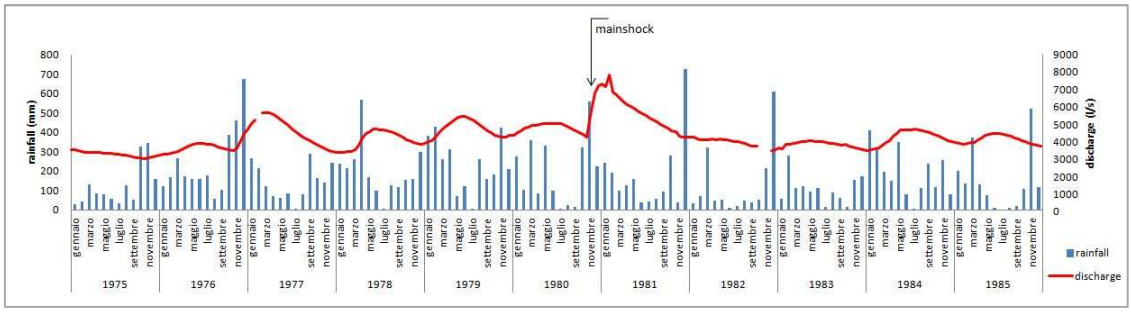

Figure 17: Caposele spring discharge and rainfall at Acerno raingouge.

In **Figure 18**, **Figure 19**, **Figure 20** and **Figure 21** reported below are graphed every ten days discharge data and monthly rain data from Cassano Irpino group and rainfall measured at Montella raingouge from January 1975 to December 1985.

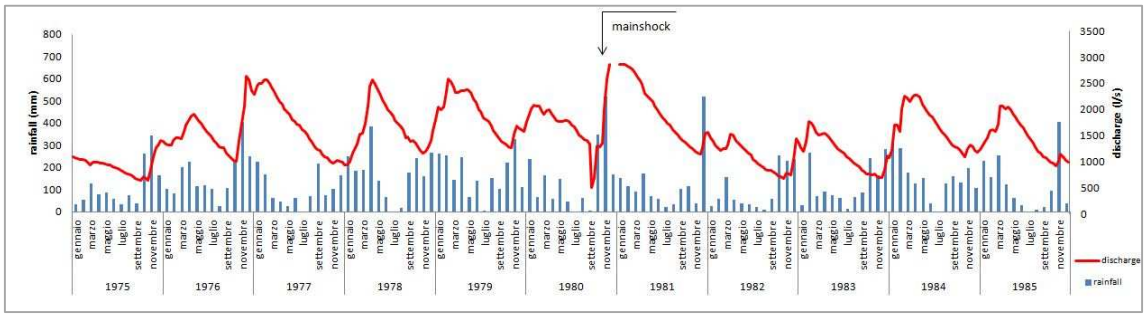

Figure 18: Cassano Irpino (Bagno della Regina) discharge and rainfall at Montella raingouge

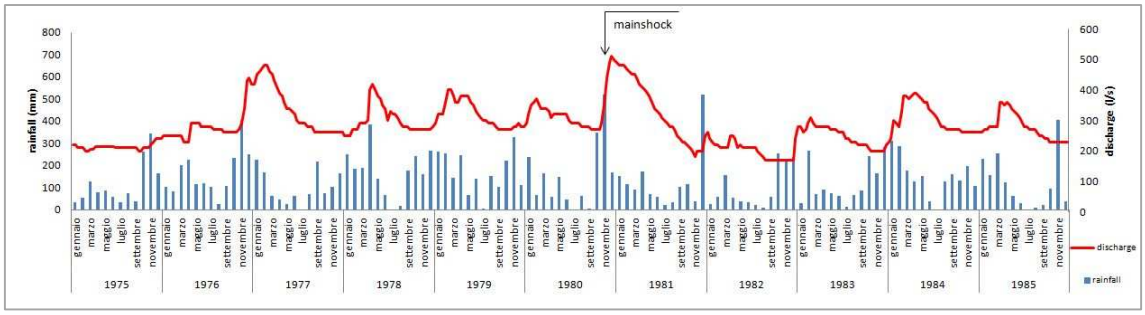

Figure 19: Cassano Irpino (Peschiera) discharge and rainfall at Montella raingouge

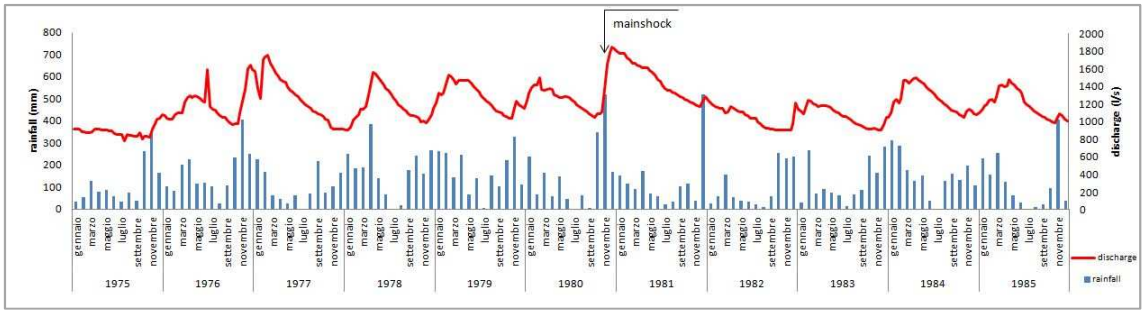

Figure 20: Cassano Irpino (Pollentina) discharge and rainfall at Montella raingouge

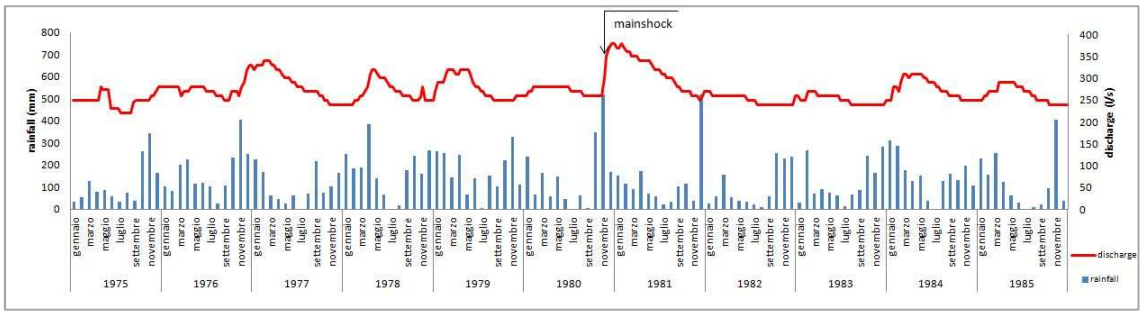

Figure 21: Cassano Irpino (Prete) discharge and rainfall at Montella raingouge

The Cervialto Mountain lies in the S. Angelo dei Lombardi Foglio 186 of the Italian Geological map.

The geological map and the tectonic setting of Cervialto Mountain has been considered to evaluate the aquifer amplitude.

In **Figure 22** the geological map and the tectonic setting of the aquifer is shown.

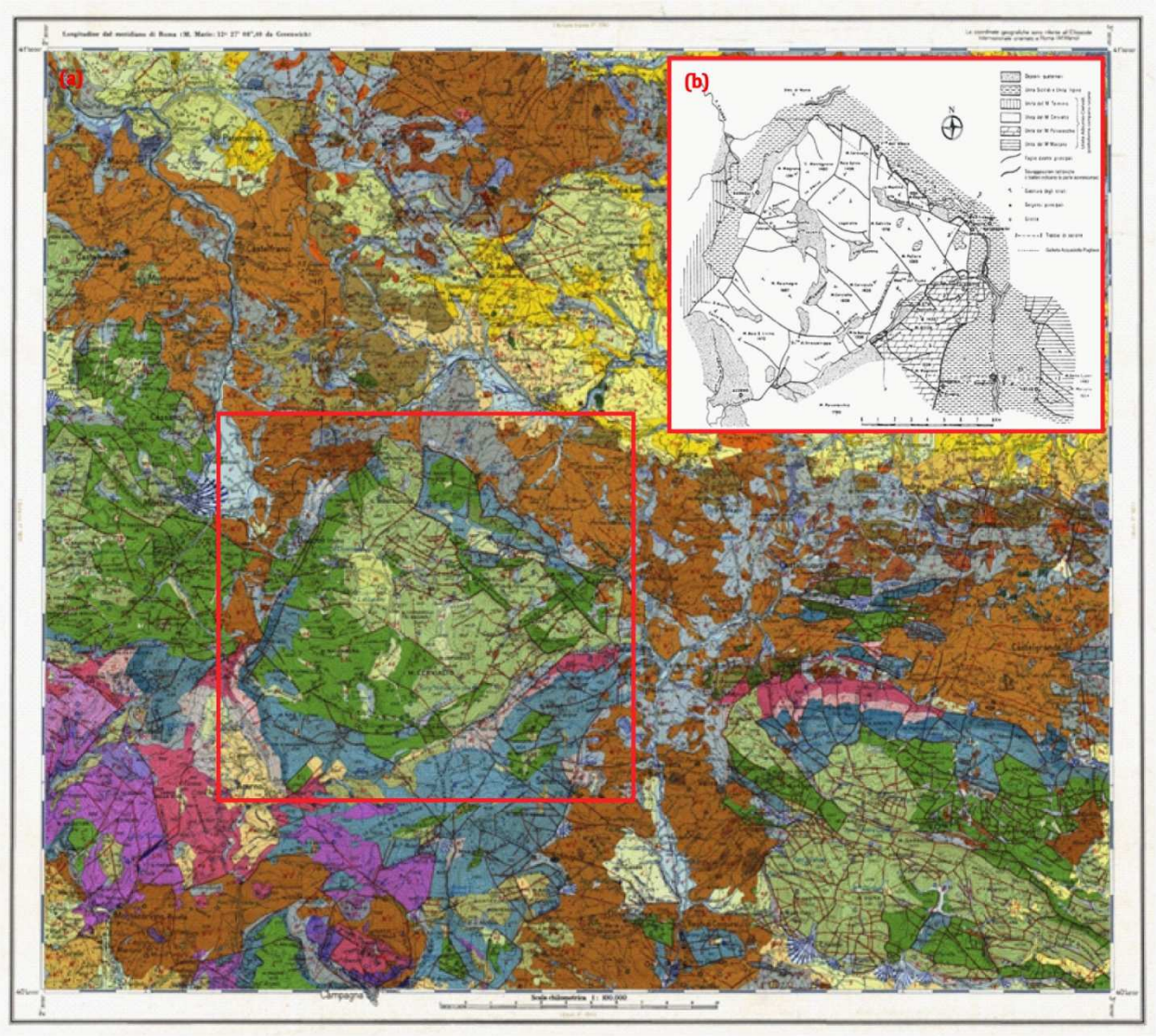

Figure 22: (a) geological map S. Angelo dei Lombardi Foglio 186; (b) tectonic setting of Cervialto Mountain from Celico & Civita (1976)

2.4.2 Methods

In this chapter it will be argued the methods utilized to study the hydrological changes observed in consequence to the 1980 Irpinia earthquake. In general the approach was to start by the hydrological changes observation in Sanità di Caposele spring discharge, than analysis of the spring hydrograph have been performed (baseflow recession analysis), based on hydrological observations and on geological background, hypothesis on the aquifer hydrogeological properties changes have been promoted, to argue the proposed conceptual model a numerical model of the Cervialto Mountain aquifer has been performed.

Baseflow recession analysis

The Caposele spring hydrograph has been analyzed before and after the Irpinia earthquake using the baseflow recession analysis.

The *recession curve* is the specific part of the flood hydrograph after the crest (and the rainfall event) where streamflow diminishes, refer Baseflow.

The slope of the recession curve flattens over time from its initial steepness as the quickflow component passes and baseflow becomes dominant. A *recession period* lasts until spring flow begins to increase again due to subsequent rainfall. Hence, recession curves are the parts of the hydrograph that are dominated by the release of water from natural storages, typically assumed to be groundwater discharge. *Recession segments* are selected from the hydrograph and can be individually or collectively analyzed to gain an understanding of these discharge processes that make up baseflow (**Figure 23**). Graphical approaches have traditionally been taken but more recently analysis has focused on defining an analytical solution or mathematical model that can adequately fit the recession segments.

Each recession segment is often considered as a classic exponential decay function as applied in other fields such as heat flow, diffusion or radioactivity, and expressed as (Maillet, 1905):

$$Q_t = Q_0 e^{-\alpha t} \qquad 2$$

where Q_t is the stream flow at time t, Q_0 is the initial stream flow at the start of the recession segment, α is a constant.

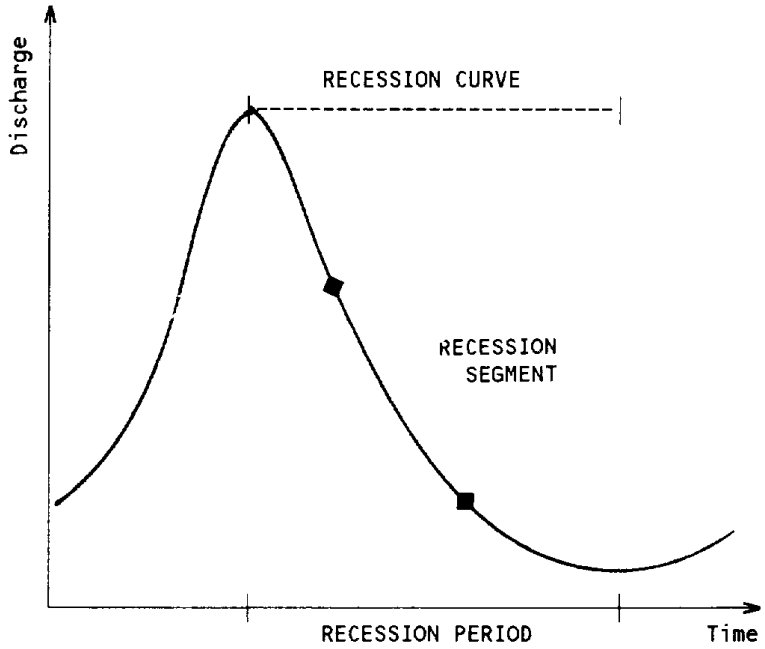

Figure 23: from (Tallaksen, 1995) Recession curve, period and segment

The recession curve, and α value, tells in general way about the natural storages feeding the spring. Accordingly, it contains valuable information concerning storage properties and aquifer characteristics, and recession analysis has been useful in many areas of water resource planning and management (Tallaksen, 1995).

Taking a leaf from Wang & Manga, 2010, which analyzed the hydrographs of streams near the epicenter of the 1989 Mw 6.9 Loma Prieta earthquake to study the aquifer permeability changes, baseflow recession analysis were used to investigate the Cervialto Mountain aquifer hydrological variations (**Figure 24**). So α value pre- and post- earthquake have been compared.

In **Figure 25** α values annual variation is represented. The α values between 1964 and 1999 have been calculated by equation 2 on Septeber-October two-month period, the α values from 2000 to 2009 were provided by prof. Fiorillo. The data represent annual values and mean values, deal with separately for the pre-earthquake and post-earthquake years. Data are also compared with precipitations.

In **Figure 26** the mean pre- and post- earthquake α values are reported organized in 2 scatterplots, also standard deviations and outliers are visualized in the graph, as it shows there is an increase in standard deviation after the earthquake occurrence.

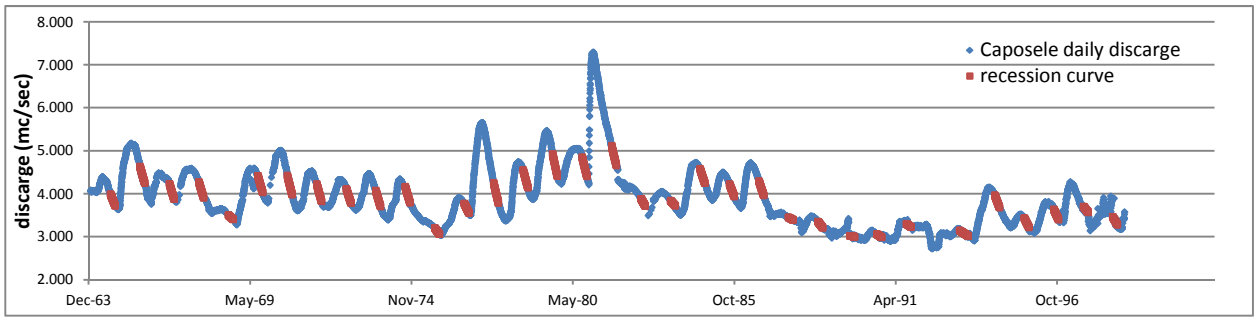

Figure 24: Caposele spring recession curve, period January 1964 – December 1999

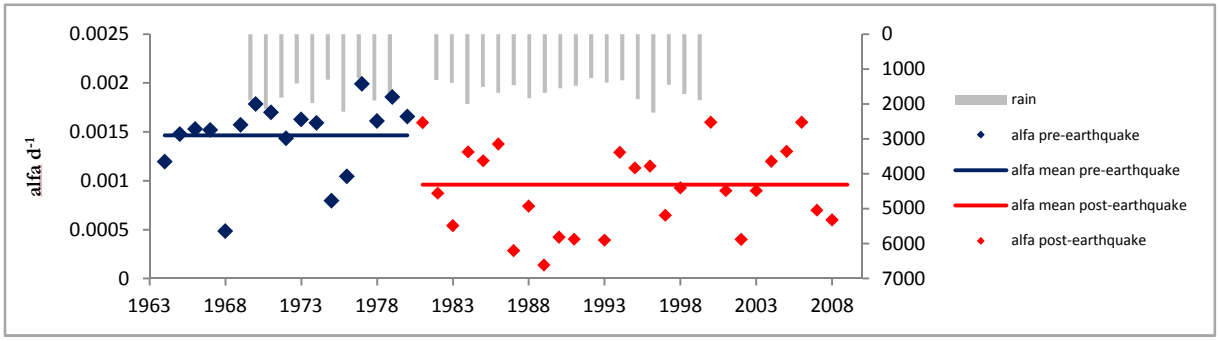

Figure 25: Representation of pre- and post-seismic α values, period January 1964 – December 2009

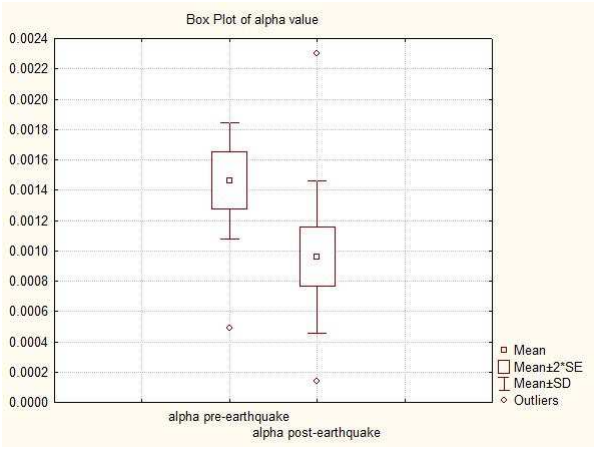

Figure 26: Representation of mean with standard deviation pre- and post-seismic α values, period January 1964 – December 2009

Geological map

To build the Cervialto Mountain hydrological model (par. 2.4.4) has been drown the geological map of the area using ARC GIS 9 (ArcMap™ Ver. 9.3) reported in **Figure 27**, on the right the rose diagram of the principal faults direction is reported. As were not possible to make a field study, lithological and structural information has been considered to build the mesh of the numerical model.

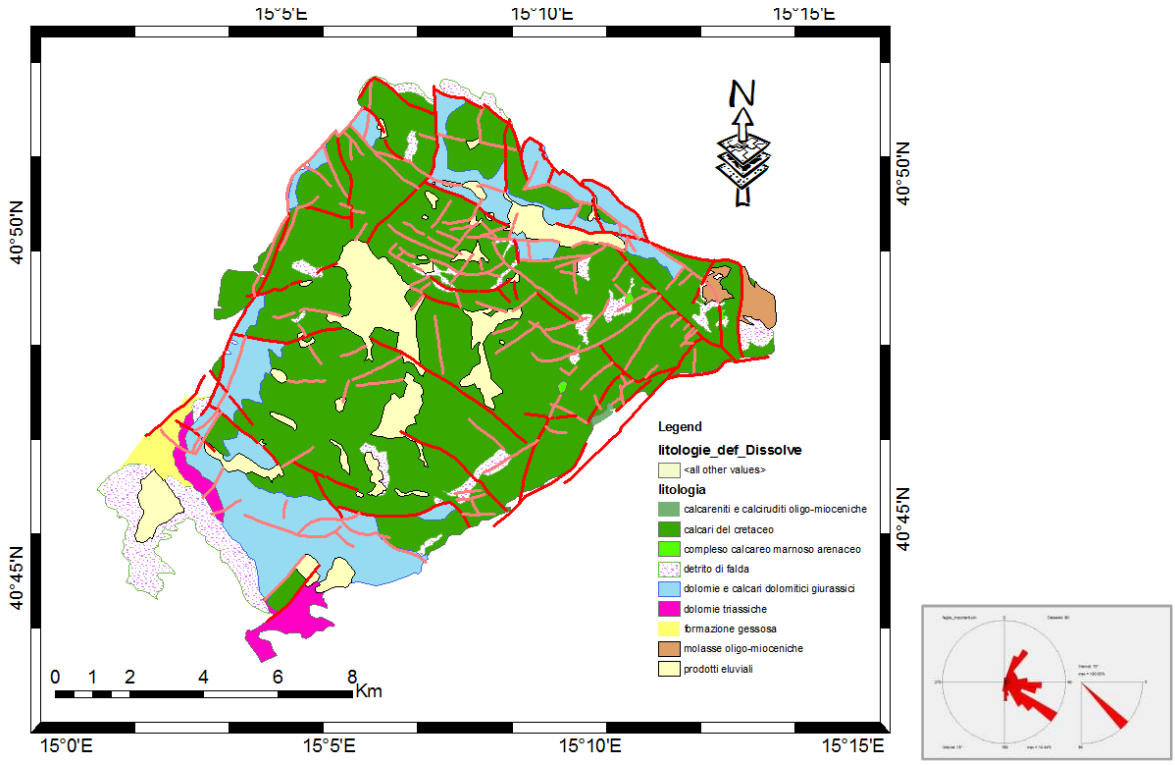

Figure 27: lithological and structural map of the Cervialto Mountain aquifer, used as base for the numerical model; on the right there is a rose diagram of the principal faults direction of the area.

As the surface aquifer is considered only the Cervialto Mountain massif were carbonatic rocks outcrops, from the map it is possible to evaluate that the aquifer recharge area is about 109 km^2, this data is supported by Fiorillo & Guadagno, 2011.

To evaluate the 3 dimensions aquifer extension six cross-sections of the Cervialto Mountain aquifer has been interpreted by the geological map. Has said before, for "Cervialto aquifer" is considered only the carbonatic portion of the aquifer, so it has been placed particular attention to the carbonate limits.

Looking at the data it could be possible to suppose that something in the aquifer (geometry/properties) changes with the occurrence of the earthquake, it could be happened that the seismogenic fault proximity has generated aquifer geometry and static stress changes which influenced the hydraulic properties, or that the seismic waves passage caused a sponge effect of the aquifer.

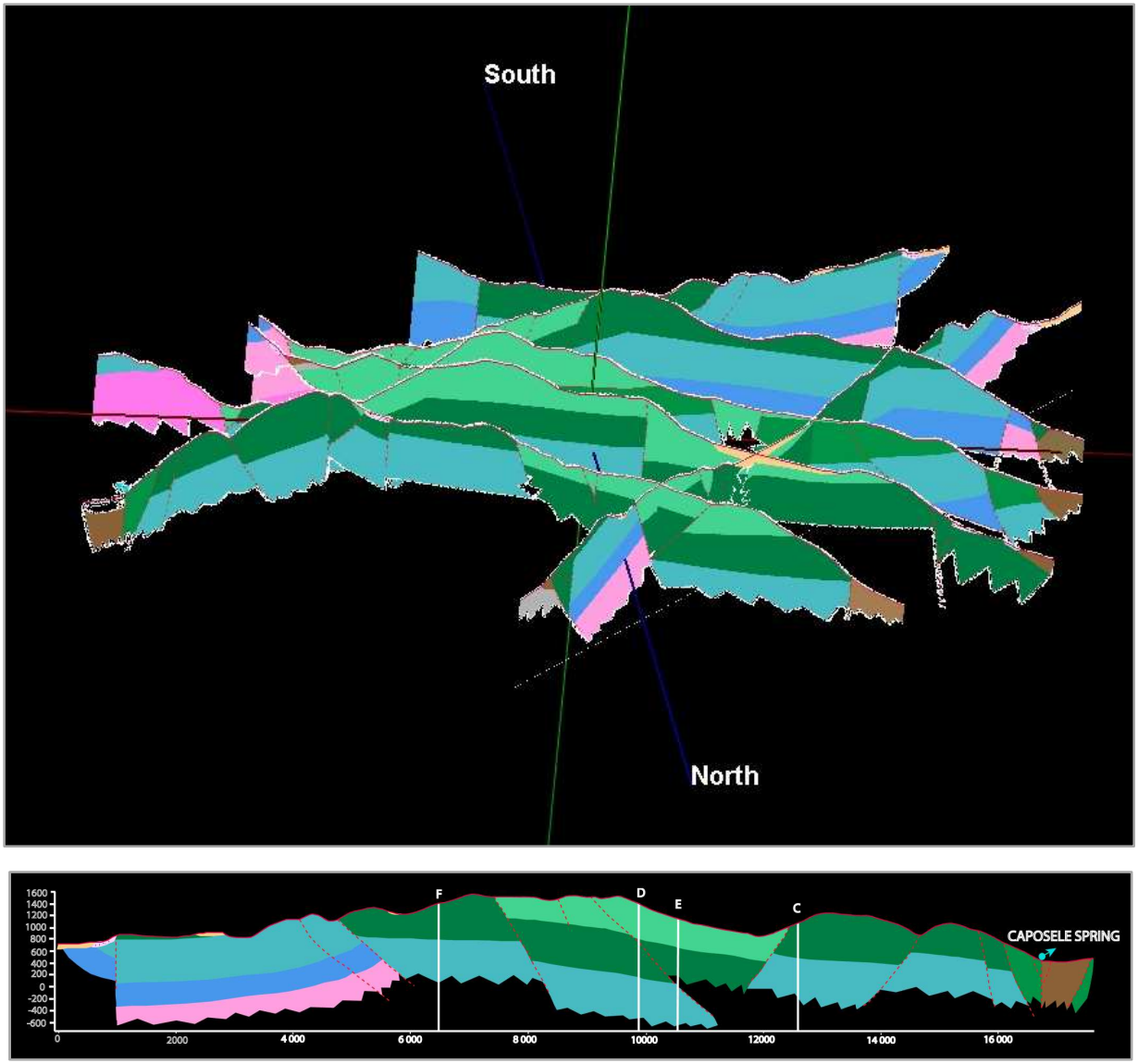

Figure 28: Interpreted cross-sections of Cervialto Mountain.

Numerical modeling

To evaluate the hypothesis of changing in aquifer hydraulic characteristic, a numerical model of the Cervialto Mountain has been performed.

The used Software is Visual Modflow Version 2011.1 Pro (Dynamic Groundwater Flow and Contaminat Transport Modeling Software). This software is based on the calculation code MODFLOW-2000.

This is a new version of the finite difference hydrological model usually called MODFLOW, released by the U.S. Geological Survey in 2000. The groundwater flow is simulated using a finite difference approach block centered.

The three-dimensional water flow at constant density and trough soils characterized by primary permeability can be described from the following equation:

$$\frac{\partial}{\partial x}\left[K_{xx}\frac{\partial h}{\partial x}\right]+\frac{\partial}{\partial y}\left[K_{yy}\frac{\partial h}{\partial y}\right]+\frac{\partial}{\partial z}\left[K_{zz}\frac{\partial h}{\partial z}\right]+W=S_S\frac{\partial h}{\partial t} \qquad 3$$

Where

K_{xx}, K_{yy} and K_{zz}	are Hydraulic Conductivity values along x, y and z axes, it is assumed that they are parallel to the principal Hydraulic Conductivity directions of the system (L/T)
h	is the potentiometric load (L)
W	is the flow per unit of volume, which represent springs or water capture with (T^{-1}): W<0,0 for waters flowing out of the system W> 0,0 for water flowing in the system
S_s	is the specific Storage (T^{-1})
t	is time (T)

This equation, together with the flow and/or hydraulic head conditions definitions at the aquifer boundaries, and the initial definition, constitute a mathematic representation of an hydrogeological system.

Except for some very simple systems, are rarely possible analytical solutions for the equation 3, for this reason several numerical methods were employed to obtain approximate solutions. One of this methods is the finite difference approach in which the continuous system described by the flow equation is replaced by a finite ensemble of discrete points in the space and time, the partial derivates are replaced with calculated value of hydraulic head difference in that points. The process lead to differential algebraic equation systems, linear, simultaneous; their solutions are hydraulic head value in specific

points and moments. This values constitute an approximation of the hydraulic head distribution in time function.

An hydrogeologic system is represented in MODFLOW as a discrete system of a block mesh called "cells", which localization are described with "rows", "columns" and "layers". It is used an indexing system i, j, k, corresponding to the elements of localization.

In **Figure 29** a schematization of an hydrogeological model is reported:

- black dots represent active cells,
- Δr_j represents the cell dimension along row direction (subscription *j* represent the column number),
- Δc_i represents the cell dimension along column direction(subscription *i* represent the row number),
- Δv_k represents the cell dimension along vertical direction (subscription *k* represent the layer number)

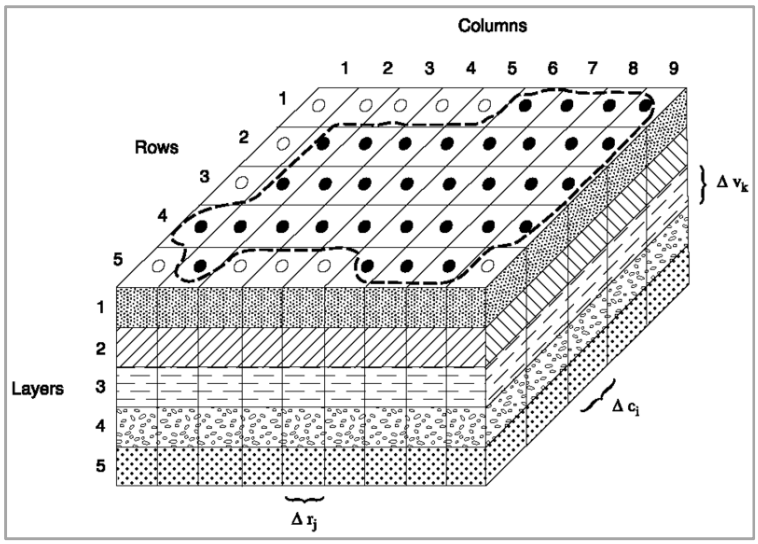

Figure 29: from Harbaugh, (2005). Discretization of an hypothetical hydrological system.

In the model equation, layers correspond to hydrogeological units, rows and columns represent two orthogonal directions within layers.

In every cell there is a "node", in MODFLOW is "block-centered", at the cell center , in correspondence of the node the hydraulic head is attributed.

To solve the general flow equation in the saturated medium, is necessary to specify the model domain boundary conditions, and in case of transitory simulations, the starting conditions. The study area model definition requires the model domain and his hydrogeological system neighboring definition. So it is necessary to identify the model limits hydrogeologically based, between the model domain and the whole system. This

limits are localized at the model boundary and in the points where external influences are present, which: rivers, wells, leaking reservoirs, etc. The utilized criteria to define boundary hydraulic conditions are correlated to topography, hydrology and geology of the study area. Once the limits are identified, the boundary conditions definition in the modeling processing consist in establishing a mathematical assumption that specify appropriate hydraulic conditions to each limit cell (usually hydraulic head o boundary flow).

Boundary conditions definition is necessary to guarantee uniqueness solution and output of the model to the flow equation. Each limit will correspond to only one boundary condition, that could be time varying. Limits could be divided in physical and faked; the first one are mathematically represented by three boundary conditions type:

1. Constant head,
2. Imposed flow,
3. Head depending flow.

While faked limits are utilized when the modeling area doesn't have "real" hydrogeologic limits, usually are imposed far away from the model grid center.

Processing

During Processing phase flow equation is solved in three dimension. The method could be chosen between several available solver. For Cervialto Mountain model Preconditioned Conjugate-Gradient Package is used.

This solver uses iterative calculation of the model equations. It permits to select a maximum number of Outer Iterations, if it doesn't converge the simulation is automatically stopped. Iteration number changes with the desired resolution for the model.

Output data coming from the solver calculation are written of specific files, it is possible to visualize them with a graphic interface.

Output results can be visualized as spatial data, as graphics. Comparing simulated and observed data is possible to perform model parameters sensitivity analysis, which mean that simulation are performed several time changing one parameter each simulation and correlating output results with singular parameter variation.

Equivalent porous medium

The Cervialto Mountain aquifer is a prevalent secondary permeability system characterized by carbonatic rocks. A MODFLOW limit is that it was created to simulate flow in primary permeability media (soils). In spite of this limit, is considered that the Cervialto numerical model scale (100 x 100 m cells) is large enough to use the equivalent porous medium approach.

2.4.3 Conceptual model and results

The conceptual model describes the Cervialto Mountain aquifer boundaries, hydraulic properties and "hydraulic balance".

Boundaries

For the Cervialto Mountain aquifer is considered only the carbonatic portion of the massif, as described in Par. 2.3 the lateral and vertical boundaries are represented by the tectonic discontinuities that make in contact the Carbonatic Unit with Terrigenous Units, also the stratigraphic transition to Dolomitic Unit is considered an aquifer limit.

The **hydraulic properties** of the aquifer are unknown, so are considered literature data to calibrate the numerical model (Par. 2.4.4). Hydraulic properties imposed in the model are: Hydraulic Conductivity (K), Specific Storage (Ss), Specific yeald (Sy), Effective Porosity.

Hydraulic conductivity

Hydraulic conductivity (K) is a property of soil or rock that describes the ease with which a fluid (usually water) can move through pore spaces or fractures. It depends on the intrinsic permeability of the material and on the degree of saturation, and on the fluid density and viscosity (Domenico and Schwartz, 1990).

In **Table 13**, **Table 14** and **Table 15** Hydraulic conductivity data for different materials and rocks are reported, in **Table 16** horizontal and vertical K are reported, in **Figure 30** is represented a summary for this property.

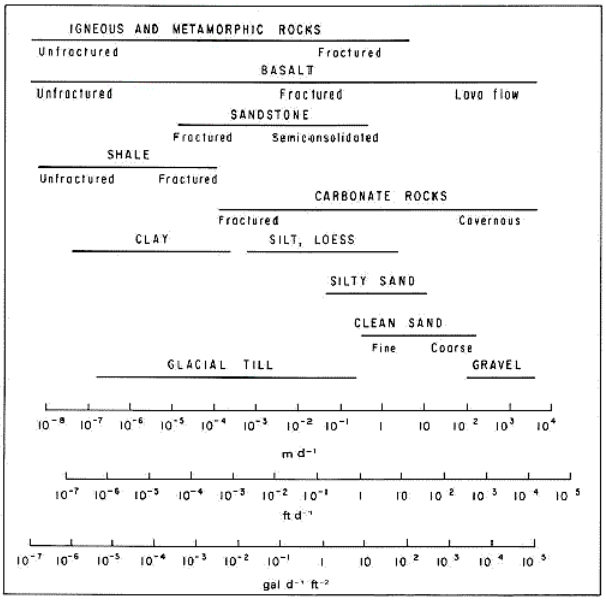

Figure 30: from Heath (1983)Hydraulic conductivity of selected consolidated and unconsolidated geologic materials.

For fissured limestone K is included between $2x10^{-2}$ m/sec (karst and reef limestone) and $1x10^{-9}$ m/sec (limestone, dolomite), horizontal K is included between 10^{-9} m/sec and 10^{-7} m/sec, vertical K is included between$5x10^{-10}$ m/sec and $5x10^{-8}$ m/sec.

Specific Storage

The Specific Storage (S_s) is a physical property that characterizes the capacity of an aquifer to release groundwater.

In **Table 17** Specific Storage representative values for different litologies are reported (Batu 1998).

For fissured limestone S_s is included between 3,3 x 10^{-6} (m^{-1}) and 6,9 x 10^{-6} (m^{-1}).

Specific yield (S_y) is defined as the volume of water released from storage by an unconfined aquifer per unit surface area of aquifer per unit decline of the water table.

In **Table 18** Specific Yield representative values for different materials are reported (Morris & Johnson, 1967).

For Limestone S_y is equal to 14 %.

Porosity is defined as the void space of a rock or unconsolidated material:

$n = V_v/V_T$

where n is porosity [dimensionless], V_v is void volume [L^3] and V_T is total volume [L^3].

The **Table 19** shows representative porosity values for sedimentary rocks (Morris & Johnson, 1967).

For Limestone Porosity is included between 7 % and 56 %.

Hydrological balance

On the whole aquifer there are no wells, there was only one high altitude raingouge (Laceno, 1.170 m a.s.l.) that operated only for 7 years from January 1974 to December 1979. There are no temperature values and no soil employment maps.

This represented a huge problem for the hydrological balance, becouse is not possible to calculate the effective infiltration with a typical balance: P - ETR = R + IE (P: rainfall; ETR: evapotranspiration; R: runoff; IE: effective infiltration).

It is known that the aquifer is laterally and basally closed, the only important rising is represented by the Caposele spring, so it is possible to consider that the rain falling on the carbonatic portion of the aquifer it will leak in, so it represents the whole amount of hypothetical aquifer recharge.

To support this hypothesis, annual Caposele spring discharge and rain felt on the considered surface of the aquifer have been compared. As described in Par. 2.4.1, the

aquifer recharge area is about 109 km^2, this data is supported by Cervialto Mountain geological map and by Fiorillo & Guadagno, 2011.

In the **Table 20** is reported the annual rainfall on the whole aquifer, the total annual discharge at the Caposele spring, in the right column is reported the percentage of the discharge in spite of the rain (considered as aquifer recharge). Looking at the table values, it is possible to confirm that the rainfall and spring discharge orders of magnitude are comparable.

Interpolation of monthly data from 9 rain gouges has been used to create rainfall maps for each month with mean monthly data, and with real monthly data of the 1980 and 1981 years. Since the Laceno rain gouge did not work in 1980, has been compared the Montevergine rain gouge (1.287 m a.s.l.) data and Laceno to recreate hypothetical Laceno 1980 and 1981 data.

2.4.4 Numerical modeling

In further paragraphs are reported input data about the model domain, hydraulic parameters, solver parameters and model results. Is important to underline that the principal aim of the numerical modeling is not to forecast the future behavior of the Mt. Cervialto aquifer, but to use this instrument to understand the mechanisms involved in the aquifer structure with the earthquake occurrence.

The model simulation is performed in transient flow with monthly time-steps to simulate the recharge on the whole aquifer and discharge at the Caposele spring.

As there are no control points on the aquifer, the model hydraulic parameters are calibrated on the Caposele spring discharge amount. Observing the output data it has been possible to "calibrate" the Cervialto Mountain numerical model in the pre-seismic period, inserting input mean data from 1974 to 1979. Once the model was calibrated, it has been insert 1980 input data (recharge) to simulate pre-seismic aquifer behavior. The same model has been performed changing the aquifer input data (recharge) to simulate the hypothetical post-seismic aquifer conditions, and output data have been compared with Caposele spring discharge in the 1981 (post earthquake year).

2.4.4.1 Input

Model domain

Cervialto Mountain model domain was initially defined considering a square around Cervialto Mountain of about 15 km side. The area was divided in 100 x 100 cells, so each squared cell has 150 x 150 m side, the model is organized in one layer representing

carbonatic rocks. The grid orientation is 40° to the North because the lateral aquifer limits and principal faults of the area has appeninic and anti-appenninic direction, as shown on the faults rose diagram on **Figure 27**.

The layer top correspond to real topography (Campania Region DEM with 20 m cells), layer bottom correspond to the bottom of the carbonatic rocks and with the top of dolomitic portion of the massif, the layer bottom is obviously not certain because is supposed by geologic sections (**Figure 28**).

At a later stage the model active domain was limited to the area where the carbonatic rocks of the Cervialto massif outcrops.

Regarding to initial cells amount (10.000), after the active domain definition, active cells results 5.362, the thickness is variable, it goes from 1 m up to 1.400 m.

In some cases cells bottom have been modified of few meters to permit a lateral communication between cells, in particular it happened where topography has steep slopes.

Model boundaries are represented by *no flow* cells all around the Cervialto aquifer, and by *drain* boundary cells where Sanità di Caposele is located.

Hydraulic parameters

As described in Par. 2.4.3, the hydraulic parameters values insert in the model derive from bibliography range data. All parameters are distributed homogeneously on the aquifer. To choose the parameter values, is taken in count the aquifer carsic network not simulated in the aquifer system, but that generate a mean increase in the system permeability.

K_x, K_y, K_z = Hydraulic Conductivity respectively in x, y and z grid direction.

$K_x = K_y = 9{,}5 \times 10^{-3}$ m/sec

$K_z = 1 \times 10^{-5}$ m/sec

$S_s = 3{,}3 \times 10^{-6}$ (m^{-1})

S_y = 14 %

P = 25 %

Initial Head = 500 m

Boundaries

Imposed boundaries in the model are represented by recharge (RCH), no flow cells and Drain (DRN).

The first one is imposed vertically on the active cells. For each cell the recharge is monthly imposed, it is expressed in mm/yr, so the rain amount felt in a month in a specific area is multiplied for 12 month, as visualized in **Figure 31**.

The Drain boundary is imposed where the Caposele spring is located (**Figure 31**), from literature data is known that the spring lies at 420 m a.s.l., in the model drain top elevation is imposed 1 m below cell top, it goes from 445 to 408 m a.s.l, drain bottom elevation is represented by the drain cell bottom.

The drain conductance is a lumped coefficient describing the head loss between the drain and the groundwater system. This loss is caused by converging flow patterns near the drain, the presence of foreign material around the drain, channel bed materials, the drain wall, and the degree to which the drain pipe openings may be blocked by chemical precipitates, plant roots, etc. There is no general formulation for calculating drain conductance. In most situations, the detailed information required to calculate drain conductance is not available to the groundwater modeler. These details include the detailed head distribution around the drain, aquifer hydraulic conductivity near the drain, distribution of fill material, number and size of the drain pipe openings, the amount of clogging materials, and the hydraulic conductivity of clogging materials. It is common to calculate drain conductance from measured values of flow rate and head difference. Drain Conductance value is usually adjusted during model calibration.

Drain conductance imposed at each drain cell is 2000 m^2/day.

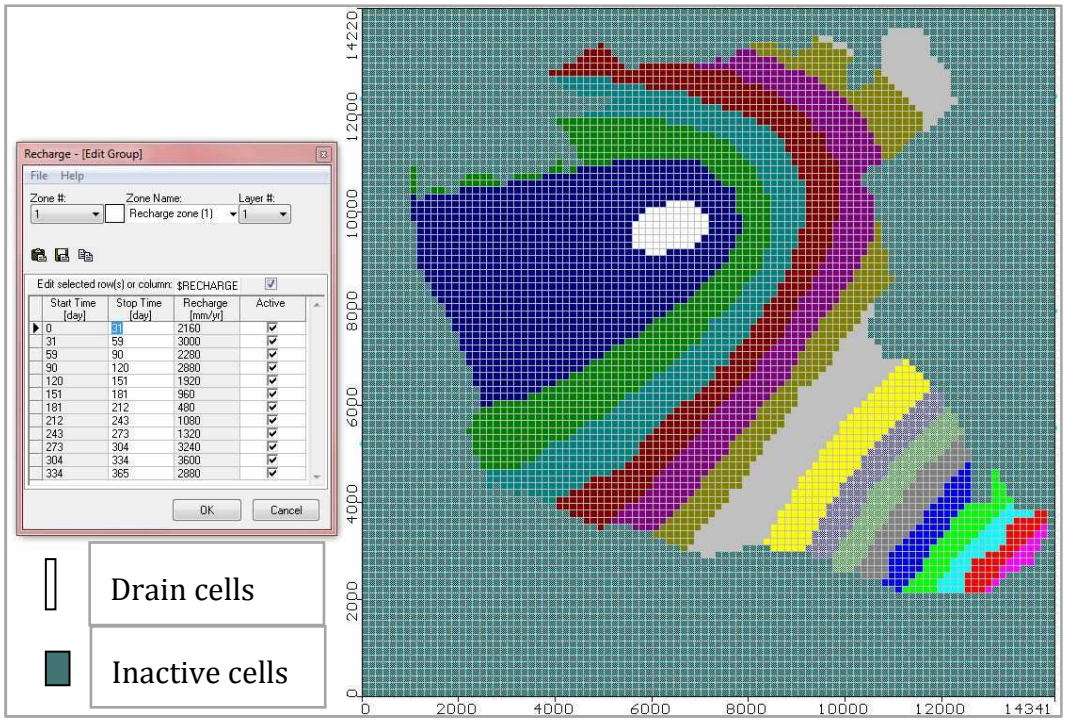

Figure 31: Model domain with different recharge areas, in the tool box on the left there is an example of input recharge data for the zone 1 (white area).

Solver parameters

For Cervialto numerical model is employed PCG Package, that uses the preconditioned conjugate-gradient method to solve the simultaneous equations produced by the model.

The Solver is set as follows:

Maximum outer iterations = 800

Maximum inner iterations = 100

Head change criterion = 0,1

Residual criterion = 0,1

Damp factor = 1

Printout interval = 10

The considered time steps are 12, one for month as reported in **Table 21**.

Calibration

As said before, unfortunately there are no control point on the whole aquifer, with the exception of the Caposele spring discharge data. So the unique calibration parameter is the Caposele spring discharge.

Comparing water amount rising from Caposele spring and water passes trough drain cells the model has been calibrated.

The calibrated parameters are K (hydraulic conductivity), Ss (Specific Storage) and Drain Conduttance.

As considered in Par. 2.4.3 initial input parameters was data coming from literature taking in account the probable existence of a carsic network, the entire accepted range value for every parameter has been tested, the final calibrated values is reported in Par. 2.4.4.1.

Resulting from calibration iterative tests is possible to assert that the Cervialto Mountain aquifer model is very sensitive to K_x, K_y and Drain Conduttance value variations.

Input data reported in Par. 2.4.4.1 are the same for pre-seismic and post-seismic simulations, because changing hydraulic properties generate output not fitting with real data.

2.4.4.2 Output

In **Figure 32**, **Figure 34** and **Figure 36** the mass balance graphs are reported respectively for model simulation of mean pre-seismic year, 1980 (pre-seismic) and 1981 (post-seismic). In **Figure 33**, **Figure 35** and **Figure 37** the output flow map are reported for the

three simulations earlier quoted. Looking at the presence and at the shape of the dry cells, is possible to consider that the geologic structures of the aquifer strongly influence the groundwater circulation, effectively the wet cells follow precisely the graben, located in the middle of the aquifer characterized by a huge thickness of the calcareous portion of the Cervialto Mountain aquifer.

In **Table 22** are reported the comparison between simulated and observed discharge data, for the three performed simulations.

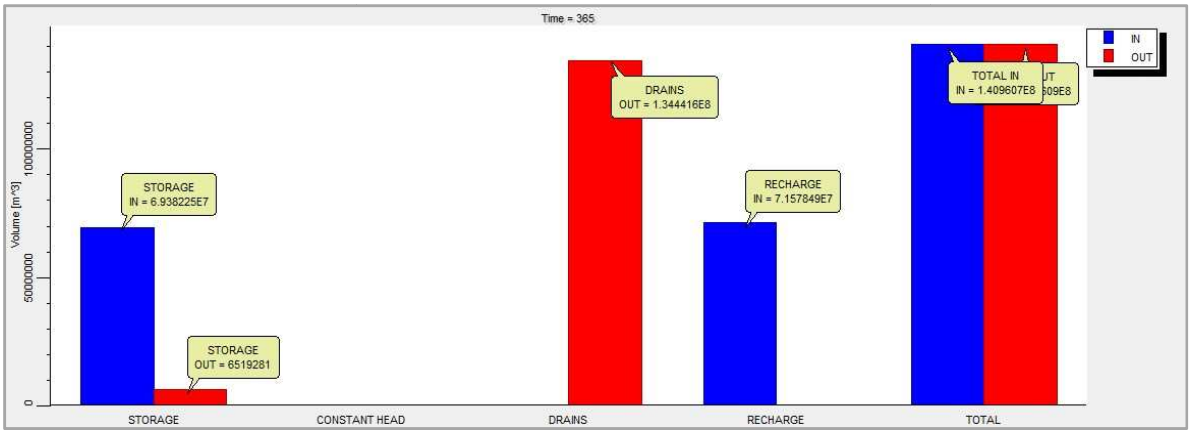

Figure 32: Output graph representing output data at 12 time step (365° day) for the simulation of the mean year.

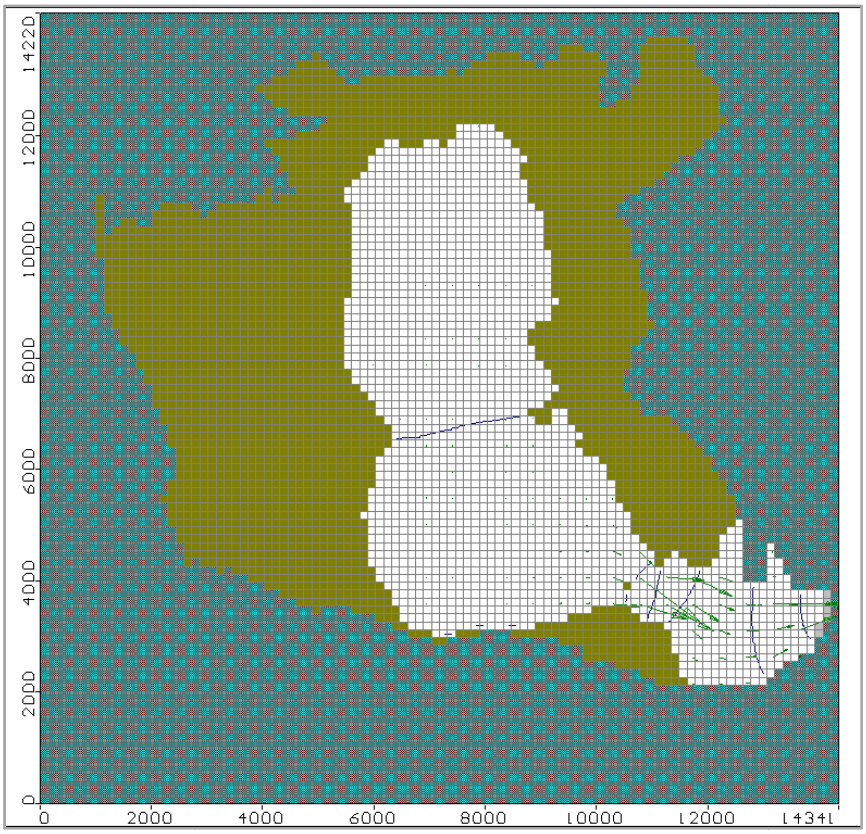

Figure 33: Output model map representing the simulation of the mean year. Green cells are dry cells, white cells are wet cells, grey cells represent the DRAIN (Caposele spring); the arrows represent the groundwater flow direction.

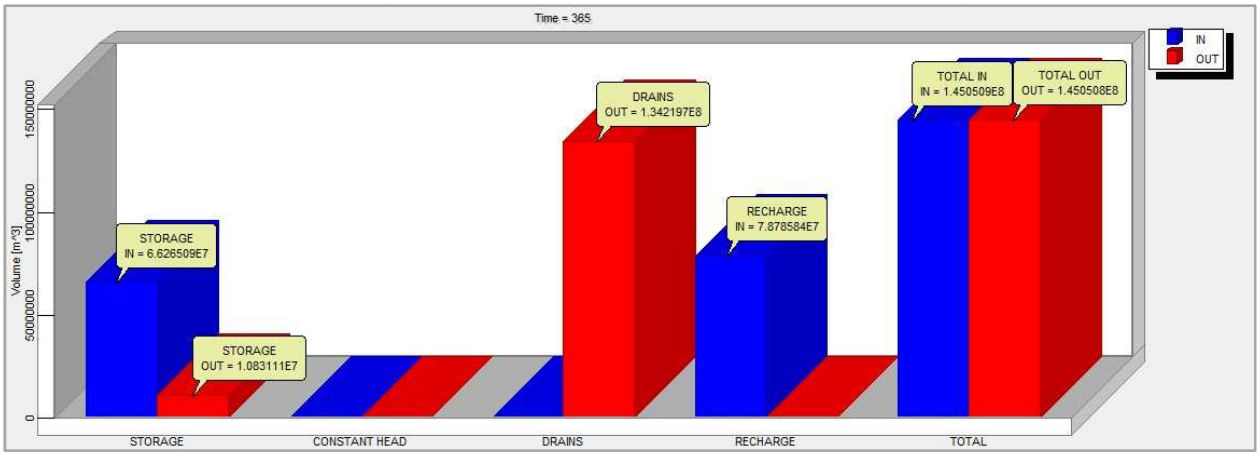

Figure 34: Output graph representing output data at 12 time step (365° day) for the simulation of the 1980, pre-earthquake year.

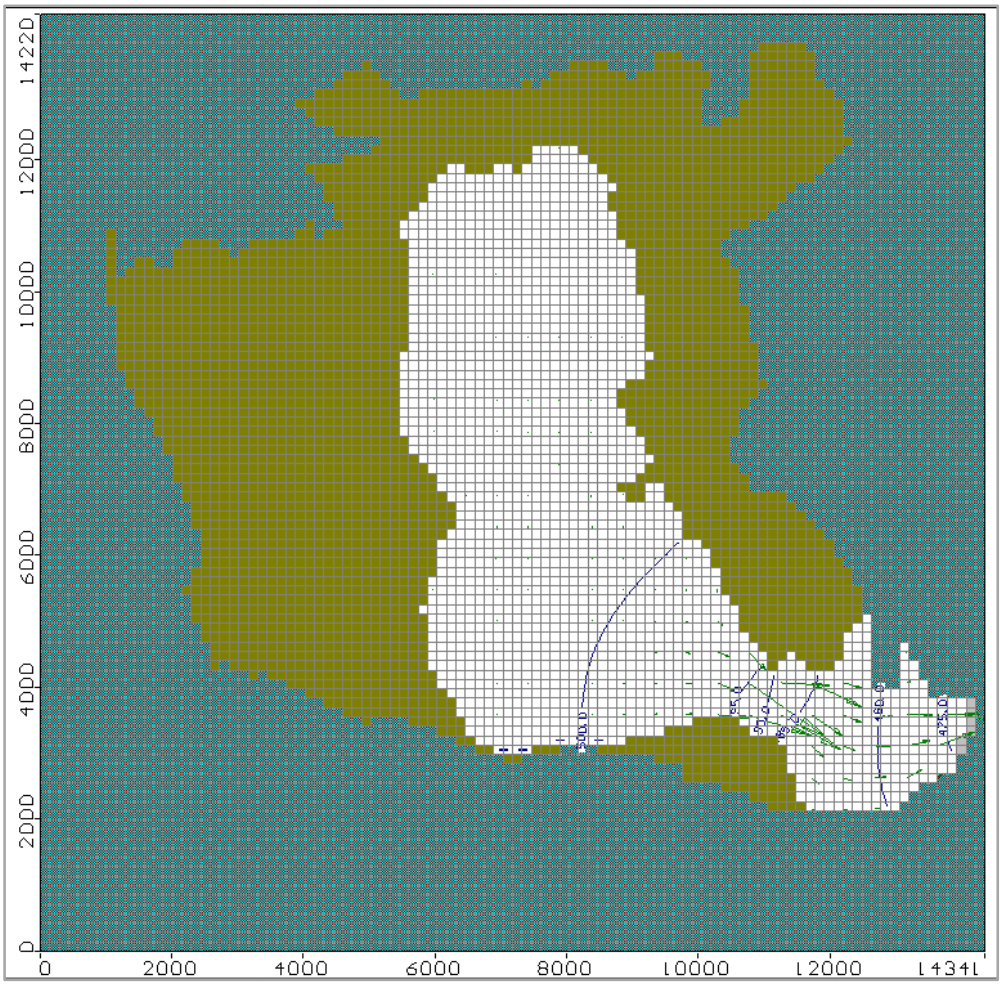

Figure 35: Output model map representing for the simulation of the 1980, pre-earthquake year. Green cells are dry cells, white cells are wet cells, grey cells represent the DRAIN (Caposele spring); the arrows represent the groundwater flow direction.

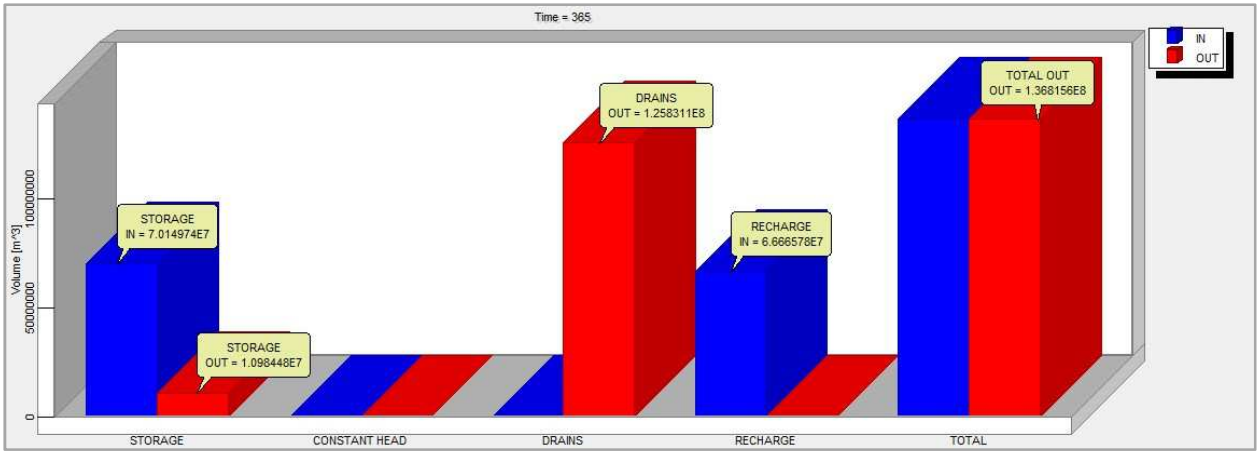

Figure 36: Output graph representing output data at 12 time step (365° day) for the simulation of the 1981, post-earthquake year.

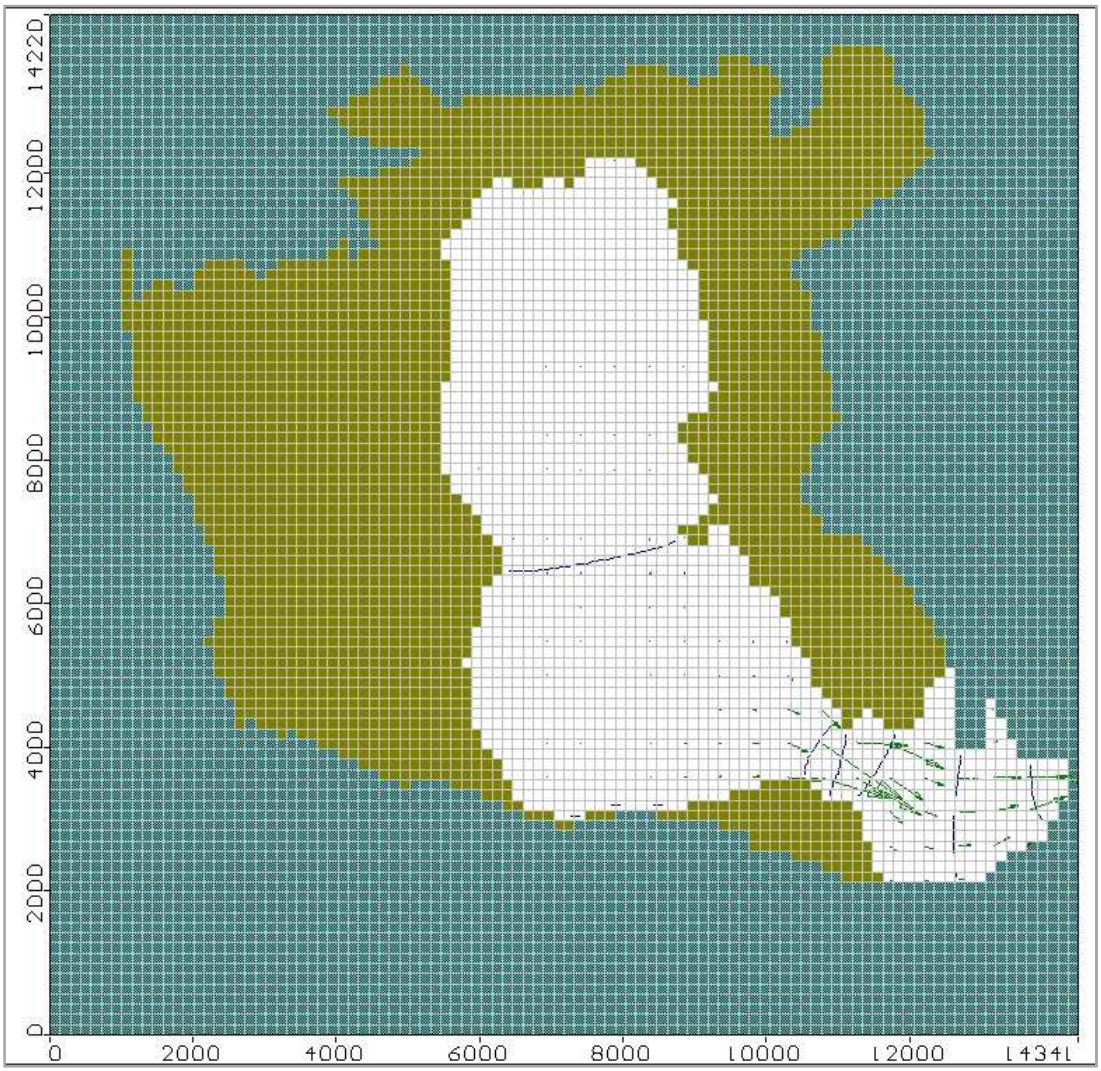

Figure 37: Output model map representing for the simulation of the 1981, post-earthquake year. Green cells are dry cells, white cells are wet cells, grey cells represent the DRAIN (Caposele spring); the arrows represent the groundwater flow direction.

2.5 Discussions and conclusions

The graph in **Figure 25** shows how the mean α values diminish after the occurrence of the Irpinia earthquake. It is widely known that this constant is aquifer hydraulic characteristic correlated. So it is possible to suppose that the occurrence of the earthquake generated some hydraulic variations in the aquifer structure (hydraulic characteristic), caused by the seismogenic fault dislocation (static stress) and/or by the seismic waves passage (dynamic strain).

Strong of this hypothesis, a numerical model has been done to simulate the aquifer behavior in pre- and post-seismic periods, with the intent to understand better the mechanisms involved in the discharge anomalies, but without the claim of build a tool for water resources management to predict the future Caposele discharge.

The pre-seismic period model simulation converge with the observed data of the Caposele spring discharge, while the post-seismic period model simulation doesn't correspond well with observed discharge Caposele spring data, in **Table 22** observed and simulated value are reported.

Several attempts has been performed to get close to observed data, the first hypothesis was to change hydraulic properties, but it was not sufficient.

A numerical modeling limit is that the water flow total amount depends directly on recharge input, the hydraulic properties make the difference on the water flow rate at the spring. In pre-seismic period, both on the mean values that on 1980 values, seems that the discharge flow amount correspond to the recharge amount (rainfall on the carbonatic portion of the aquifer). In the post-seismic period results undeniable that the rainfall is not the only source of the Caposele spring discharge flow, especially the 1981.

Three hypothetic scenarios could be involved to explain discharge increase at the Caposele spring:

1. geometrical variation of the aquifer,
2. "sponge effect" with permanent changes in the aquifer characteristics,
3. "sponge effect" with no permanent changes in the aquifer characteristics.

Hypothesis number 1 is abandoned because there were no field evidences on the aquifer limits, for example no new springs appeared after the earthquake.

Hypothesis number 2 and 3 are considered achievable, but at the moment is difficult to simulate the effect by numerical modeling. Based on the α value variation after the earthquake occurrence, the hypothesis 1 is more substantiated. In future it will be possible to implement new numerical models to validate this hypothesis with more data.

The “sponge effect” hypothesis involves a rapid expulsion of fluid from the aquifer reservoir just after the earthquake occurrence, caused by the crack closing in consequence of the seismogenic fault dislocation (change in static stress) and by the fracture cleaning with the passage of the seismic waves (dynamic strain). This explanation is supported by Muir-Wood and King (1993).

Effectively the 4 hydrologic post-seismic years show a discharge decrease, is like if the aquifer needed years to recover the water lost with the “sponge effect” due to the seismic waves transit.

By a numerical modeling point of view, is very difficult to simulate this effect, it means to imply the involvement of an increase in spring discharge equal hydrological balance. In effect it seems that the discharge increase at Caposele spring after the earthquake is due to a release of water lying under the threshold permeability level of the spring. This hypothesis could validate the rapid increase in discharge just after the Irpinia earthquake and the mean discharge value decrease for the four hydrological years after. The recharge (infiltration by rainfall) use time to refill all the voids of the aquifer portion lying under the threshold permeability level.

The model results underline the difficulty of hydrological effects due to earthquakes simulation, especially on a wide aquifer with no control point as the Cervialto Mountain. It doesn’t have the intent of simulate the aquifer behavior to predict the Caposele spring discharge, but represents a medium to suppose that the recharge (rainfall) doesn’t justify the increase in discharge observed after the earthquake occurrence.

The evidence of the α values general decrease after the Irpinia earthquake occurrence allow us to hypothesize an hydrologic characteristic change after the earthquake, it was not possible to simulate this variations but the α data are more robust than simulation data to build a conceptual model.

In

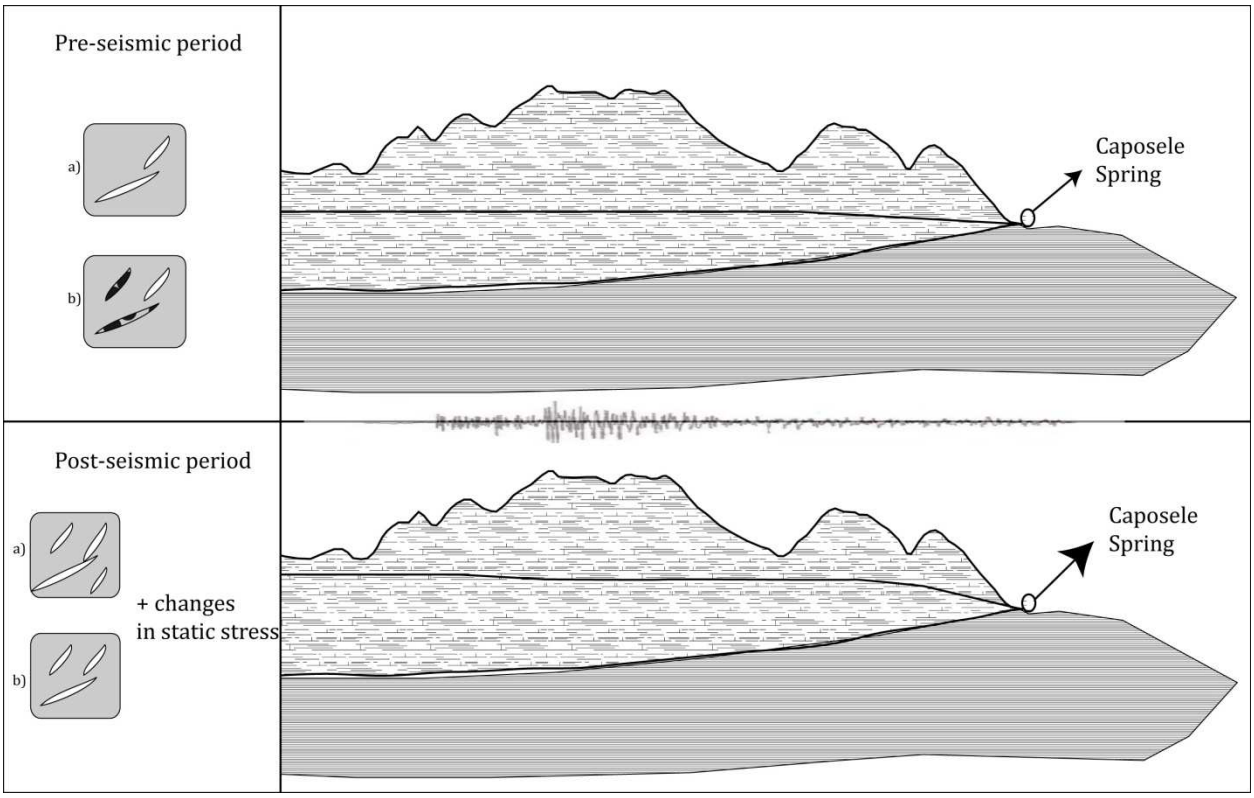

Figure 38 the conceptual model of the hydraulic variations hypothesis is shown.

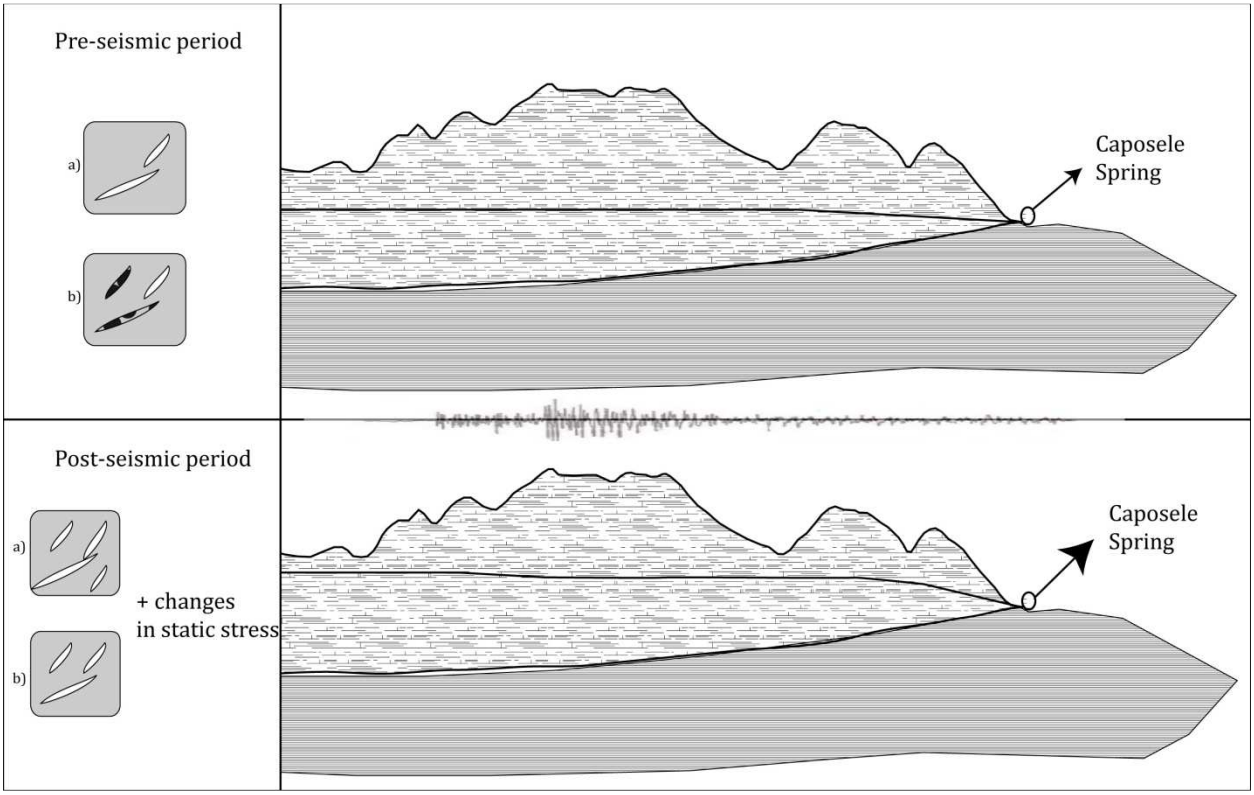

Figure 38: Conceptual model of Cervialto aquifer variations.

3 CASE STUDY 2: INTERMEDIATE FIELD HYDROGEOLOGIC RESPONSE TO L'AQUILA EARTHQUAKE 6TH APRIL 2009 (MW 6.3)

3.1 Central Appennine geological setting

The Apennine chain is a Neogene E-verging thrust system which involved pre-orogenic Triassic-to-Miocene carbonate platform, slope and basin paleogeographic domains and synorogenic Miocene siliciclastic turbidites of orogen foredeep (e.g DArgenio & Alvarez, 1980, Oldow et al., 1993, Argnani & Ricci Lucchi, 2001; Patacca & Scandone, 2007).

In the central Apennines (**Figure 39**), thrusting affected the western calcareous ridges (Lepini–Ausoni–Aurunci Mts.) during late Tortonian–early Messinian times, the Simbruini Mts. and Marsica area during Messinian–early Pliocene, and finally the Maiella Mt. and Adriatic foothills during middle–late Pliocene (Speranza et al. 2003 and references therein). The Gran Sasso arc underwent both late Messinian and early–middle Pliocene shortening episodes (Speranza et al., 2003 and reference therein).

Since the Quaternary, the Central Apennines has been deforming by active extensional tectonics following the eastward migration of the Apenninic compressional front (e.g. Malinverno & Ryan, 1986, Cavinato & De Cellis, 1999). A broad and complex pattern of normal faults is the result of superposition of extensional systems in areas previously affected by compression (Roberts & Michetti, 2004; Galadini & P. Galli, 2000 and references therein).

The extension affected first the western ridges during late Messinian–early Pliocene times, subsequently migrated eastward, and is still active today in the central–eastern belt sector (D'Agostino et al., 1998)

Currently, the NE-SW extensional processes are mainly focused along the axis of the chain, as shown by the global positioning system velocities that do not exceed 3 mm/yr in the L'Aquila Apennines (Giaccio et al., 2012 and reference therein). Here, the active faults are arranged in systems that generally do not exceed 30 km in lengths. According to previous paleo-seismological studies, for Mw >6.5 earthquakes, these active faults are generally characterised by recurrence times of 1-2 ka (Giaccio et al., 2012 and reference therein), or even less (P. Galli & Naso, 2009; Galli et al., 2011).

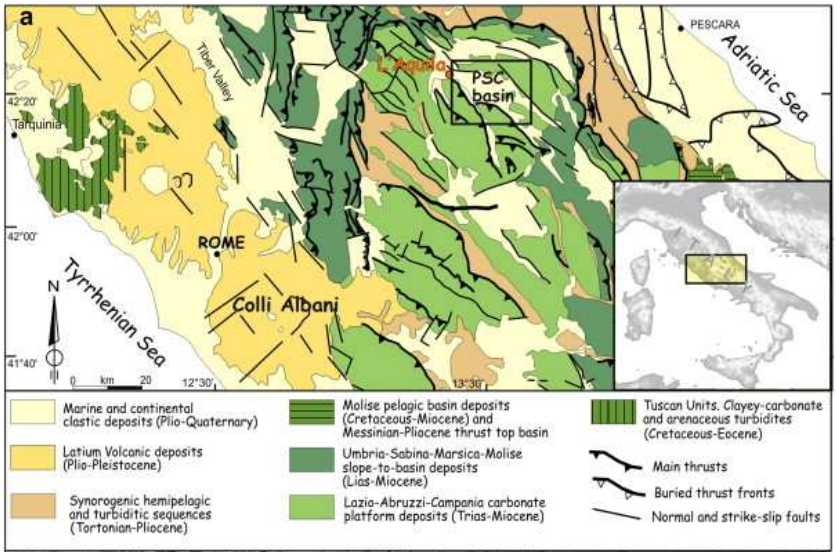

Figure 39: from Giaccio et al., 2012,Geological–structural sketch of the central Apennine (a).

3.2 Earthquake kinematics

Central Apennines suffered several of the strongest historical earthquakes in Italy. Earthquake catalogs (e.g. http://emidius.mi.ingv.it/CPTI08/) show the persistent occurrence of destructive earthquakes in this area: 9 September 1349 (MW 6.5), 26 November 1461 (MW 6.5), 2 February 1703 (MW 6.7), 6 October 1762 (MW 6.0).

A M_W 6.3 earthquake struck on April 6, 2009 the Abruzzi region (central Italy) producing vast damage in the L'Aquila town and surroundings villages of the Abruzzi region, causing 300 deaths and leaving sixty thousand homeless.

Large earthquakes originate mainly on a narrow belt along the central Apennines, accommodating a NE-trending extension, with a rate of about 3 mm/yr, progressively thinning the Apennines thrust and fold belt. The normal fault system is elongated NW–SE and composed of adjacent, west-dipping, and echelon fault segments. The extension in this region is accommodated by two sub-parallel sets of faults, the eastern and western normal fault systems which include several Quaternary normal faults with clear signature at the surface and paleoseismological evidence of Holocene surface faulting earthquakes. The deep geometry of most of these faults is poorly constrained by sub-surface data.

Chiarabba et al., 2009 used data from the INGV national and regional permanent networks and some of the temporary seismic networks to define the space-time evolution of the seismicity, providing accurate earthquake locations and the geometry of faults that accommodate the extension in this portion of the Apennines.

Anzidei et al., 2009 used data of five GPS stations (CADO, ROIO, SELL, CPAG, SMAR) and estimate with high accuracy the near field displacements of the seismogenic fault.

Pondrelli et al., 2010 computed seismic moment tensors for 26 events with M_w between 3.9 and 6.3 belonging to the 2009 L'Aquila (Central Italy) seismic sequence. It gave immediately the indication that this seismicity, from the seismotectonic point of view, is similar to previous extensional activity occurred along this mountain belt, also in the vertical distribution of hypocenters and deformation styles. NW–SE striking focal planes agree with mapped faults of the region, allowing to infer which tectonic structures have been activated.

All Authors agree that the main event has a pure normal faulting mechanism (www.bo.ingv.it/RCMT). Its location, obtained integrating arrival times at all the available permanent seismic stations including the accelerometric network managed by the Dipartimento di Protezione Civile (DPC) is at 9.5 km depth and at distance of about 2 kilometers from L'Aquila town center.

The extent of aftershocks near the surface coincides with an active fault recognized in the field that has a poorly constrained geometry, lateral continuity and doubtful seismogenic role (the Paganica fault). This poorly known fault is located close to other larger Quaternary faults previously considered to be the main seismogenic sources of the region. Most of the aftershocks occur on the main fault plane around three patches that accounted for the largest slip during the main shock (Chiarabba et al., 2009).

The aftershock data clearly show the location and geometry of the fault ruptured by the L'Aquila earthquake. The rupture developed on a planar, 45° SW-dipping fault evident from 10 to 2 km depth. The seismicity cutoff at 2 km depth suggests that the upper portion of the fault did not slip much. In the southern portion of the fault, the seismicity distribution is cloudy, suggesting a change in the fault plane orientation along strike or, more likely, the transition to a more distributed deformation on several small faults (**Figure 40**).

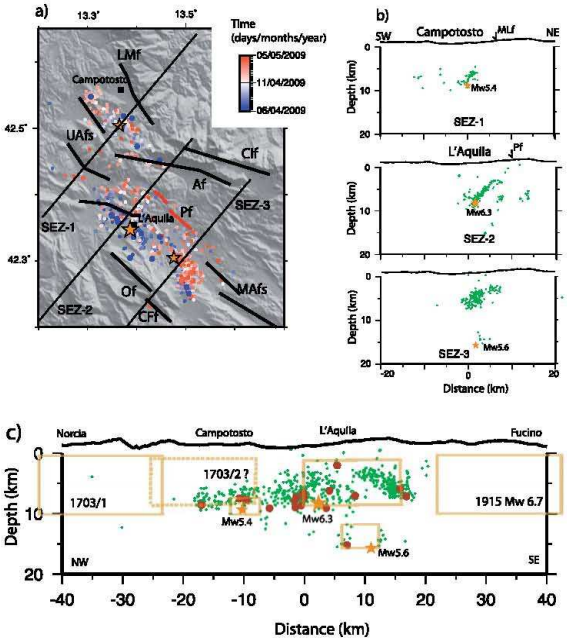

Figure 40: from Chiarabba et al. (2009)(a) Map of the 712 relocated events, with a color code indicating time after the main event. The dashed lines are the traces of vertical sections shown in Figure 2, and the solid lines are the mapped Quaternary faults [Barchi et al., 2000]: (LMf, Laga Mts. fault; UAfs, Upper Aterno fault system; Af, Assergi fault; CIf, Campo Imperatore fault; MAfs, Middle Aterno valley fault system; OPf, Ovindoli Pezza fault; CFf, Campo Felice fault; Of, Ocre fault; Pf, Paganica fault). The box is a projection of the ruptured main fault. (b) Vertical sections across the Laga Mts. fault (SEZ-1) and the Paganica fault (SEZ-2, and SEZ-3). The fault geometry is consistently defined by the largest aftershocks. (c) Vertical section along the fault system, showing the geometry of the ruptured faults. Red dots are the ML ≤ 4.0 earthquakes. The 1703 and the 1915 earthquakes occurred at the north and southern border of the Paganica fault.

The aftershock data suggest a size of about 10 x 6 km^2 for the main ruptured patch, whereas the second shallower patch is smaller, about 5 x 5 km^2. The third patch is smaller and located northward of the first two(Gerald P Roberts et al., 2010) (**Figure 40**).

In the study of (Anzidei et al., 2009) the deployment of five GPS stations (CADO, ROIO, SELL, CPAG, SMAR) before the L'Aquila earthquake of April 6, 2009 allow them to estimate with high accuracy the near field displacements. The maximum horizontal and vertical coseismic offsets (10.39 ± 0.45 cm and _15.64 ± 1.55 cm, respectively) are both recorded at CADO. Significant permanent deformations are detected within a radius of 60 km, covering a wide sector of central Italy, in agreement with the well-known long term extensional tectonic style across the central Apennines. The modeled source geometry is typical of the Apennine chain normal faults (i.e., NW striking and 40°–50° dipping).

3.2.1 Documented hydrogeological response to seismic event

The consequences of seismicity on aquifers are usually related to post-mainshock situations such as the possible permanent aquifer deformation (Manga and Wang, 2007). Fracture-dominated aquifers often show different velocities and flowpaths of groundwater. For example, a fast flow rate occurs through main discontinuities and karst features, while

a lower velocity flow rate occurs by seepage in fracture networks (Emblanch et al., 2003; Adinolfi Falcone et al., 2008). This dual-flow system, peculiar to karst aquifers like the Gran Sasso carbonate aquifer, can cause non-standard aquifer responses to earthquakes (Amoruso et al., 2010, Adinolfi Falcone et al., 2012).

The Gran Sasso **Figure 41** represents one of the most important aquifer of Central-Southern Apennines. The thick carbonate sequences of Gran Sasso aquifer are imbricated eastward onto Neogene flysch deposits and dislocated by recent normal NW–SE fault systems. These carbonate structures, which, due to fractures and karst are highly permeable, are bound by low permeability deposits (Boni et al., 1986 and Salvati, 2002). Only a small portion of the infiltrating water recharges small springs located at high altitudes, while the majority recharges the regional aquifer, feeding moderate springs at relatively high altitudes (800–1300 m a.s.l.) and large basal springs, located at low-altitudes (200–500 m a.s.l.) at the border of the carbonate ridges (Barbieri et al., 2005 and Boni et al., 1986). The Gran Sasso aquifer feds also two large flow rate water discharges at high elevation (960 m a.s.l.), which are the water drainage of the Gran Sasso motorway tunnel.

The seismic event observed on 6 April 2009 in the Gran Sasso carbonate fractured aquifer produced changes in the groundwater flow system that had different short and mid-term effects on the recharge and discharge areas. These effects were observed through spring discharge and groundwater-level monitoring in wells (Amoruso et al., 2010) and changes in water chemistry (Adinolfi Falcone et al., 2012).

An increase in spring discharge (quick increase) and water table levels (progressive rise) with respect to historical recording made prior to the main-shock were universally recorded, especially at the boundaries of the aquifer. The water table changes along the constant head boundaries cannot be attributed to seasonal recharges. Only locally along the Paganica Fault was an immediate decline in discharge and water table directly observed (Tempera springs) by Amoruso et al., 2010.

Adinolfi Falcone et al.(2012) substain that close to the PF, at the Tempera group springs the seismically-induced rising up of deep crustal fluids, including ^{222}Rn and CO_2 along seismic faults, makes groundwater more reactive. The coseismic phase caused a discharge and a mineralization increase, attributable to the elasto-static pore pressure and to the deep fluids upwelling; this pore pressure, coupled with a general SI undersaturation and a lowering of pH of groundwater, was quickly widespread into the whole aquifer, both in recharge area and, during the early post-seismic period (September2009), in the peripheral discharge zones too.

Short-term responses were attributed to pore pressure coseismic changes related to aquifer deformation. Mid-term responses cannot be due to the same process.

Observed hydrogeological data suggest that a variation in groundwater aquifer bulk hydraulic properties occurred in the portion of the aquifer near the Paganica Fault activated by the main-shock. A possible local and transient increase of bulk hydraulic conductivities in the recharge area was supposed by (Amoruso et al., 2010), supported by hydraulic head decrease in the core aquifer, to explain the observed water table elevation and discharge increases along the boundaries of the aquifer in the discharge areas.

Amoruso et al., 2010 exclude the contribution of seasonal recharge, the short-term hydrologic effects registered immediately after the mainshock are determined to have been caused by a pore pressure increase related to aquifer deformation. Mid-term effects observed in the months following the mainshock suggest that there was a change in groundwater hydrodynamics. Supplementary groundwater that flows towards aquifer boundaries and springs in discharge areas reflects a possible increase in hydraulic conductivity in the recharge area, nearby the earthquake fault zone (**Figure 42)**.

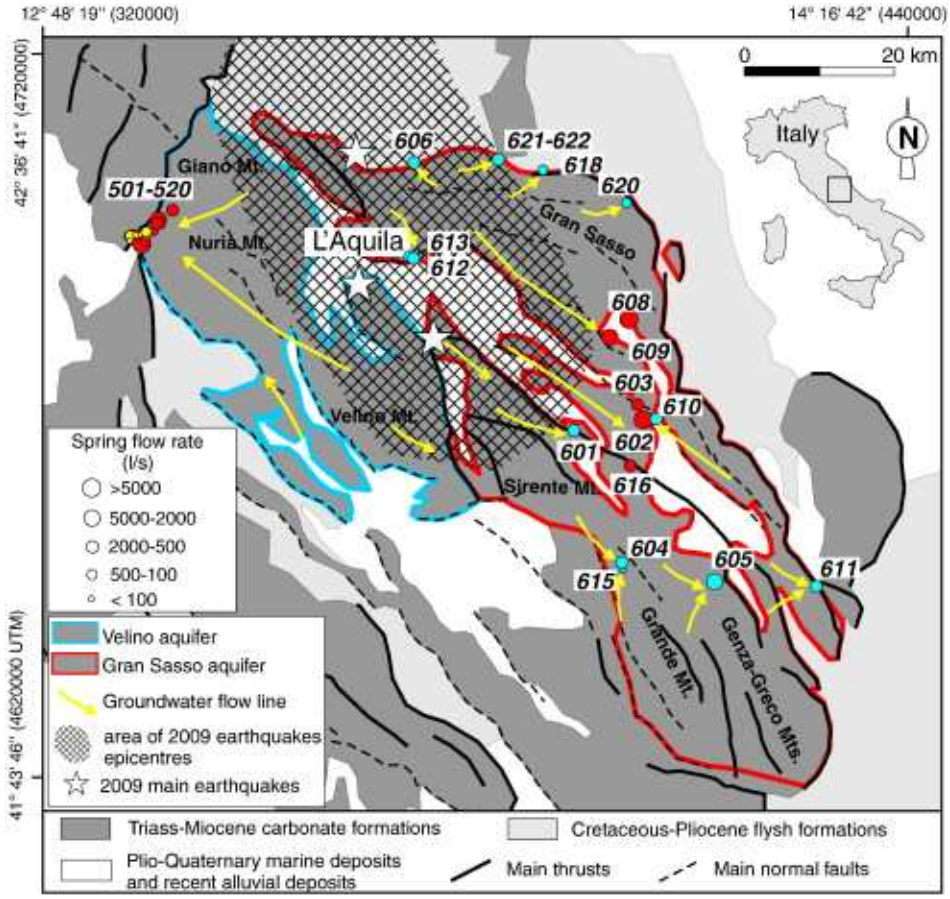

Figure 41: from Chiodini et al. (2011) Schematic geological map with the location of the Gran Sasso aquifer (red line) and the Abruzzo earthquakes (ISIDE, 2009).

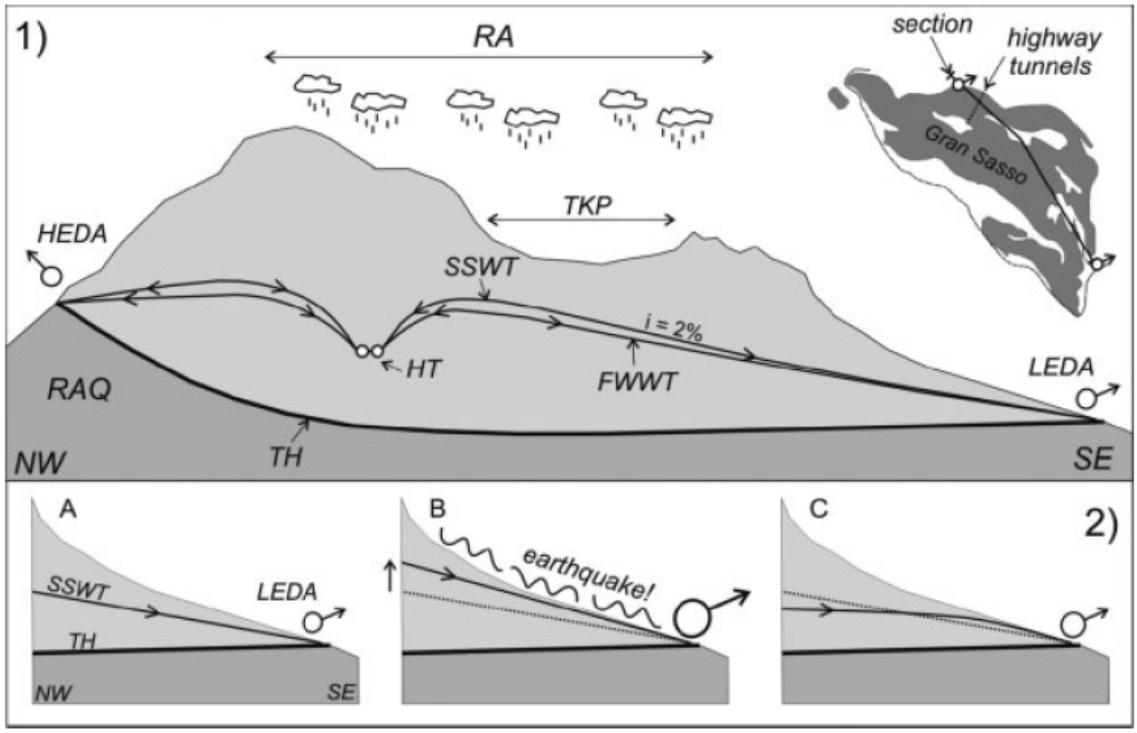

Figure 42: from Amorus et al. (2010) (1) Conceptual scheme of groundwater changes caused by the L'Aquila earthquake; RAQ—regional aquiclude; TH—permeability boundary (main regional thrust); HT—highway tunnels (950–1000 m asl); RA—high-elevation recharge area (2700–1500 m asl); TKP—high-elevation tectono-karstic plain (preferential recharge area); HEDA—high-elevation discharge area (750–1600 m asl); LEDA—low-elevation discharge area (270–350 m asl); SSWT—spring–summer water table (groundwater recharge period); FWWT—Fall–winter water table (groundwater exhaustion period). (2) Conceptual sketch of groundwater changes caused by the L'Aquila earthquake in the main discharge area (LEDA). A—Situation before the mainshock; B—short-term response after the mainshock. Pore pressure causes the water table to raise with instantaneous spring discharge increases relative to the pre-mainshock state (dotted line); and C—mid-term response associated with a change in the bulk hydraulic conductivity of the recharge area. This causes spring discharge increases with respect to those of the pre-mainshock period (dotted line)

3.3 Hydrogeological setting of the Acque Albule aquifer

The Acque Albule Basin (AAB) plain is located over a subsiding basin in the Latium region (central Italy) that is close to the northeastern suburbs of the city of Rome. The plain is tilted southward and is bounded by the Apennine chain (Cornicolani and Lucretili Mountains) on the north and east sides, the Colli Albani volcano complex on the south side and low hills on the west side. The Aniene River, which is a tributary of the Tiber River, flows across the southern portion of the plain to in a southwest direction (**Figure 43**).

The geology of the AAB is strongly influenced by subsidence, due to strike-slip fault activity (Faccenna et al.,1994). The Mesozoic subsided carbonate bedrock, which outcrops in the Cornicolani and Lucretili Mountains, composes the bottom of a pull-apart basin that is filled with very thick marine and continental Pliocene sandy-clayey and gravelly deposits. Since the development of the north-south strike-slip fault system occurred approximately 115.000 years ago and during the late activity of the Colli Albani Volcano, intense

hydrothermal activity produced travertine deposits that are up to 80 m thick (Faccenna et al., 1994; Faccenna et al., 2008). The Regina and Colonnelle hydrothermal springs (approximately 2000 l/s; Capelli et al., 1987) and several minor sources (approximately 300 l/s, La Vigna, 2009) that are distributed throughout the plain provide evidence of current hydrothermal activity.

Travertine outcrops extensively throughout the plain, and it overlies Pliocene marine deposits and volcanic units.

From a hydrogeological viewpoint, the AAB is characterised by the following three main units (**Figure 44**):

1) Mesozoic carbonate bedrock,
2) Pliocene clayey marine deposits,
3) Pleistocene travertine plate (maximum thickness of 80-90 m) that is hydrogeologically associated with the volcanic units, the Holocene alluvial sediments, the ancient debris and the upper gravelly and sandy facies of the Pliocene deposits.

In the AAB, the fractured carbonate bedrock constitutes a leaky confined aquifer, while an unconfined aquifer is characterised by fractured travertine and associated porous sediments.

Pliocene deposits (clayey facies) may be considered to be non-continuous aquiclude. The two aquifers are thought to be connected in the centre of the plain, where deep hydrothermal water (its thermalisation and mineralisation is caused by the upwelling of endogenous fluids) that originates from the limestone bedrock flows through the Pliocene deposits into the travertine and mixes with the shallow aquifer (La Vigna, 2009). Regional faults contribute to the local vertical permeability and expand in the aquiclude, which facilitates hydrothermal upwelling and subsidence of the AAB plain.

The contribution to the shallow aquifer recharge that occurs due to the lateral transfer of water from outcropping limestones seems to be fairly small, which has been shown in recent studies (La Vigna, 2009). As a result, the main recharge of the plain must come from the bottom via the upwelling of the deep-water carbonate circulation. The general recharge system (Capelli et al., 1987) shows that the hydrogeology of the plain is sensitive to rainfall in the recharge area of the Cornicolani and Lucretili Mountains. In the Cornicolani Mountains, the level of the “Pozzo del Merro” (PdM), Karst Lake, is commonly considered to be the local expression of the top of the saturated zone of the carbonate system (Caramanna, 2001; Caramanna & Gary, 2004).

The piezometric map of the AAB (**Figure 43**) shows the general discharge of the groundwater into the Aniene River. The natural groundwater flow appears to be

substantially perturbed by the large dewatering depression that is induced by activity in the travertine quarries in the centre of the plain. Superficial extensions of the depression cone follow the main quarry distribution to the north.

In agreement with the main hydrothermal springs of the Colonnelle and Regina Lakes, the water table reaches up to 60 m a.s.l., which is higher than its surroundings, due to the concentrated vertical upwelling of deep groundwater flow, which generates a local gradient increase. The water table pattern shows that groundwater flows up towards the lakes, and it principally flows to the south and east. The groundwater flow is attracted by the depression, which induces lateral recharge from the Aniene River.

Major ion chemistry data show that groundwater stratification in the travertine aquifer is associated with mixing of the shallow groundwater with mineralised fluids discharges from the deep aquifer (Carucci et al., 2010). The groundwater hydrochemistry in the Tivoli Plain and adjacent recharge areas is characterised by a mixing of the three following end-members:

1) Ca – HCO_3-type groundwater of the recharge area: TDS (0-0.8 g L^{-1}), SO_4 (0-250 mg L^{-1}), DIC (0-7 mmol kg^{-1}) and EC (0-2 mS cm^{-1}).
2) Ca – HCO_3–SO_4-type groundwater of the shallow travertine aquifer (Acque Albule Basin): TDS (0.8-2.4 g L^{-1}), SO_4 (250-800 mg L^{-1}), DIC (7-16 mmol kg^{-1}) and EC (2-3.5 mS cm^{-1}).
3) Ca-Mg – HCO_3-SO^4-type groundwater of deep carbonate aquifer: TDS (2.4-3.6 g L^{-1}), SO_4 (800-1200 mg L^{-1}), DIC (16-18 mmol kg^{-1}) and EC (3.5-4.5 mS cm^{-1}).

3.4 Available data and methods

3.4.1 Data and Methods

To understand the intermediate-field hydrogeological response to the L'Aquila earthquake, data from the quarry-monitoring network in the AAB have been analyzed (**Figure 43** and **Figure 44**).

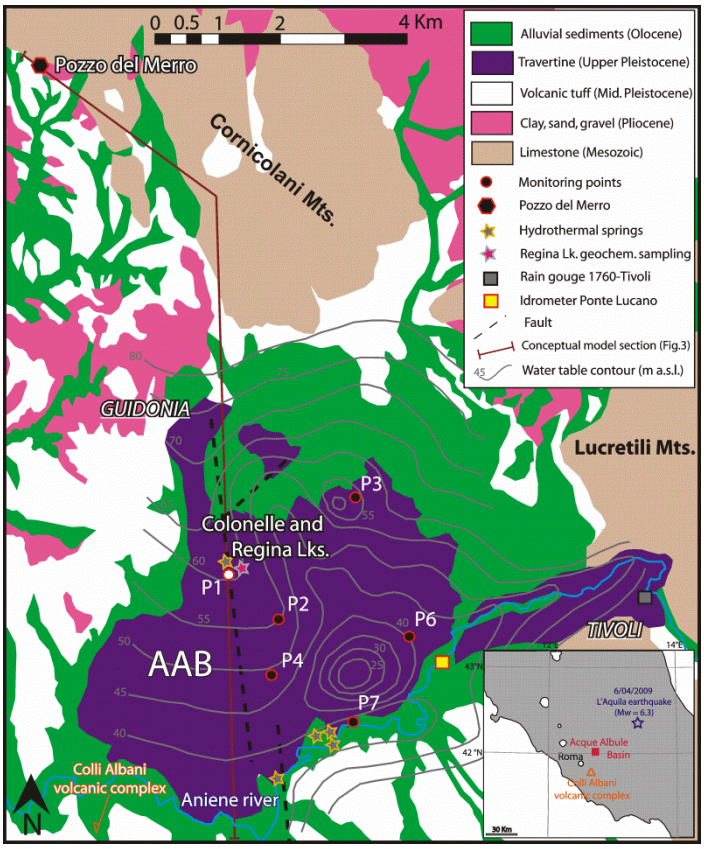

Figure 43: Simplified geological and hydrogeological map of the Acque Albule basin. The legend describes the symbols that are used in the map, and a map shows the location of the basin with respect to the L'Aquila earthquake epicenter.

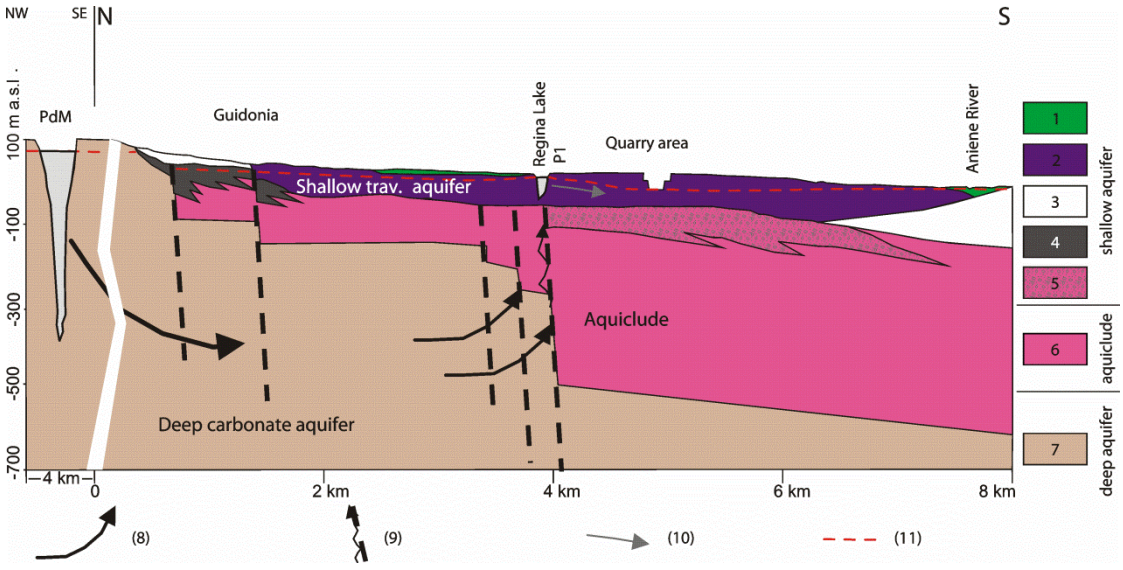

Figure 44: Hydrogeological conceptual model of the Acque Albule basin. The first NW-SE segment is not presented to scale. 1 – alluvial and recent deposits, 2 – travertine (Pleistocene), 3 – volcanic deposits (Pleistocene), 4 – ancient debris (Pleistocene), 5 – gravel facies of Pliocene deposits, 6 – marine clay (Pliocene), 7 – limestone (Mesozoic), 8 – flow path lines in the deep carbonate aquifer, 9 – high-permeability zone of the aquiclude, 10 – flow path lines in the shallow travertine aquifer and 11 – water table.

A monitoring network containing six piezometric dataloggers (P1, P2, P3, P4, P6 and P7, which were installed in 2006) records the shallow groundwater levels and temperatures on an hourly schedule, and the accuracies are approximately 1 cm and 0.1°C, respectively (La Vigna et al., 2007). The monitoring points are distributed within the AAB; P1 is located in the N-W sector near the Regina and Colonnelle Lakes' hydrothermal springs, and P7 is located near the Aniene River and is close to other minor hydrothermal springs. **Figure 45** shows the groundwater levels from February to June 2009, which allows for the analysis of changes during the earthquake event.

Hydrometric data regarding the groundwater levels in the Aniene River and PdM were recorded to clarify the general behaviour of the shallow travertine aquifer during the selected period in comparison with the daily rainfall. Because the quarry dewatering has been active for at least twenty years, it can be considered as a constant anthropic external stress in this system. The monitoring network of the Hydrographic Survey of the Latium Region (http://www.idrografico.roma.it/default.aspx) (**Figure 45**) collected hourly rainfall amounts at the rain gauge of Tivoli (station N°1760), Aniene River water levels at the hydrometer of Ponte Lucano (station N°4532) and water levels of the PdM Lake (recorded since 2008).

The data from a sampling location in the Acque Albule Basin are considered for a geochemical comparison before and after the L'Aquila earthquake, which is displayed in **Figure 43**. The geochemical samples were derived from Regina Lake in the main spring of Acque Albule Basin near monitoring point P1.

The samples were collected and stored in PE bottles. An aliquot that was used for the cation analysis was filtered through 0.45 μm Millipore filters and acidified with HNO_3 before storage. Temperature, Eh, pH and electrical conductivity (EC) were measured in the field using electric probes, and alkalinity was measured by a titration with 0.1 N HCl. The pH measurements were accurate and reproducible to 0.1 pH unit. The precision of the conductivity meter that was used for the analyses was approximately 1%. The major ion concentrations (Cl-, SO_4^{-2}, Ca^{2+}, $Mg^{2+,}$ K^+ and Na^+) were measured using Ion chromatograph techniques.

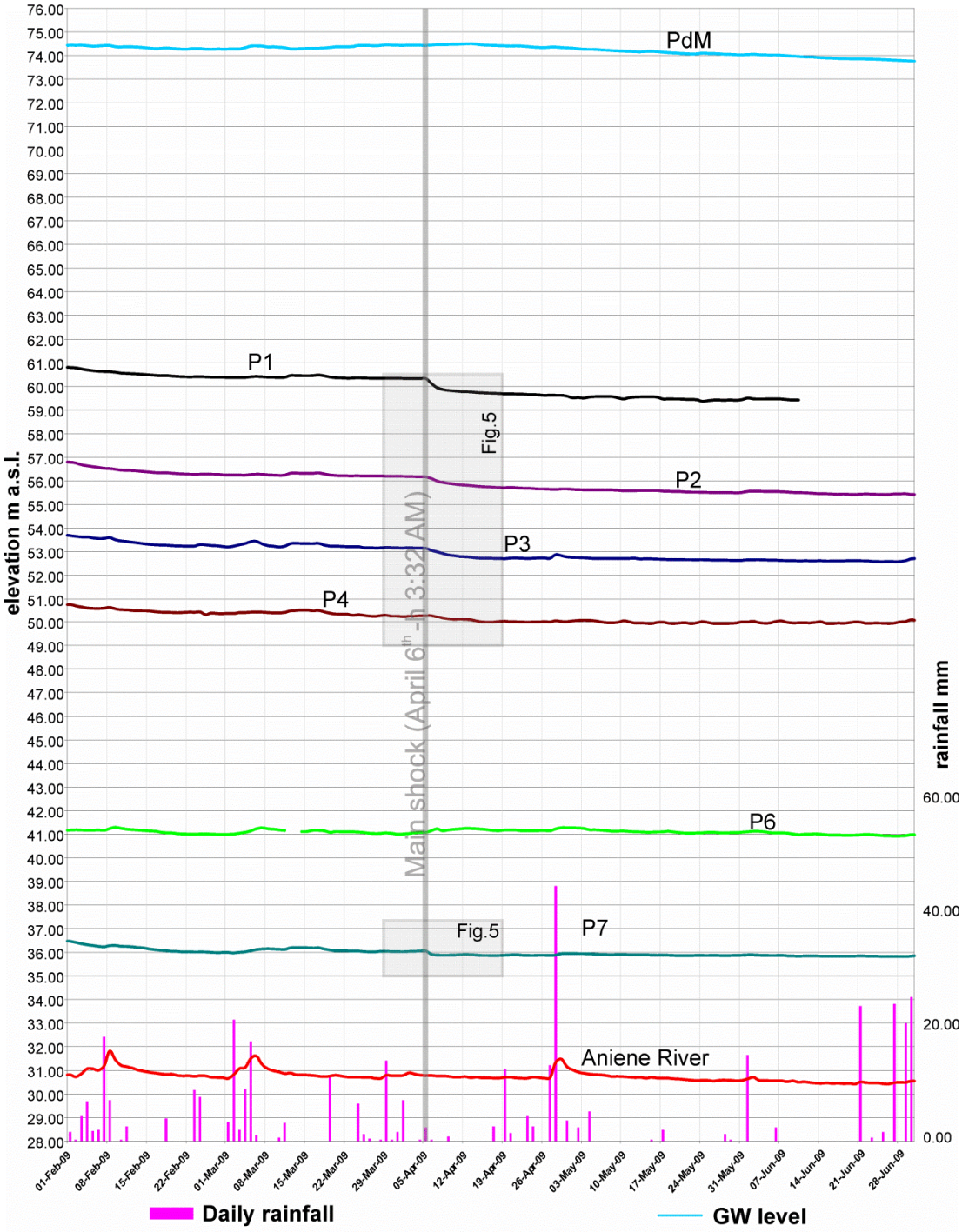

Figure 45: Groundwater level comparison for the AAB monitoring network, which shows six hourly groundwater monitoring points that sample the shallow travertine aquifer, hourly Aniene River hydrometric levels (referring to hydrometer N°4532 of Ponte Lucano), hourly groundwater levels of the Pozzo del Merro (PdM) in the carbonate aquifer, and the daily rainfall, as determined by the rain gauge that is N°1760 of Tivoli from February through June 2009. The vertical grey bar represents the time of the L'Aquila earthquake (6 April 2009 01:32 GMT). The rectangle shows the area that is highlighted in figure 6.

3.4.2 Conceptual model and results

Figure 45 shows the groundwater levels of the monitoring points in the AAB and the PdM compared with the Aniene River levels and the daily rainfall data. The graph shows the presence of 1 to 1.5 m of variability in the groundwater table elevations in the northern travertine aquifer (P1, P2, P3 and P4, which are shown in figure 3), with a general decreasing trend. Conversely, the levels at the monitoring points in the southern travertine aquifer (P6 and P7) are less variable and correlate well with the Aniene River variations. The groundwater level of the PdM (deep limestone aquifer) appears to be less dynamic with variability of no more than 0.5 m in the same period. The comparison of all of the groundwater levels with the daily rainfall at the Tivoli rain gauge shows a direct correlation, especially in the southern portion of the plain. This relationship with rainfall is damped at the PdM, where a positive level variation was recorded during a dry period in the first half of April.

This aquifer is normally characterised by frequent, rapid variations that are induced by quarry dewatering, but this type of variation did not occur during the selected time period (**Figure 45**). The trend in groundwater levels in the AAB and the Cornicolani Mountains is constant in the observed time period, and the fluctuations are related exclusively to the recharge of the aquifers.

A sudden decrease step in the groundwater levels was recorded concurrent with the L'Aquila earthquake at five of the six monitoring points (P1, P2, P3, P4 and P7) (**Figure 45** and **Figure 46**).

Within approximately twelve days of the mainshock, all of the groundwater levels decreased to a new average level.

All of the monitoring points showed level decreases in two steps: an abrupt decrease occurred during the first six hours after the mainshock, and a second gradual lowering to the new average level occurred over the next twelve days (**Figure 46**).

The total recorded change in the groundwater level (the sum of the first and second steps) is the largest at P1 (approximately 70 cm), and it gradually decreases at the other monitoring points, as follows:

P1 – First step: 22 cm; Total: 70 cm until 18 April

P2 – First step: 6 cm; Total: 50 cm until 18 April

P3 – First step: 10 cm; Total: 45 cm until 18 April

P4 – First step: 0 cm (No abrupt decrease observed); Total: 30 cm until 18 April

P7 – First step: 20 cm; Total: 20 cm until 18 April (no gradual decrease was observed)

No level changes were registered at the monitoring point near the Ainene River (P6) in the AAB (**Figure 45**).

Instead, the deep aquifer behaved differently. The PdM time series (**Figure 45**) shows the presence of a general water level increase since March, which probably occurred due to seasonal effects. On the day after the mainshock, a slight slope change in the general trend was observed, and it peaked on 15 April.

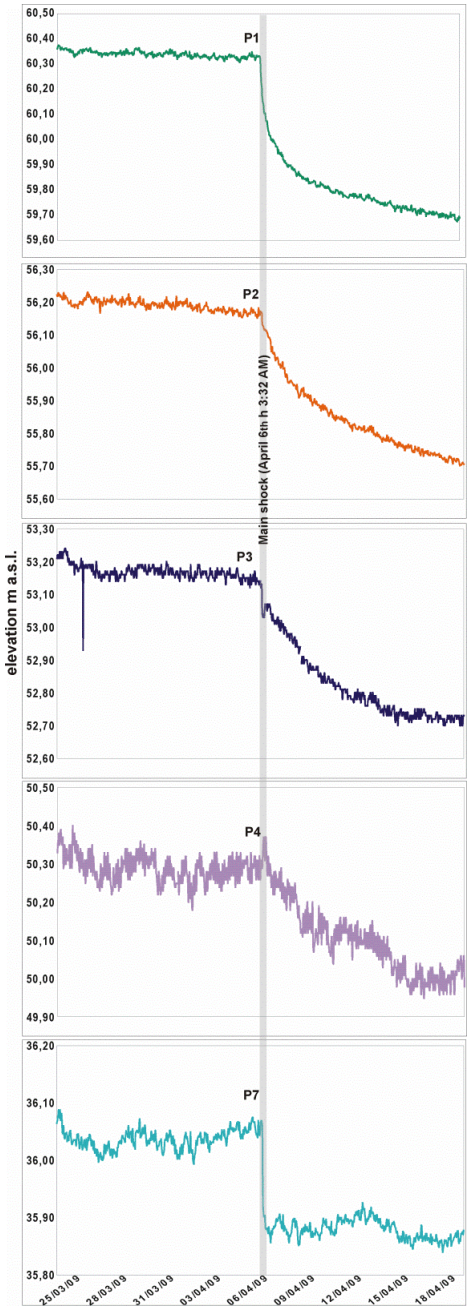

Figure 46: The shallow aquifer response to the L'Aquila earthquake. Five of the six monitoring points (P1, P2, P3, P4 and P7) show a decrease in the groundwater level corresponding to the L'Aquila mainshock. The five monitoring points show decreases in two steps: the first is characterised by an abrupt decrease, the second is characterized by a slight and sustained decrease. Point P7 does not show the second decrease.

To verify whether other earthquakes have influenced the groundwater levels in the AAB, M_L>4 earthquakes that occurred between 41° N – 44° N and 10° E – 15° E were downloaded from the INGV website (http://iside.rm.ingv.it - *Italian Seismic Instrumental and Parametric Data-Base*). During the selected period (February – June 2009), all 32 earthquakes that fit these criteria were related to the L'Aquila seismic sequence. Of these earthquakes, only the mainshock appeared to affect the AAB groundwater levels.

The most representative hydrothermal spring in the Tivoli Plain and the Acque Albule Basin (Regina Lake) has been considered to verify the occurrence of anomalous geochemical behaviours in the travertine aquifer. Due to steady groundwater exploitation in the travertine aquifer, seasonal changes may not largely affect the water's chemical composition, and samplings at the P1 monitoring point that were obtained prior to the earthquake showed a stable chemical composition (CARUCCI, 2010). The comparison of these mean pre-earthquake values with the measurements from November 2010 (approximately 7 months after the L'Aquila earthquake) (Tab. 1) shows no appreciable pH or temperature differences. The only evident variations in the post-seismic period are decreases in electrical conductivity and sulphate contents.

3.5 Discussion and conclusions

The data show two main behaviours in the groundwater level time series of the travertine shallow aquifer and the limestone bedrock relative to the earthquake (**Figure 47 c**). In the travertine aquifer (P1, P2, P3, P4 and P7) (**Figure 45** and **Figure 46**), the groundwater table shows a widespread decrease of up 0.7 m in the monitoring points near the main hydrothermal upwelling zone (P1 and P7). Conversely, the PdM station in the bedrock limestone reservoir shows a slight gradual rise that began on the day after the mainshock (**Figure 45**).

Figure 47 shows the proposed possible conceptual model of the hydrogeological response of the Acque Albule hydrothermal system to the L'Aquila earthquake.

The observed water table decrease in the travertine aquifer is caused by the two following different mechanisms:

A permeability enhancement occurred in the travertine (**Figure 47 a**). This increase may be caused by three separate processes induced by the dynamic stress changes that occurred due to the passing of seismic waves through these rocks: the opening of new micro-cracks (BRACE *et alii*, 1966), the interconnection of pre-existing cracks and isolated pores of travertine, and the removal of infill from cracks (BRODSKY *et alii*, 2003; MATSUMOTO *et alii*, 2003; WANG & CHIA, 2008).

A permeability decrease occurred in the high-permeability zones of the aquiclude (**Figure 47 b**). The process responsible for the permeability decrease was caused by the pore reorganisation (compaction) of the porous media constituting the high-permeability zones of the aquiclude (sand, clay and gravel) (MANGA & WANG, 2007), which reduced the upwelling flow to the shallow aquifer.

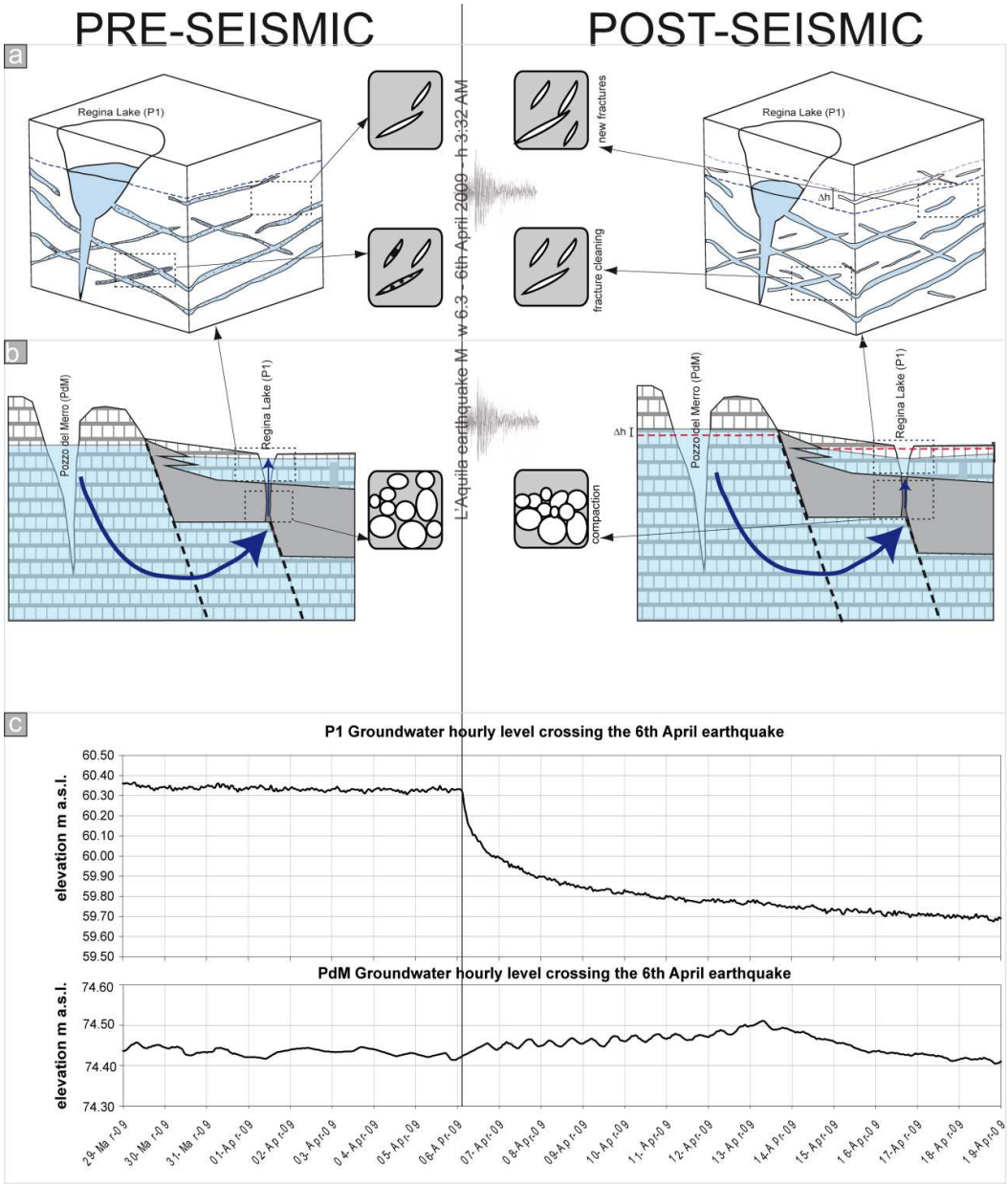

Figure 47: Possible conceptual model of the hydrogeological response of the AAB hydrogeological system induced by the L'Aquila earthquake. (a) Shallow travertine aquifer behaviour showing a permeability increase due to the opening of new fractures and/or fracture cleaning. (b) Deep carbonate aquifer behaviour showing a permeability decrease (compaction) in the high-permeability zone in the aquiclude. (c) Zoom-ins of the variations in the two aquifers showing decreasing water levels in the shallow travertine aquifer and a slight increase in the Pozzo del Merro (PdM) shaft (deep carbonate aquifer)

The first and second steps of the decrease that are displayed in **Figure 46** are related to the following two mechanisms:

The first step may be caused by compaction in the high-permeability zones of the aquiclude and a rapid decrease in the upwelling deep flow. The monitoring points P1 and P7, which are located near the hydrothermal upwelling zones, displayed the largest decreases (P1 = 22 cm and P7 = 20 cm).

The second step may be caused by the permeability enhancement in the travertine aquifer because the decrease is gradual and sustained over time (WANG & MANGA, 2010). Site P7 is an exception because it is probably more influenced by the Aniene River fluctuations.

The different magnitudes of the total groundwater level decreases (the sum of the first and second steps) that were recorded at the monitoring points can be explained by their different locations with respect to the AAB and by the non-homogeneous permeability of the travertine aquifer.

Based on the hydrogeological setting (**Figure 44**) and the recharge conditions of the travertine aquifer, the different behaviour of the groundwater level that was observed in the PdM shaft may confirm the previous assumptions. The observed water level rise may be connected to the permeability variation in the high-permeability zones of the aquiclude (**Figure 47 b**) because a temporary permeability decrease may have increased the pressure in the confined carbonate aquifer.

The subsequent negative variation in the PdM groundwater level after the observed peak (**Figure 45**, **Figure 47 c**) may instead be related to the seasonal lowering of the regional aquifer (LA VIGNA, 2011) or to a gradual return to the pre-seismic permeability conditions of the aquiclude, due to the pressure increase in the deep limestone reservoir. This eventual recovery must have been notably slow because no corresponding level increases in the travertine aquifer failed to return to pre-seismic levels by the end of the observation period. From a geochemical viewpoint, a consistent decrease in dissolved sulphate content, which was likely due to a TDS decrease (there are no post-seismic total major ions analyses), may confirm the hypothesis of the opening of new cracks and permeability enhancement, which were contemporaneous to minor upwelling of deep hydrothermal flow. These phenomena could cause the dilution of dissolved salts and a minor increase in the H_2S fluid contribution, respectively. The latter is responsible for high SO_4^{-2} concentrations in the Acque Albule travertine aquifer, due to sulphide oxidation near the surface and inside the main fractures.

Based on the groundwater level time series, only the 6 April 2009 L'Aquila earthquake mainshock produced groundwater level changes. None of the other selected earthquakes affected the AAB hydrogeological system; according to Manga & Wang (2010), this finding

was probably caused by the ratio of their small magnitude relative to their epicentral distance (**Figure 48**).

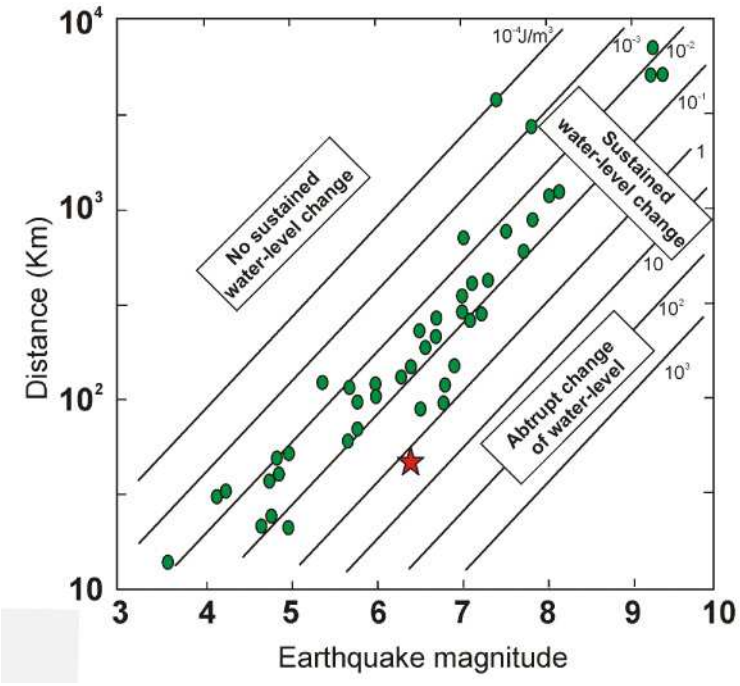

Figure 48: Hypocentral distance (in km) of the groundwater level changes plotted against the earthquake magnitude. The contours of the constant seismic energy density and the domains in which different types of coseismic water-level responses occur are shown. The sustained water-level changes in a global dataset are indicated with green circles; the intermediate-field water-level changes, which were observed in the Acque Albule basin in response to the 6 April L'Aquila earthquake (Mw 6.3), are indicated with red stars (modified from MANGA & WANG, 2007).

In conclusion, the observations that are presented in this study highlight the importance of groundwater monitoring in tectonically active regions, such as Italy. The groundwater variations discussed here can be studied only where a monitoring network is installed; in complex groundwater systems that are characterised by different aquifers, every aquifer should be monitored. Sampling intervals of 1 hour were useful in this work; however, a smaller sampling interval is required for aquifers with high seismic sensitivities (ITABA *et alii,* 2010).

The sensitivity of the AAB hydrogeological system to seismic events is probably due to its tectonic setting (ACOCELLA & FUNICIELLO, 2006; FACCENNA *et alii*, 1994) and its hydrothermal character.

The groundwater level changes that were observed in the AAB groundwater-monitoring network are clearly connected to the 6 April 2009 L'Aquila earthquake (Mw 6.3). The data provide evidence that dynamic strains can create permanent (within the analysed period of February-June 2009) changes in the aquifer properties also in the intermediate-field.

The groundwater level data that were collected and analysed in this study show an abrupt decrease that was followed by a sustained decrease in the shallow travertine aquifer and a

gradual increase in groundwater level in the deep limestone aquifer that was observed at the PdM shaft.

The conceptual model presented here shows a permeability increase in the travertine aquifer, due to the opening of new micro-cracks and/or the cleaning of infilling fractures and local compaction in the aquiclude.

The permeability increase is supported by the sustained gradual decrease of the groundwater level that was observed in the second step of water table decrease.

The compaction, which induces a local permeability decrease in the aquiclude, is supported by the observed abrupt decrease in the groundwater level in the travertine aquifer (the first observed step) and a slow increase in the groundwater level of the PdM shaft.

4 CASE STUDY 3: NEAR FIELD HYDROGEOLOGIC RESPONSE TO EMILIA EARTHQUAKE 21TH MAY 2012 (MW 6.1)

4.1 Northern Appennine geological setting

The Emilia region is located in the Po plain, which represents the east–west continental collisional boundary between the subducting Adria plate to the north, and the overriding Northern Apennine block to the south (Picotti & Pazzaglia, 2008).

The Po Basin, covers an area of approximately 46.000 km^2 and is bound to the N by the Alps, to the SW by the Apennines and to the E by the Adriatic Sea; moreover, it represents the Northern Apennine Foredeep.

The Apennine chain is a thrust and fold belt composed of several units, structurally homogeneous, that were emplaced toward the N–NE from Early Cretaceous to present during the closure of the Piedmont-Ligurian Ocean and the collision of the European and Adria plates. In the north-western Apennines, the allochthonous Ligurian Internal units (Mesozoic oceanic and forearc sedimentary deposits) and the overlying Epiligurian units (Middle Eocene–Early Messinian turbidites and shallow water primary evaporites) representing the upper structural level that translated to the foredeep, reached the foreland and overthrust the more recent turbidites of the foredeep (Argnani & Ricci Lucchi, 2001).

During the Miocene and up to the Quaternary, the Po basin has been gradually reduced by the compression, that originated the frontal buried thrusts of the northern Apennines and southern Alps. The buried structures, resulting from embricational tectonics, mostly developed in submarine conditions, and consisting of folds strongly compressed and thrust toward north–east, forming (from west to east) the Monferrato, Emilia and Ferrara–Romagna arcs. The huge thickness of Neogenic deposits is evidenced by the bottom of Pliocene rocks, that reaches 8 km depth inside the Ferrarese fold system, attesting a stately subsidence phase during this time. The bottom surface of the Pliocene sequence is the result of Pliocene or post-Pliocene deformations (Pieri & Groppi, 1981). The whole area was interested by a strong crustal shortening (Castellarin et al., 1985, Perotti, 1991). Variation in thickness of the pre-Pliocene sequences suggests vertical motions and extensional tectonics during the Mesozoic and lower Tertiary, followed by a compressional phase in the upper Miocene. The last compressive episodes occurred in the upper Pliocene and in Pleistocene (Bernini & Clerici, 1983, Bernini et al., 1990). The amount of compression and shortening decreases from east to west analogously to the decrease in amount of amplitude of deformation in the belt (Amato et al., 1993).

The lower structural level of the Apennines corresponds to the Tuscan (nappe)-Umbrian (foredeep) units consisting of crystalline rocks of the metamorphic Paleozoic basement and

Mesozoic carbonates (Triassic evaporite and dolostone, **Figure 49**), that represent the main regional reservoir. In the Emilia Romagna Region, one of the most important structures of the Appenninic lower level is the Ferrara anticline known as Dorsale Ferrarese, where the Mesozoic substratum has been uplifted to a depth of less than 100 m (Pieri & Groppi, 1981; Regione Emilia-Romagna and Eni-Agip, 1998). The Dorsale Ferrarese is part of a series of fold-faulted Apennines units dipping southward (Rebai et al., 1992) and the Po Plain covers them.

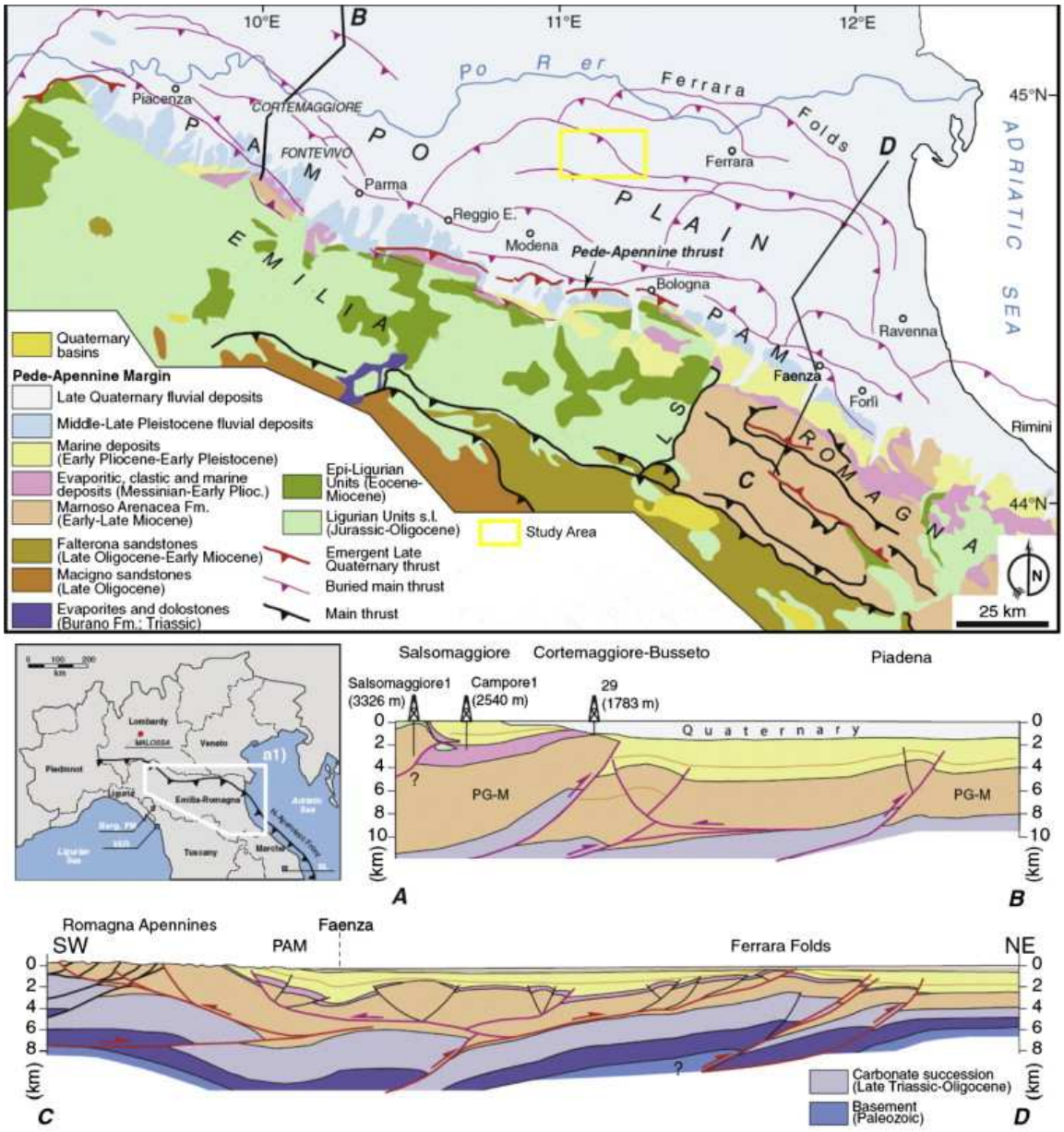

Figure 49: from Sciarra et al. (2013) Simplified geological map of the Northern Apennine and study area. PAM Pede-Apennine Margin; LSL Livorno-Sillaro lineament, PG-M, undifferentiated Paleogene-Miocene sediments. Two cross sections A–B and C–D are shown.

4.2 Earthquake kinematics

On May 20 2012, a seismic event of ML 5.9 (M_W 5.6) struck the southern edge of the Po river flood plain (Pianura Padana), approximately 30 km West of the town of Ferrara, and 10 km to the NW of the village of Finale Emilia (INGV). On 05/19/2012 at 23:13:27 the earthquake was preceded by a foreshock of ML 4.1 (M_W 3.8). Hypocentral depths were 6.3 km for both events; centroid depths were 5 and 6 km (main and foreshock, respectively). Fault was a reverse one, dipping 45 to the South (**Figure 50**) (Malagnini et al., 2012).

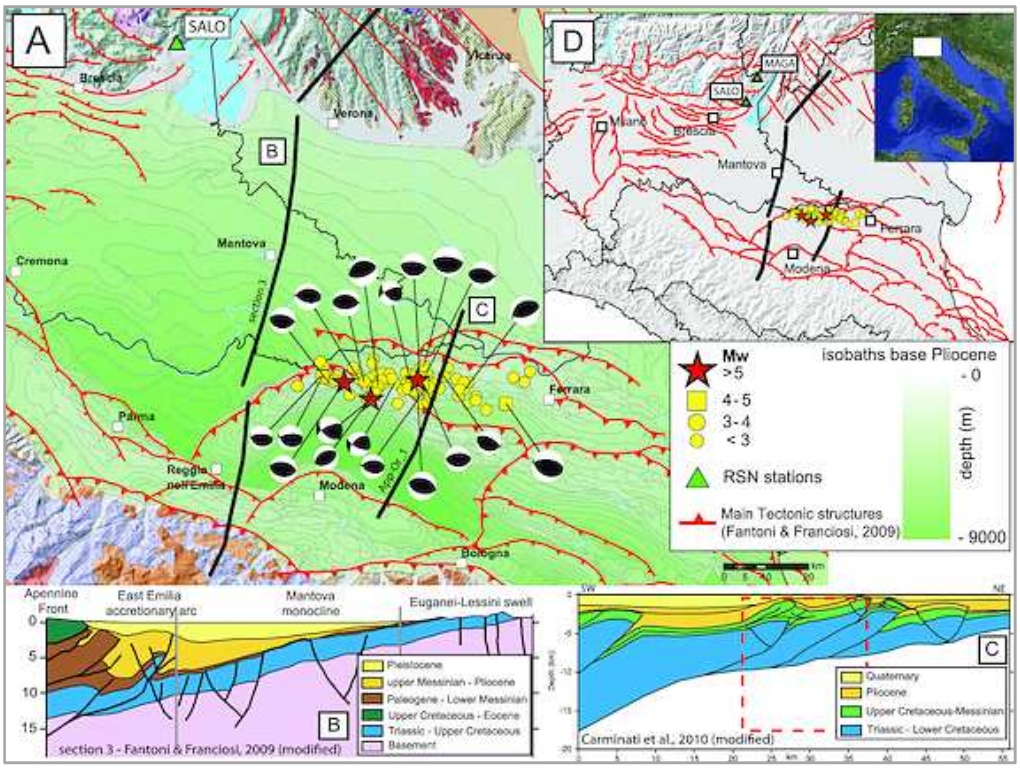

Figure 50: from Malagnini et al. (2012), Map of the area where occurred the May 2012 seismic events . Isobaths contours of Pliocene base surface below the whole Po Plain highlight the buried architecture of the area. 78 events of the entire 2012 seismic sequence and our 22 MT solutions are plotted. (b) Geological cross section modified from Fantoni and Franciosi (2010, three-pieces profile B of Figure 1a): gray vertical lines mark the discontinuities of the profile. (c) Geological cross section built on the interpretation of the App_Or_1 seismic profile (modified from *Carminati et al.,* 2010, profile C in Figure 1a); dashed box indicates a section of the volume that is potentially interested by the seismic activity.

This seismic sequence occurred in the central Po plain tectonic domain, characterized, below the Plio-Quaternary sedimentary cover, by arcuate thrust systems and related growth folds (Pezzo et al., 2013 and reference therein). These structures are well imaged by several seismic sections acquired by the petroleum industry in the last 30 years (Boccaletti, M., 2004) these thrusts are considered blind, because no fault traces can be seen at the surface (P. Burrato et al., 2003).

The activity of the thrust–fold system has been debated for many years. Some authors, based on field studies and seismic reflection lines, maintain the hypothesis that, following a major geodynamic change, thrusting and related folding between the northern front of the

Apennine and the Po plain ceased in Early Pleistocene time (Argnani et al., 1997; Bertotti et al., 1997; Di Bucci and Mazzoli, 2002; Argnani et al., 2003).

Other authors, based on geomorphological analysis, subsurface geology, seismicity, and present day stress field, suggest that the tectonic activity of the frontal part of the Northern Apennine accretionary wedge is still going on. In particular, Scrocca et al. (2007) and Burrato et al. (2003) suggest that this activity is mainly going on along the external thrust fronts below the Po plain. Active thrusting is also in agreement with recent horizontal GPS measurements (Serpelloni et al., 2006; Devoti et al., 2011) which suggest ~1 mm=yr of shortening is accommodated in this area. Such low deformation rates are in agreement with the low historical seismicity levels of the area. In fact, since at least the year 1000 A.D. this area has never experienced earthquakes of magnitude larger than ML ~ 4:7 (1574 Finale Emilia earthquake, Rovida et al., 2011). Larger magnitude earthquakes occurred west and east of the 2012 epicentral area, the most significant one being the 1570 ML ~ 5:4 Ferrara earthquake (Rovida et al., 2011). The sources of such historical events (the Mirandola and Ferrara thrusts) were defined based on seismic reflection profiles and geomorphological studies (Basili et al., 2008), their location roughly corresponding to the area of the 2012 sequence. In particular, Burrato et al. (2003) describe active fold growth in this area, observing the northward migration of the Po River and other smaller watercourses during the Late Quaternary. The short-term coseismic deformation observed during the seismic sequence may provide the opportunity to harmonize all geological long-term observations with the present day rates. The 2012 earthquakes have actually confirmed the present activity of the external thrust belt (at least in the central Po plain): the main focal solutions show west-northwest to east–west nodal planes and a ~north–south compressional kinematics (Malagnini et al., 2012), in agreement with the seismotectonic setting (Boccaletti et al., 2010).

4.2.1 Documented hydrogeological response to seismic event

The May-June 2012 seismic sequence occurred in the low plain area, where fine sediments generate multilayered confined aquifers, and phreatic aquifers are limited to the first 10 m to 30 m in depth.

Marcaccio &Martinelli, 2012, analysed the water level recorded in some automatic stations of the regional well network. These data can be considered useful to understand the relationships between seismic events and the local groundwater.

Most of the stations located in the whole of the Emilia-Romagna region did not record significant signals that are attributable to seismic events, while some stations located in the provinces of Modena and Ferrara recorded sudden water uprising phenomena, of up to 1.5 m (**Figure 51**).

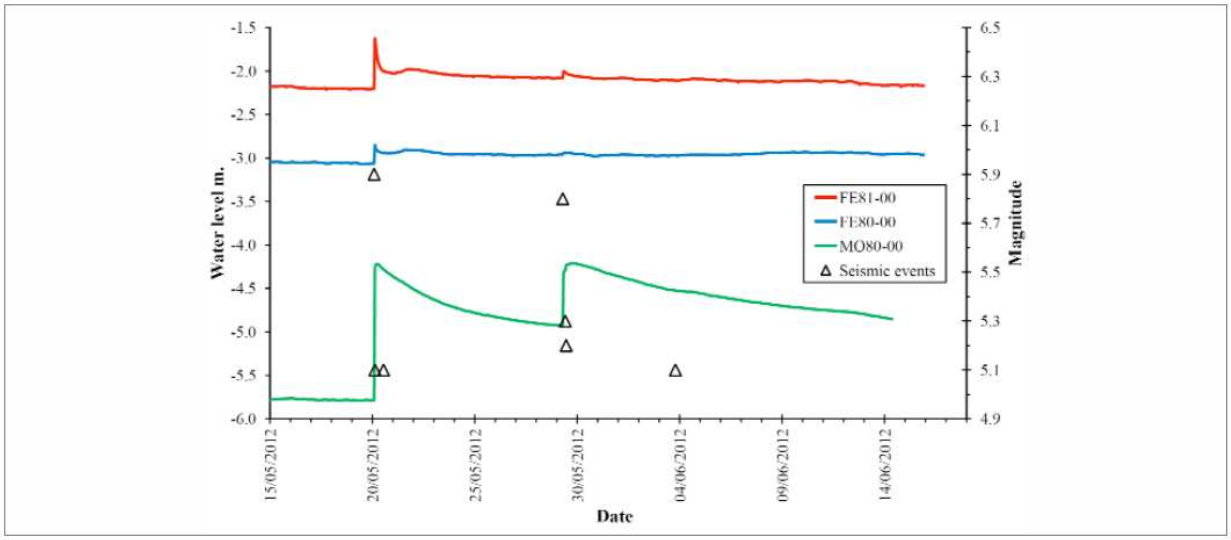

Relevant seismic events (magnitude)	Seismic events occurrence date	Seismic events occurrence time (UTC)	Pre-seismic recording time (UTC)	Post-seismic recording time (UTC)
5.9	20/05/2012	02.03.52	02.00.00	03.00.00
5.8	29/05/2012	07.00.03	07.00.00	08.00.00

Figure 51: from Marcaccio & Martinelli et al. (2012), Water-level changes in concomitance with some significant seismic events. The events characterized by 5.1 ≤M ≤5.9 were considered. In the table are shown the occurrences of the two most relevant seismic events, with the pre and post recording times.

Two different water level variations were recorded in concomitance with most of the relevant seismic events, which were characterized by the M 5.9 (full dot) and M 5.8 (empty dot) seismic events (**Figure 52**).

The sizes of the recorded anomalies can be tentatively related to the aquifer characteristics, to the distances of the recording station from the hypocentral area, and to the locations of the monitored aquifers in areas probably subjected to compressive strain. The step-like signals observed indicate that all of the monitoring stations in the near-field area, in which

undrained consolidation is the dominant mechanism for coseismic groundwater level changes, were affected by significant water level variations.

Data are in agreement with Severi et al. (2013), the Authors analyze the behavior of the aquifer water table and the first confined aquifer near the right bank of the Po River in consequence of the Emilia earthquakes occurrence, their study is part of the project "Seismic Verification of embankments on the right bank of the Po River from Boreham (RE) in Ro (FE)".

They observed that in the stations of Ro Ferrarese, Ferrara, Occhiobello, Bondeno, Felonica, Sermide, Carbonara Po, Guastalla and Boreham (ie in all but Gualtieri and Pieve Saliceto), changes were noted at the same time of the earthquakes of May 2012. The distance to which these changes have been observed, therefore, comes up to more than 40 kilometers from the epicenter points.

The changes concerned abnormal oscillations of level, conductivity and temperature.

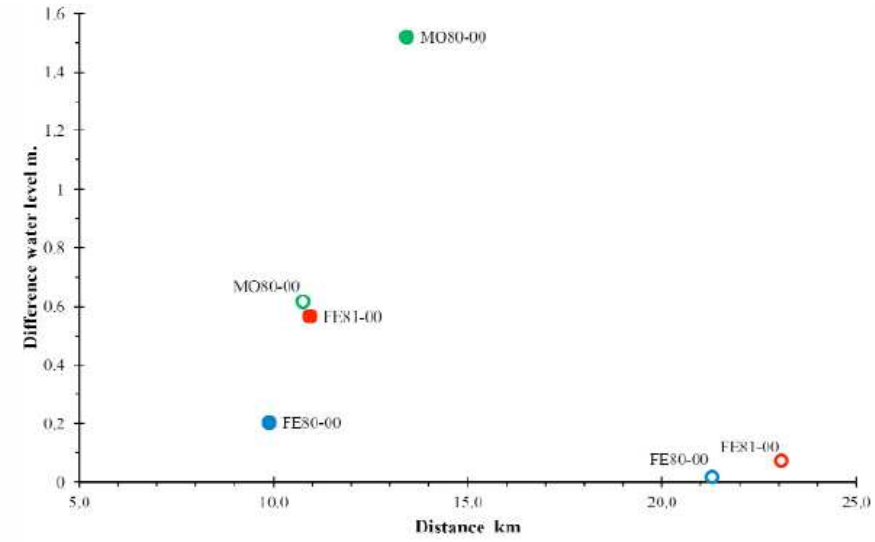

Figure 52: from Marcaccio & Martinelli et al. (2012), Differences in the water levels at the three monitoring stations, as related to the distance in concomitance with the two relevant seismic events characterized by M 5.9 (full dot) and M 5.8 (empty dot).

4.3 Hydrogeological setting of Po Plain

The Po sedimentary basin is filled by sediments of Alpine and Apennine origin (Ori 1993). The sedimentation processes have filled the sedimentary basin with alternate layers of sands and clay (Ori 1993, and references therein). Gravels are present near the Apenninic chain front in the alluvial fan areas, while the bottom of the Quaternary sediments is at depths of 100 m to 700 m. These multilayered sequences constitute the Po aquifer system (Regione Emilia-Romagna and ENI-AGIP 1998).

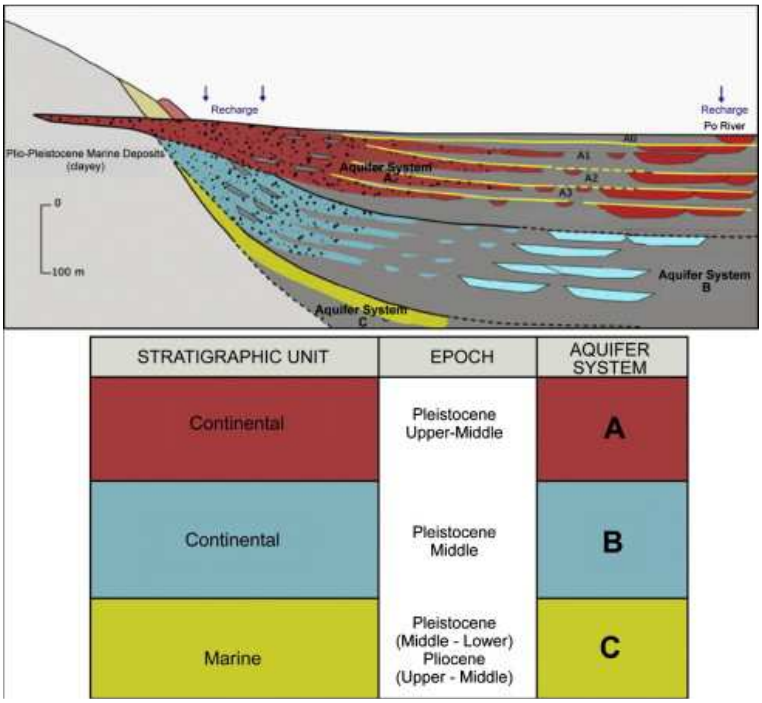

Figure 53: from Sciarra et al. (2013)On the basis of the available stratigraphic data, three main aquifer systems (A–C) are identified by Regione Emilia Romagna joined with ENI-AGIP (Regione Emilia-Romagna and Eni-Agip, 1998). The A and B aquifer systems are hosted in the Quaternary continental sediments, whereas the C aquifer system into Quaternary marine delta deposits.

In the part of the basin close to the Apenninic chain front (the belt of alluvial fans), the aquifers are located in undersaturated sediments and are subject to seasonal variations in their recharging processes. Fine sediments host confined or semiconfined aquifers are characterized by low circulation velocities. Isotopic data indicate that deep groundwaters in this area are of Alpine origin, while ^{3}H and ^{14}C data indicate ages of 15000 to 30000 years (Martinelli et al. 1998, and references therein). At depths shallower than 50 m, load fluctuations are observed in connection with rainfall, although lenses of confined aquifers that are poorly sensitive to rainfall are known to be at shallow depths too.

4.4 Available data and methods

4.4.1 Data and Methods

To understand the hydrogeological response to the Emilia earthquake, data from 19 monitoring wells in the Po Plain have been analyzed.

Most of the stations located in the whole of the Emilia-Romagna region did not record significant signals that are attributable to seismic events, while some stations located in the provinces of Modena and Ferrara (**Figure 54**) recorded sudden water uprising phenomena, of up to 1.5 m (**Figure 55**). The internal clock of the monitoring stations was synchronized according to Coordinated Universal Time (UTC). In this way, the first measures after the M 5.9 and M 5.8 shocks were recorded about 1 h after these seismic events.

Data are about wells draining aquifers at several depths, from 1 up to 45 m depth.

At depths shallower than 50 m, load fluctuations are observed in connection with rainfall, although lenses of confined aquifers that are poorly sensitive to rainfall are known to be at shallow depths too (Marcaccio & Martinelli, 2012).

In **Figure 54a** the study area is shown, in **Figure 54b** the area zoom with the location of the 3 monitoring wells where variations at the Emilia earthquake were univocally observed are reported.

A monitoring network containing 5 piezometric dataloggers (Fe8100, Fe8000, Bof800, Mo4301 and Mo8000) records the shallow and deep groundwater levels on an hourly schedule, and the accuracies are approximately 1 cm. The monitoring points are

distributed within the area of **Figure 54b.**

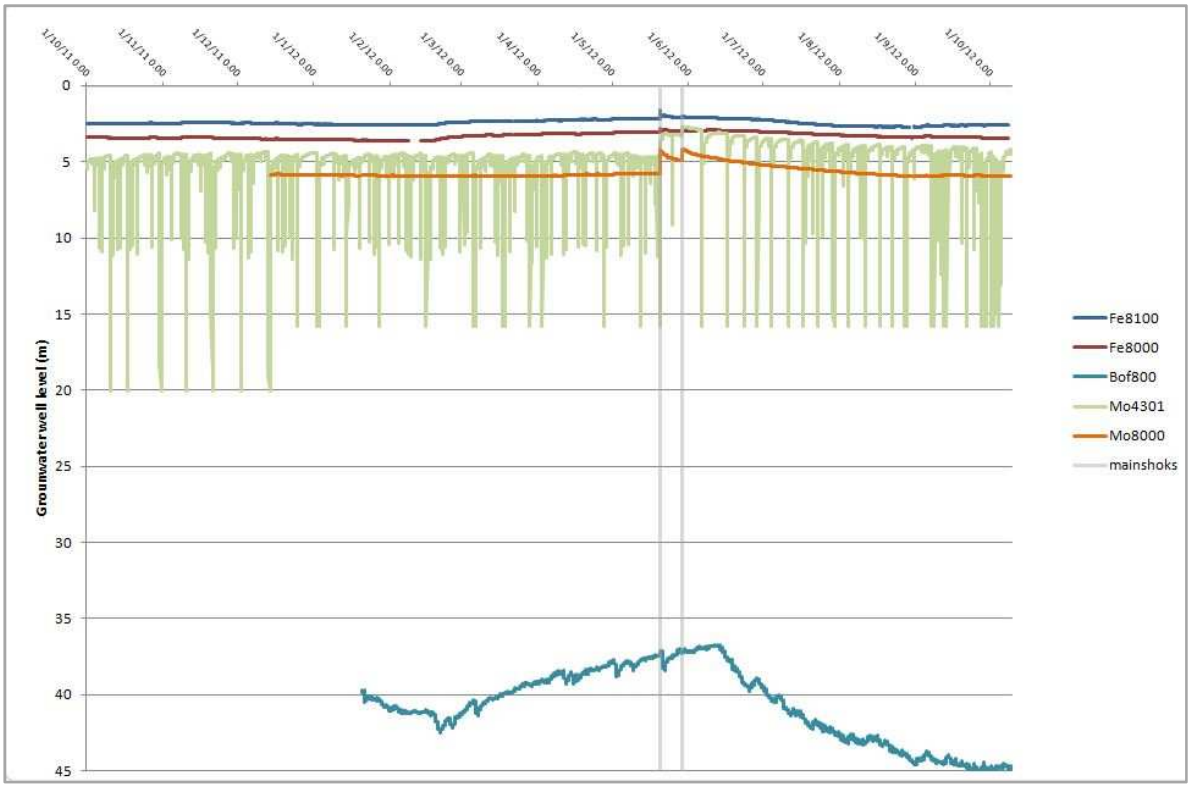

Figure 55 shows the groundwater levels from October 2011 to October 2012, which allows for the analysis of changes during the earthquake event. The data of residual 14 piezometric dataloggers are not reported because variations due to Emilia earthquake are not observed.

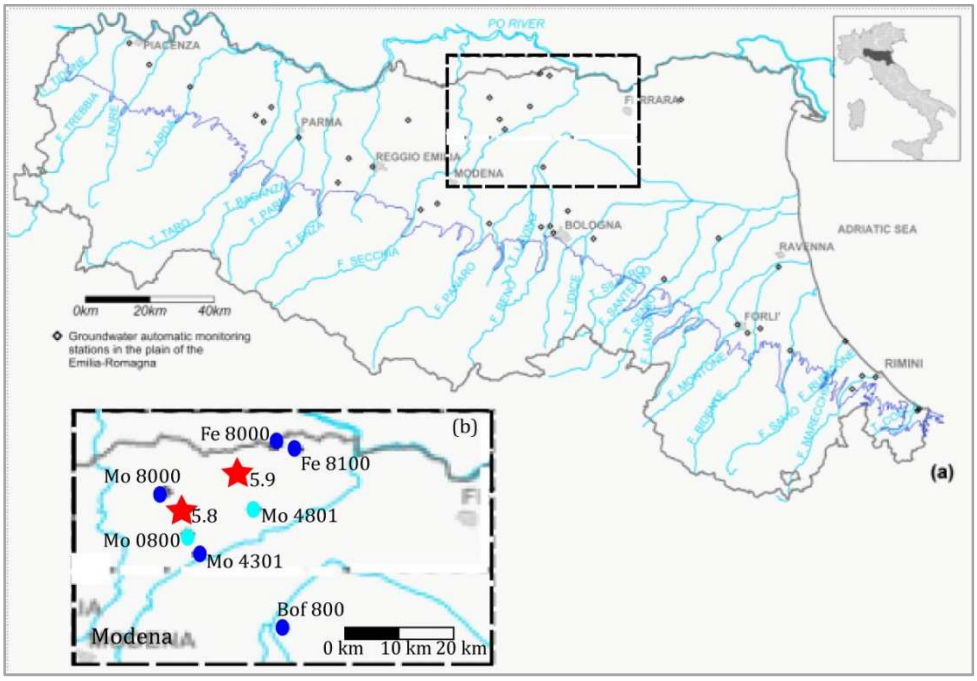

Figure 54: modified from Marcaccio & Martinelli (2012) - (a) Geographical sketch of the Emilia-Romagna region showing all of the groundwater automatic monitoring stations managed by ARPA Emilia-Romagna. (b) Monitoring stations considered (blue points) and epicenters of the most relevant seismic events (red stars) [INGV 2012].

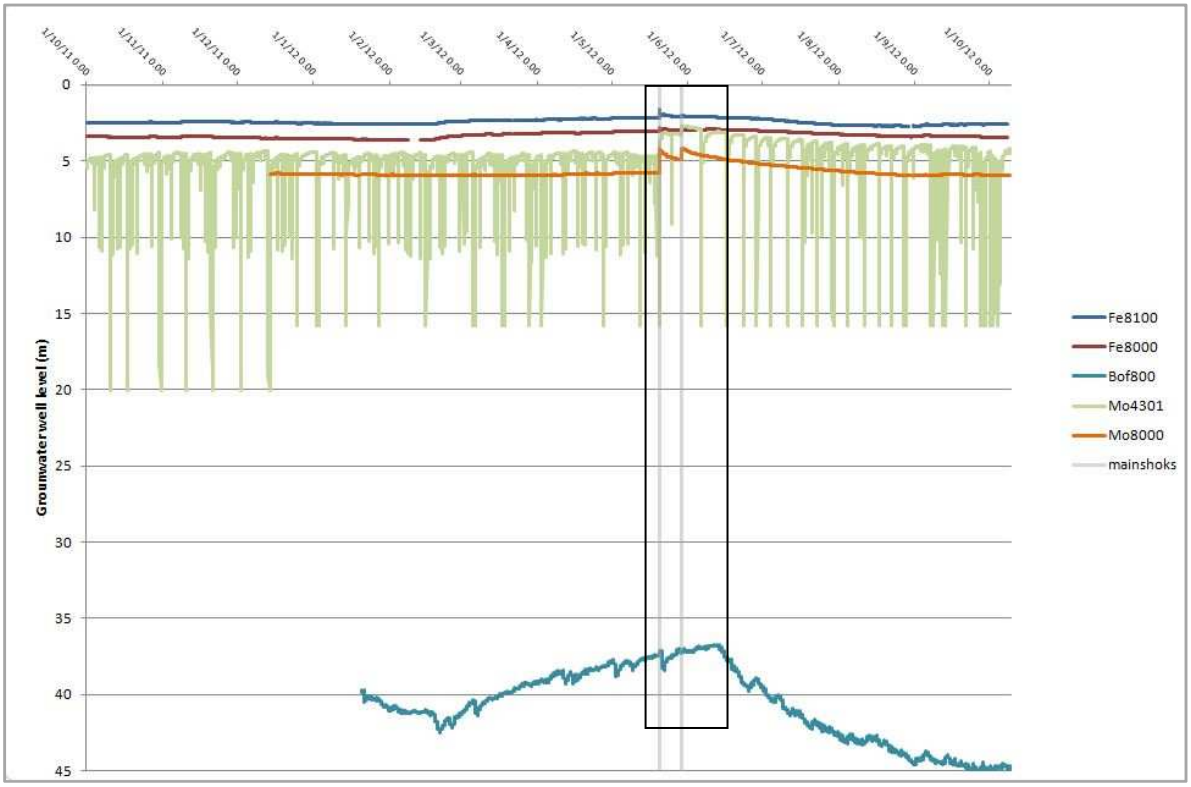

Figure 55: Groundwater level comparison for Po Plain monitoring network, which shows five hourly groundwater monitoring points that sample the shallow and deep aquifer. The vertical grey bar represents the time of the Emilia earthquake mainshoks (20 May 2012 at 02:03 and 29 May 2012 at 07:00). The rectangle shows the area that is highlighted in Figure 56 with exception of Mo4301 well.

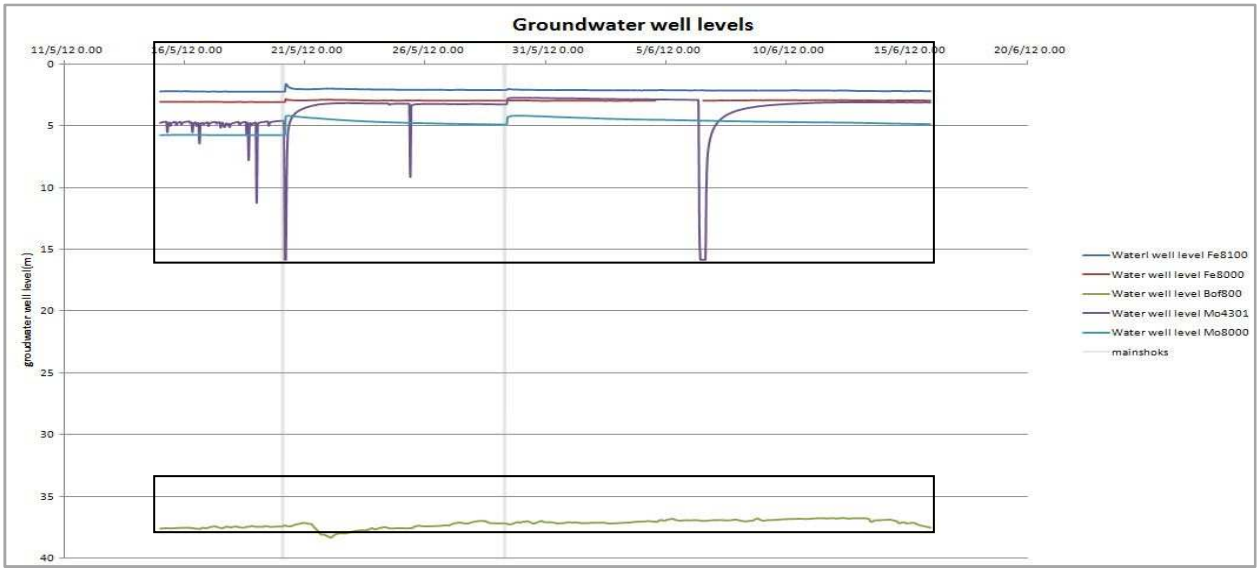

Figure 56: Groundwater level comparison for Po Plain monitoring network, which shows five hourly groundwater monitoring points that sample the shallow and deep aquifer from 15/05/2012 to 15/06/2012. The vertical grey bar represents the time of the Emilia earthquake mainshoks (20 May 2012 at 02:03 and 29 May 2012 at 07:00). The rectangle shows the area that is highlighted in Figure 57.

4.4.2 Conceptual model and results

In **Figure 54** is shown the spatial location of the epicenter of the two Emilia earthquake mainshocks and the monitored wells close to. With dark blue are highlighted wells were hydrological variations are observed, while in light blue are indicated monitored wells where no level variations are observed.

Figure 55 and **Figure 56** show the groundwater levels of the monitoring points in the Ferrara and Modena regions levels data. The graph shows the presence of 1 to 1.5 m of variability in the groundwater table elevations in the shallow aquifers (Fe8100, Fe800, Mo4301 and Mo8000, which are shown in **Figure 57a**), with a general increasing trend. Conversely, the level at the monitoring point in the deep aquifer (Bof800) appears to show no immediate variations, but only a slight increase after the 20 May mainshok (**Figure 57b**).

The M 5.9, May 20, 2012, seismic event occurred at a distance of about 5 km to 20 km from the monitoring stations Mo4801, Mo0800, Fe8100, Fe800, Mo4301 and Mo8000, while up to 35 km from the monitoring well Bof800. The observed signal amplitude was relevant in monitoring stations Fe8100, Fe800, Mo4301 and Mo8000, but no variations was observed in Mo4801 and Mo0800 that are located close to epicenter, and no apparent variations in Bof800 located about 35 km away from the epicenter (**Figure 54**).

The M 5.8, May 29, 2012, seismic event occurred at a distance of about 10 km from the Mo8000, Mo4801, Mo0800 and Mo4301 stations, at about 20 km from the Fe8000 and Fe8100 stations, and at about 30 km from Bof800. These distance differences might explain the higher effects recorded at the Mo8000 and Mo4301 stations, but is difficult to explain why Mo4801 and Mo0800 didn't show any effect.

The Mo4301 monitoring station shows a peculiar behavior in the whole monitored period, his hydrograph displays a fluctuating trend with frequent negative peaks, in spite of this irregular trend is possible to observe two positive peaks corresponding to the earthquakes occurrences.

Similar important groundwater variations occurred in concomitance with other earthquakes in the near-field were described by several Authors (Par. 1.1.2).

As reported in previous literature, water well level variations can be positive or negative according to the well location and to the aquifer characteristics. If the area is subjected to compressive strain, the expected anomaly is positive. The amplitude of the recorded variation can be related to the aquifer characteristics, to the distances of the well from the seismogenic fault.

The water well level variations in the well located in the shallow aquifer show a step-like increase in the near-field area. The mechanism proposed to explain step-like groundwater

level increase is the undrained consolidation hypothesis, it consist in the fact that ground shaking causes sediments around a well to consolidate or dilate independently from the tectonic stresses.

This hypothesis is proposed because the step-like increase are not permanent, the water well levels recovered preseismic values in few months in all the wells where coseismic level variations were observed.

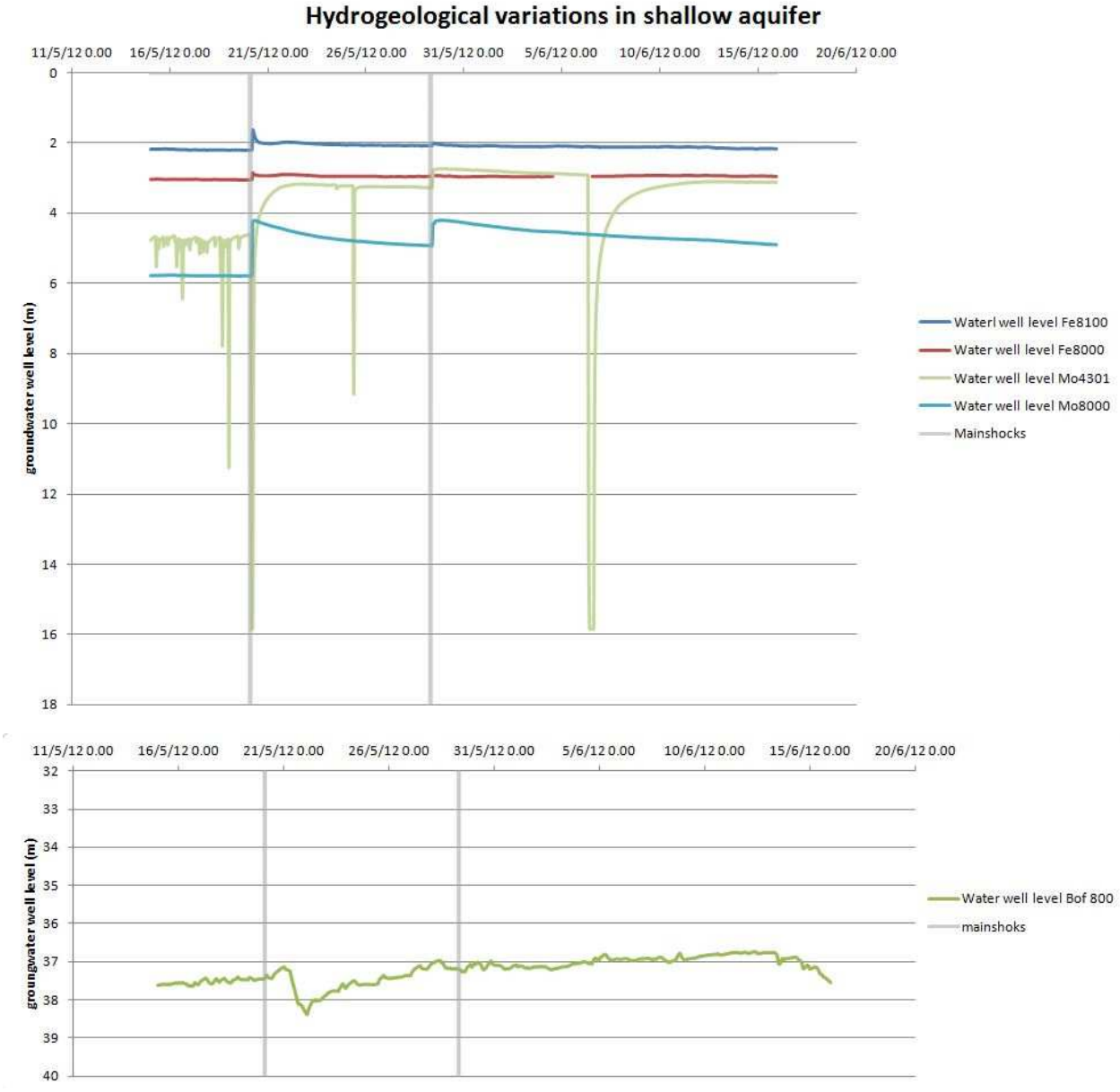

Figure 57: (a)The shallow aquifer response to the Emilia earthquake (Fe8100, Fe8000, Mo4301and Mo8000) show an increase in the groundwater level corresponding to the mainshocks; (b) The deep aquifer response to Emilia earthquake (Bof800) shows no evident response to the mainshocks.

4.5 Discussion and conclusions

The available data show step-like increase in the shallow aquifer groundwater level time series (Fe8100, Fe8000, Mo4301and Mo8000) in consequence of the two mainshok of the Emilia earthquake, while a slight increase after the 20 May mainshok in the deep aquifer monitoring well (Bof800) is observed.

In consequence of the Emilia earthquake the observed hydrological variations are within the characteristics reported in the common scientific literature relating to undrained consolidation phenomena linked to earthquakes occurrence. Their amplitudes are probably a function of their relatively small distances from the earthquake epicenter and to their location in an area subjected to compressive strain.

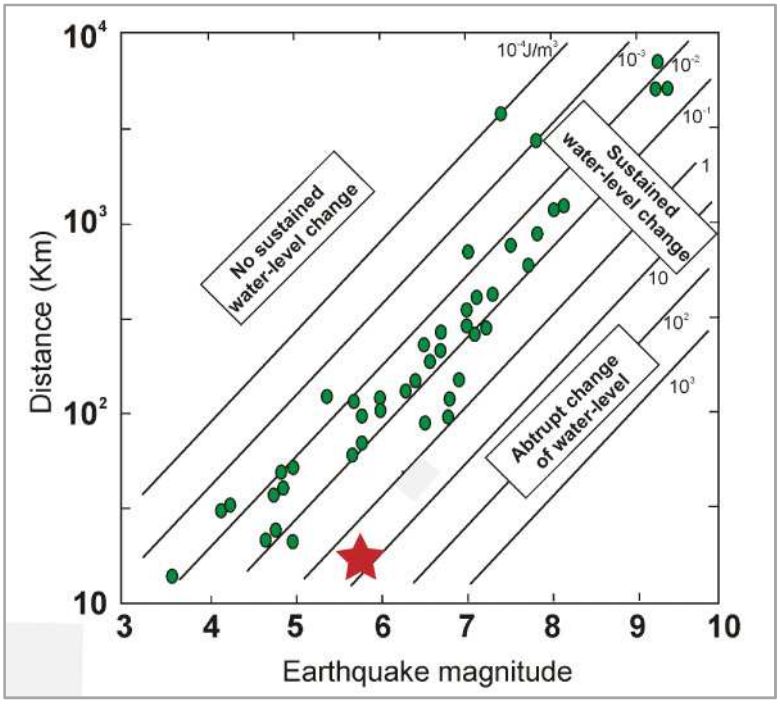

Figure 58: Hypocentral distance (in km) of the groundwater level changes plotted against the earthquake magnitude. The contours of the constant seismic energy density and the domains in which different types of coseismic water-level responses occur are shown. The sustained water-level changes in a global dataset are indicated with green circles; the near-field water-level changes, which were observed in the Ferrara Modena Region in response to the 20 and 29 Emilia earthquakes (Mw 5.9 and 5.8), are indicated with red stars (modified from MANGA & WANG, 2007).

5 DISCUSSION AND CONCLUSIONS

It is widely thought that it would be possible to predict the earthquakes occurrence with a suitable monitoring net of springs, wells and streams. Unfortunately it doesn't exist a physical model that explains the hydrogeologic responses to seismic events, in literature there are different proposed mechanisms for different hydrological changes, but it doesn't exist a specific and universal law that explain all the processes.

In brief, the factors which influences the water-earthquake interaction are as follows: the geology of mainshock area, the stress conditions in force both before and after the earthquake (on regional and local basis), the possible presence of volcanism, the isotherms trend and some situ situation (such as: the geology, the hydrogeology, the structural setting, the rate and duration of shaking, the rainfall, the distance from seismogenic zone, human activity etc.) and also, obviously, the seismicity.

In this thesis three case studies of hydrogeological variations due to earthquakes have been analyzed. The first one consists in a near-field spring discharge increase observed at the Caposele spring, Campania Region, just after the November 23th,1980 Irpinia earthquake (M_w 6.9). The second one consists in an intermediate-field water well level decrease observed in the Acque Albule Basin travertine shallow aquifer and in a slight increase in the water well level at the Pozzo del Merro carst shaft, limestone bedrock, just after the April 6th, 2009 L'Aquila earthquake (M_w 6.3). The third one consists in step-like water well level increase near field effects at the May 20th and 29th, 2012 Emilia earthquakes (M_w 5.9 and 5.8 respectively).

The three hydrogeological variations cases allow to consider that the changes in the water well levels and spring discharge trend are caused by the earthquakes occurrence, but the involved causal mechanisms are different for each case.

For the Irpinia earthquake case a "sponge effect" is involved to explain the rapid discharge increase observed at the Caposele spring, located close to the earthquake epicenter and the seismogenic faults. This hypothesis is based on the α value variation after the earthquake occurrence (**Figure 25**), this value variation implies a change in the hydrological characteristic of the aquifer. To valuate this hypothesis a numerical model with MODFLOW Software have been performed.

Has been done three numerical models to simulate the Cervialto Mountain aquifer, the models simulate:

- pre-seismic period using mean input data;
- pre-seismic period using 1980 year input data;
- post-seismic period using 1981 year input data.

Each output result has been compared with observed corresponding data (**Table 22**).

The pre-seismic models simulations converge with observed data, so is possible to consider that the hydraulic characteristics and the aquifer geometry are similar to reality. The post-seismic model simulation doesn't converge with observed data. Even if several attempts has been performed on the post-seismic simulation, changing on the hydraulic characteristics, the outflow data doesn't correspond with the real data.

To explain the discharge increase at the Caposele spring different hypothesis has been conjectured:

4. geometrical variation of the aquifer,
5. "sponge effect" with permanent changes in the aquifer characteristics,
6. "sponge effect" with no permanent changes in the aquifer characteristics.

Number 1 is rejected because there are no evidences on the aquifer limits, for example no new springs appeared after the earthquake.

Number 2 and 3 are considered achievable. In future it will be possible to implement new numerical models to validate this hypothesis with more data.

Unfortunately at the moment the implementation of this numerical models highlights the impossibility of the simulation of an hydrogeological changes due to earthquake. It is obvious that, for these phenomena, the development of a numerical model (or empirical model) is very difficult considering the amount of variables to put in it. Nevertheless, studying this particular aspect of geology, at times, is the unique instrument to understand deep geodynamic and tectonic processes.

For the L'Aquila earthquake case study a conceptual model to explain variations observed in the Acque Albule Basin and on the Pozzo del Merro is proposed, assuming that the variations in groundwater level are given by variation of permeability in the aquifers caused by the dynamic stress change, at the seismic waves passage.

Two different behaviour have been observed in the groundwater levels of the Acque Albule basin in correspondence of the L'Aquila earthquake. The first one, observed in the shallow travertine aquifer (AAB), is an abrupt level drop down; the second one is a gradual and slightly rising of level observed in the deep limestone aquifer (Pozzo del Merro).

A first conceptual model is proposed for the first behaviour: the level lowering is associated to an increase of permeability due to the opening of new micro cracks and the fracture filling cleaning in the travertine.

A second conceptual model is proposed for the second behaviour: the level rising is associated to an increase of pressure in the confined aquifer due to a temporary

obstruction or permeability decrease of the higher permeability zone of the aquitard, which confines the reservoir.

For the Emilia earthquake case study step-like increase in the shallow aquifer groundwater level time series in consequence of the two mainshok of the Emilia earthquake (on 20th and 29th May 2012), while a slight increase after the 20th May mainshock in the deep aquifer monitoring well is observed.

The mechanism proposed to explain step-like groundwater level increase is the undrained consolidation hypothesis, it consist in the fact that ground shaking causes sediments around a well to consolidate or dilate independently from the tectonic stresses.

This hypothesis is proposed because the step-like increase are not permanent, the water well levels recovered pre-seismic values in few months in all the wells where coseismic level variations were observed, in spite of the monitoring wells are located close to the two epicenters, it seems that no permanent hydrological variations occurred.

6 REFERENCES

Adinolfi Falcone, R., Carucci, V., Falgiani, A., Manetta, M., Parisse, B., Petitta, M., et al. (2012). Changes on groundwater flow and hydrochemistry of the Gran Sasso carbonate aquifer after 2009 L ' Aquila earthquake. *Ital. J. Geosci.*, *131*(3), 459-474.

Adinolfi Falcone, R., Falgiani, A., Parisse, B., Petitta, M., Spizzico, M., & Tallini, M. (2008). Chemical and isotopic multi-tracing for groundwater conceptual model of carbonate aquifer (Gran Sasso INFN underground laboratory—central Italy). *Journal of Hydrology*, *357*, 368–388.

Amato, A., Alessandrini, B., Cimini, G. B., Frepoli, A., & Selvaggi, G. (1993). Active and remnant slabs beneath Italy: evidence from seismic tomography and seismicity. *Annali di Geofisica*, *36*, 201–214.

Amato, A., & Montone, P. (1997). Present day stress field and active tectonics in southern peninsular Italy. *Geophysical Journal International*, *130*, 519– 534.

Amato, A., & Selvaggi, G. (1993). Aftershock location and P-wave velocity structure in the epicentral region of the 1980 Irpinia earthquake. *Annals of Geophysics*, *36*(1), 3-15.

Amoruso, A., Crescentini, L., Petitta, Marco, Rusi, Sergio, & Tallini, Marco. (2010). Impact of the 6 April 2009 L'Aquila earthquake on groundwater flow in the Gran Sasso carbonate aquifer, Central Italy. *Hydrological Processes*, (April 2009).

Anzidei, M., Boschi, E., Cannelli, V., Devoti, R., Esposito, A., Galvani, A., et al. (2009). Coseismic deformation of the destructive April 6, 2009 L'Aquila earthquake (central Italy) from GPS data. *Geophysical Research Letters*, *36*(17), 3-7.

Aquino, S., & Aquino, A. (2008). Assetto idrogeologico del Monte Cervialto e del Sele. *Acque & Territorio*, *17-18*, 52-54.

Argnani, A., & Ricci Lucchi, F. (2001). Tertiary turbidite systems of the Northern Apennines. In: Vai, G.B., Martini, I.P. *Anatomy of an Orogen: The Apennines and Adjacent Mediterranean Basin* (pp. 327-350).

Barbieri, M., Boschetti, T., Petitta, M., & Tallini, M. (2005). Stable isotope 2H, 18O and 87Sr/86Sr and hydrochemistry monitoring for ground water hydrodynamics analysis in a karst aquifer (Gran Sasso, central Italy). *Appl. Geochem*, *20*, 2063–2081.

Basili, R., Valensise, Gianluca, Vannoli, P., Burrato, Pierfrancesco, Fracassi, U., Mariano, S., et al. (2008). The Database of Individual Seismogenic Sources (DISS), version 3 : Summarizing 20 years of research on Italy ' s earthquake geology. *Tectonophysics*, *453*, 20 - 43.

Bernini, M., Boccaletti, M., Moratti, G., Papani, G., Sani, F., & Torelli, L. (1990). Episodi compressivi neogenico-quaternari nell'area estensionale tirrenica nord-orientale. Dati in mare e a terra. *Mem. Soc. Geol. Ital*, *45*, 577– 589.

Bernini, M., & Clerici, A. (1983). Individuazione di un campo di sforzi compressivo in alcuni affioramenti del Pleistocene continentale del margine appenninico presso Collecchio (Parma). *Bollettino della Società Geologica Italiana*, *102*, 369– 384.

Boccaletti, M., and L. M. (Ed.). (2004). *Carta sismo-tettonica della Regione Emilia-Romagna scala 1:250.000 e note illustrative* (S.EL.CA.). Florence.

Boni, C., Bono, P., & Capelli, G. (1986). Schema idrogeologico dell'Italia Centrale. *Memorie della Società Geologica Italiana*, *36*, 991–1012.

Braca, G., Bussettini, M., Lastoria, B., & Mariani, S. (2013). *Linee guida per l'analisi e l'elaborazione statistica di base delle serie storiche di dati idrologici* (p. 148). ISPRA.

Briggs, R. O. (1991). Effects of Loma Prieta earthquake on surface waters in Waddel Valley. *Journal of American Water Resources Association*, *27*(6), 991-999.

Brodsky, E. E. (2003). A mechanism for sustained groundwater pressure changes induced by distant earthquakes. *Journal of Geophysical Research*, *108*(B8), 1-10.

Burrato, P., Ciucci, F., & Valensise, G. (2003). An inventory of river anomalies in the Po plain, northern Italy: Evidence for active blind thrust faulting. *Annals of Geophysics*, *46*(5), 865–882.

Capelli, G., Cosentino, D., Messina, P., Raffi, R., & Ventura, G. (1987). Modalità di ricarica e assetto strutturale dell'acquifero delle sorgenti Capore – S.Angelo (Monti Lucretili – Sabina Meridionale). *Geologia romana*, *26*, 419-447.

Caramanna, G. (2001). L'immersione scientifica avanzata nelle ricerche geologiche subacquee – Un caso di studio: il sinkhole pozzo del Merro. *Rivista della Federazione Italiana di Scienze della Terra*, *7*, 28-29.

Caramanna, G., & Gary, M. (2004). Applicazioni di metodologie di immersione scientifica e ROV (Remote, Operated, Vehicle) nello studio geologico comparato dei due sinkholes allagati più profondi del pianeta: pozzo del Merro (Lazio, Italia centrale) El Zacaton (Taumalipas, Messico). In Nisio (Eds.), (pp. 211-277). APAT.

Carucci, V., Petitta, M., & Aravena, R. (2010). Multi-chemical and isotope approach for studying shallow and deep groundwater interaction in an urban area: the case of Tivoli plain (central Italy). *Groundwater Quality Conference held in Zurich, Switzerland*. IAHS.

Casero, P., Roure, F., Endignoux, L., Moretti, L., Muller, C., Sage, L., et al. (1988). Neogene geodynamic evolution of the Southern Apennines. *Mem. Soc. Geol. Ital*, *41*, 109– 120.

Casero, P., Roure, F., & Vially, F. (1991). Tectonic framework and petroleum potential of the Southern Apennines. In Spencer A.M. (Eds.), *Generation, Accumulation, and Production of Europe's Hydrocarbons. European Association of Petroleum Geoscientists, Special Publication* (p. 381– 387). Oxford University Press, Oxford, UK.

Casnadei, R. (1988). Subsurface basin analysis of fault-controlled turbidite system in Bradano Trough, Southern Adriatic foredeep, Italy. *Bull. Am. Assoc. Pet. Geol*, *72*(11), 1370–1380.

Castellarin, A., Eva, C., Giglia, G., & Vai, G. B. (1985). Analisi strutturale del Fronte Appenninico Padano. *Giornale Di Geologia*, *47*, 47–75.

Cavinato, G. P., & De Cellis, P. G. (1999). Extensional basins in the tectonically bimodal central Apennines fold-thrust belt, Italy: response to corner flow above a subduction slab in retrograde motion. *Geology*, *27*, 955-958.

Celico, P. (1981). Relazioni tra idrodinamica sotterranea e terremoti in Irpinia (Campania). *Rend. Soc. Geol. It.*, *4*, 103-108.

Celico, P., & Civita, M. (1976). Sulla tettonica del massiccio del Cervialto (Campania) e le implicazioni idrogeologiche ad essa connesse. *Boll. Soc. Natur. in Napoli*, *85*, 555-580.

Chia, Y.-P., Wang, Y.-S., Huang, C.-C., Chen, J.-S., & Wu, H.-P. (2002). Coseismic Changes of groundwater level in response to rhe 1999 Chi-Chi earthquake. *Western Pacific Earth Sciences*, *2*(3), 261-272.

Chia, Y., Chiu, J. J., Chiang, Y.-H., Lee, T.-P., Wu, Y.-M., & Horng, M.-J. (2007). Implications of coseismic groungwater level changes observed at multiple-well monitoring stations. *Geophysical Journal International*, *172*(1), 293-301.

Chia, Y., Wang, Y.-S., Chiu, J. J., & Liu, C.-W. (2001). Changes of Groundwater Level due to the 1999 Chi-Chi Earthquake in the Choshui River Alluvial Fan in Taiwan. *Bulletin of the Seismological Society of America*, *91*(5), 1062-1068.

Chiarabba, C., Amato, A., Anselmi, M., Baccheschi, P., Bianchi, I., Cattaneo, M., et al. (2009). The 2009 L'Aquila (central Italy) M W 6.3 earthquake: Main shock and aftershocks. *Geophysical Research Letters*, *36*(18), 1-6.

Cinque, A., Patacca, E., Scandone, P., & Tozzi, M. (1993). Quaternary kinematic evolution of the Southern Apennines. *Annals of Geophysics*, *36*(2), 249-260.

Cotecchia, V., & Salvemini, A. (1981). Correlazione fra eventi sismici e variazioni di portata alle sorgenti di Caposele e Cassano Irpino, con particolare riferimento al sisma del 23 novembre 1980. *Geologia Applicata e Idrogeologia*, *XVI*, 167–191.

Doglioni, C., Harabaglia, P., Martinelli, G., Mongelli, F., & Zito, G. (1996). A geodynamic model of Southern Appenines accretionary prism. *Terra Nova*, *8*(6), 540-547.

D'Agostino, N., Chamot-Rooke, N., Funiciello, R., Jolivet, L., & Speranza, F. (1998). The role of pre-existing thrust faults and topography on the styles of extension in the Gran Sasso range (central Italy). *Tectonophysics*, *292*, 229–254.

D'Argenio, B., & Alvarez, W. (1980). Stratigraphic evidence for crustal thickness changes on the southern Tethyan margin during the Alpine cycle. *Geological Society of America Bulletin*, *91*, 2558-2587.

D'Argenio, B., Ferranti, L., Marsella, E., Pappone, G., & Sacchi, M. (1993). From the Lost Lagonegro Basin to the present Tyrrhenian. *4th International Lithospheric Project Origin of Sedimentary Basins, International Lithosphere Program*.

D'Argenio, B., Letto, A., & Oldow, J. S. (1987). Low angle normal faults in the Picentini Mountains (southern Italy). *Rend. Soc. Geol. ltal*, *9*, 113-125.

D'Argenio, B., Pescatore, T., & Scandone, P. (1974). Schema geologico dell'Appennino Meridionale (Campania e Lucania). *Atti del Convegno: Moderne Vedute Sulla Geologia dell'Appennino Meridionale. Accad. Naz. Lincei* (pp. 49-72).

Emblanch, C., Zuppi, G., Mudry, J., Blavoux, B., & Batiot, C. (2003). Carbon 13 of TDIC to quantify the role of the unsaturated zone: the example of the Vaucluse karst systems (Southeastern France). *Journal of Hydrology*, *279*, 262–274.

Eni-Agip, R. E.-R. and. (1998). *Riserve idriche sotterranee della regione Emilia-Romagna* (S.EL.CA.). Florence.

Esposito, E., Pece, R., Porfido, S., & Tranfaglia, G. (2001). Hydrological anomalies connected to earthquakes in southern Apennines (Italy). *Natural Hazards and Earth System Science*, *1*(3), 137-144.

Faccenna, C., Funiciello, R., Montone, P., Parotto, M., & Voltaggio, M. (1994). Late pleistocene strike-slip tectonics in the Acque Albule basin (Tivoli – Latium). *Mem. Descr. Car. Geol. It*. Istituto Poligrafico e Zecca dello Stato, Roma.

Faccenna, C., Soligo, M., Billi, A., De Filippis, L., Funiciello, R., Rossetti, C., et al. (2008). Late pleistocene depositional cycles of the lapis tiburtinus travertine (Tivoli – central Italy). *Global and Planetary Change*, *63*(4), 299-308.

Ferranti, L., & Oldow, J. S. (1999). History and tectonic implications of low-angle detachment faults and orogen parallel extension, Picentini Mountains, Southern Apennines fold and thrust belt, Italy. *Tectonics*, *18*(3), 498-526.

Ferranti, L., Oldow, J. S., & Sacchi, M. (1995). Prequaternary crustal extension in the Southern Apennine belt, Italy: Arcuation and orogen parallel collapse. *Tectonophysics*, *2*(60), 325-347.

Fiorillo, F. (2009). Spring hydrographs as indicators of droughts in a karst environment. *Journal of Hydrology*, *373*, 290-301. doi: 10.1016/j.jhydrol.2009.04.034.

Fiorillo, F., & Guadagno, F. M. (2011). Long karst spring discharge time series and droughts occurrence in Southern Italy. *Environment Earth Science*, (Special Issue). doi: 10.1007/s12665-011-1495-9.

Fiorillo, F., & Ventafridda, G. (2010). LE PORTATE DELLE SORGENTI DI CASSANO IRPINO E CAPOSELE (CAMPANIA) DURANTE PERIODI SICCITOSI. *Geologi e Territorio - Ordine Regionale dei Geologi - Puglia*, 11-18.

Galadini, F., & Galli, P. (2000). Active tectonics in the central Apennines (Italy) e input data for seismic hazard assessment. *Natural Hazards*, *22*.

Galli, P., & Naso, G. (2009). Unmasking the 1349 earthquake source (southern Italy). Paleoseismological and archaeoseismological indications from the Aquae Iuliae fault. *Journal of Structural Geology*, *31*, 128-149.

Galli, P. A. C., Giaccio, B., Messina, P., Peronace, E., & Zuppi, G. M. (2011). Palaeoseismology of the L'Aquila faults (Central Italy, 2009, Mw 6.3 earthquake): implications for active fault linkage. *Geophysical Journal International*, *187*, 1119-1134.

Giaccio, B., Galli, P., Messina, P., Peronace, E., Scardia, G., Sottili, G., et al. (2012). Fault and basin depocentre migration over the last 2 Ma in the L'Aquila 2009 earthquake region, central Italian Apennines. *Quaternary Science Review*, *56*, 69-88.

Gorokhovich, Y. (2005). Abandonment of Minoan palaces on Crete in relation to the earthquake induced changes in groundwater supply. *Journal of Archaeological Science*, *32*(2), 217-222.

Gudmundsson, A. (2012). Active fault zones and groundwater flow. *Geophysical Research Letters*, *27*(18), 2993-2996.

Heath, R. C. (1983). Basic ground-water hydrology. *U.S. Geological Survey Water-Supply Paper* (p. 86).

Hippolyte, J. C., Angelier, J., Roure, F., & Casero, P. (1994). Piggyback basin development and thrust evolution: structural and paleostress analyses of PlioQuaternary basins in the Southern Apennines. *Journal of Structural Geology*, *16*, 159-173.

Ietto, A. (1965). Su alcune particolari strutture connesse alla tettonica di sovrascorrimento nei M. Picentini (Appennino meridionale). *Boll. Soc. Natur. in Napoli*, *74*, 65-85.

Improta, L. (2003). An integrated geophysical investigation of the upper crust in the epicentral area of the 1980, Ms=6.9, Irpinia earthquake (Southern Italy). *Tectonophysics*, *361*(1-2), 139-169.

Jonsson, S., Segall, P., Pedersen, R., & Bjornsson, G. (2003). Post-earthquake ground movements Post-earthquake ground movements correlated to pore-pressure transients. *Science*, *424*, 179-183.

Keskin, T. E. (2010). Groundwater changes in relation to seismic activity : a case study from Eskipazar (Karabuk, Turkey). *Hydrogeology Journal*, *18*, 1205-1218.

Kitagawa, Y., & Koizumi, N. (2011). Groundwater changes related to the 2011 Off the Pacific Coast of. *Distribution*, 11-18.

La Vigna, F. (2009). *Modello numerico del flusso dell'unità idrogeologica termominerale delle Acque Albule (Roma)* (PhD Thesis.).

La Vigna, F., Mazza, R., Taviani, S., Teoli, P., & Capelli, G. (2007). Development of a modern hydrogeological monitoring network in urban contest – the case of Acque Albule plain; central Italy; Latium region; Rome. *Geophys. Res. Abs*, *9*, 1124.

Lai, W.-chi, Koizumi, N., Matsumoto, Norio, Kitagawa, Y., Lin, C.-wee, Shieh, C.-lun, et al. (2004). Effects of seismic ground motion and geological setting on the coseismic groundwater level changes caused by the 1999 Chi-Chi earthquake , Taiwan. *Earth Planets Space*, *56*, 873-880.

Maillet, E. (1905). *Essais d'hydraulique souterraine et fluviale* (p. 218). Librairie Sci. Hermann Paris.

Malagnini, L., Herrmann, R. B., Munafò, I., Buttinelli, M., Anselmi, Mario, Akinci, A., et al. (2012). The 2012 Ferrara seismic sequence : Regional crustal structure , earthquake sources , and seismic hazard. *Geophysical Research Letters*, *39*, 1-6.

Malinverno, A., & Ryan, W. B. F. (1986). Extention in the Tyrrhenian Sea and shortening in the Appennines as result of arc migration driven by sinking of the lithosphere. *Tectonics*, *5*(2), 227-245.

Manga, M, & Wang, C.-Y. (2007). Earthquake Hydrology. *Elsevier*, (4.10), 293-320.

Manga, Michael. (2001). Origin of postseismic streamflow changes inferred from baseflow recession and magnitude-distance relations. *Geophysical Research Letters*, *28*(10), 2133. doi: 10.1029/2000GL012481.

Manga, Michael. (2003). Response of streamflow to multiple earthquakes. *Geophysical Research Letters*, *30*(5), 10-13.

Marcaccio, M., & Martinelli, G. (2012). Effects on the groundwater levels of the May-June 2012 Emilia seismic sequence. *Annals of Geophysics*, *55*(4), 811-814.

Matsumoto, N, & Roeloffs, E. A. (2003a). Hydrological response to earthquakes in the Haibara well , central Japan – II . Possible mechanism inferred from time-varying hydraulic properties. *Group*, 899-913.

Matsumoto, N, & Roeloffs, E. A. (2003b). Hydrological response to earthquakes in the Haibara well , central Japan – II . Possible mechanism inferred from time-varying hydraulic properties. *Geophysical Journal International*, 899-913.

Menardi, A., & Rea, G. (2000). Deep structure of the Campania– Lucanian arc (Southern Apennine, Italy). *Tectonophysics*, *324*, 239–265.

Montgomery, D. R., & Manga, Michael. (2003). Streamflow and water well responses to earthquakes. *Science (New York, N.Y.)*, *300*(5628), 2047-9.

Morris, D. A., & Johnson, A. I. (1967). Summary of hydrologic and physical properties of rock and soil materials and analyzed by Hydrologic Laboratory of the U.S. Geological Survey. *U.S. Geological Survey Water-Supply Paper* (p. 42).

Mostardini, F., & Merlini, S. (1986). Appennino centro-meridionale. Sezioni geologiche e proposta di modello strutturale. *Mem. Soc. Geol. Ital*, *35*, 177-202.

Muir-Wood R. & King G. C. P. (1993). Hydrological Signatures of earthquake strain. *Journal of Geophysical Research*, *90*(B12), 22.035-22.068. Journal of geophysical reseach.

Oldow, J. S., D'Argenio, B., Ferranti, L., Pappone, G., Marsella, E., & Sacchi, M. (1993). Large scale longitudinal extension in the Southern Apennines contractional belt, Italy. *Geology*, *2*(1), 1123-1126.

Pantosti, D., & Valensise, G. (1990). Faulting mechanism and complexity of the November 23, 1980, Campania– Lucania earthquake, inferred from surface observations. *Journal of Geodynamics*, *95*(15), 319– 341.

Patacca, E., Sartori, R., & Scandone, P. (1990). Tyrrhenian Basin and Apenninic arcs: kinematic relations since Late Tortonian times. *Mem. Soc. Geol. Ital*, *45*, 425– 451.

Patacca, E., & Scandone, P. (1989). Post-Tortonian mountain building in the Apennines. The role of the passive sinking of a relic lithospheric slab. *Accad. Naz. Lincei*, *80*, 157–176.

Patacca, E., & Scandone, P. (2001). Late thrust propagation and sedimentary response in the thrust belt – foredeep system of the Southern Apennines (Pliocene– Pleistocene). Dordrecht, Netherlands.

Patacca, E., & Scandone, P. (2007). Patacca 2007.pdf. *Geology of the Southern Apennines*, *7*, 75-119.

Patacca, E., Scandone, P., Ballatalla, M., Perilli, N., & Santini, U. (1992). The Numidian-sand event in the Southern Apennines. *Mem. Soc. Geol. Padova*, *43*, 297–337.

Pece, R., Tranfaglia, G., & Avino, R. (1999). Geochemical monitoring integrated in a real time hydrological network. *Il nuovo Cimento*, *22 C*, 483–490.

Perotti, C. R. (1991). Osservazioni sull'assetto strutturale del versante padano dell'Appennino nord-occidentale. *Atti Tic. Sc. Terra*, *34*, 11 –22.

Pezzo, G., Peter, J., Boncori, M., Tolomei, C., Salvi, S., Atzori, S., et al. (2013). Coseismic Deformation and Source Modeling of the May 2012 Emilia (Northern Italy) Earthquakes. *Seismological Research Letters*, *84*(4), 645-655.

Picotti, V., & Pazzaglia, F. J. (2008). A new active tectonic model for the construction of the Northern Apennines mountain front near Bologna (Italy). *Journal of Geophysical Research*, *113*(B08412), 1-24.

Pieri, M., & Groppi, G. (1981). Subsurface geological structure of the Po Plain (Italy). Agip's contribution to Oil Exploration Technology.

Pondrelli, S., Salimbeni, S., Morelli, A., EkstrÃ¶m, G., Olivieri, M., & Boschi, E. (2010). Seismic moment tensors of the April 2009, L' Aquila (Central Italy), earthquake sequence. *Geophysical Journal International*, *180*(1), 238-242.

Postpischl, D., Branno, A., Esposito, E., Ferrari, G., Marturano, A., Porfido, S., et al. (1985). Atlas of isoseismal maps of Italian earthquakes. In D. Postpischl (Ed.), *Quaderni della Ricerca Scientifica*. CNR-PFG.

Rebai, S., Philip, H., & Taboada, A. (1992). Modern tectonic stress field in the Mediterranean region: evidence for variation in stress direction at different scales. *Geophys. J*, *110*, 106–140.

Roberts, G.P., & Michetti, A.M. (2004). Spatial and temporal variations in growth rates along active normal fault systems; an example from the Lazzio-Abruzzo Apennines, central Italy. *Journal of Structural Geology*, *26*, 339-376.

Roberts, Gerald P, Raithatha, B., Sileo, G., Pizzi, A., Pucci, S., Walker, J. F., et al. (2010). Shallow subsurface structure of the 2009 April 6Mw 6.3 L'Aquila earthquake surface rupture at Paganica, investigated with ground-penetrating radar. *Geophysical Journal International*, *183*, 774-790.

Roeloffs. (2009). Persistent water level changes in a well near Parkfield, California, due to local and distant earthquakes. *Geophysical Research Letters*, *103*, 869-889. Journal of geophysical reseach.

Rojstaczer, S., Wolf, S., & Michel, R. (1995). Permeability enhancement in the shallow crust as a cause of earthquake-induced hydrological changes. *Nature*, *373*, 237-239.

Rojstaczer, Suart, & Wolf, Stephen. (1992). Permeability changes associated with large earthquakes: An example for Loma Prieta, California. *Geology*, *20*, 211-214.

Roure, F., Casero, P., & Vially, R. (1991). Growth processes and melange formation in the Southern Apennines accretionary wedge. *Earth Planet. Sci. Lett*, 395– 412.

Salvati, R. (2002). Natural hydrogeological laboratories; a new concept in regional hydrogeology studies; a case history from central Italy. *Environmental Geology*, *41*, 960–965.

Sato, T., Sakai, R., Furuja, K., & Kodama, T. (2000). Coseismic spring flow associated with the 1995 Kobe Earthquake. *Geophysical Research Abstracts*, *27*(8), 1219-1222.

Sciarra, A., Cinti, D., Pizzino, L., Procesi, M., Voltattorni, N., Mecozzi, S., et al. (2013). Applied Geochemistry Geochemistry of shallow aquifers and soil gas surveys in a feasibility study at the Rivara natural gas storage site (Po Plain , Northern Italy). *Applied Geochemistry*, *34*, 3-22. Elsevier Ltd.

Severi, P., Biavati, G., & Pignone, R. (2013). *Definizione del modello geologico e idrogeologico della zona arginale del fiume Po in destra idrografica da Boretto (RE) a Ro (FE)* (p. 127). Regione Emilia-Romagna Servizio Geologico Sismico e Dei Suoli.

Speranza, F., Adamoli, L., Maniscalco, R., & Florindo, F. (2003). Genesis and evolution of a curved mountain front: paleomagnetic and geological evidence from the Gran Sasso range (central Apennines, Italy). *Tectonophysics*, *362*(1-4), 183-197.

Tallaksen, L. M. (1995). A review of baseflow recession analysis. *Journal of Hydrology*, *165*, 349-370.

Wang, C.-Y., Cheng, L.-H., Chin, C.-V., & Yu, S.-B. (2001). Coseismic hydrologic response of an alluvial fan to the 1999 Chi-Chi earthquake, Taiwan. *Geology*, *29*(9), 831-834.

Wang, C.-Y., & Chia, Y. (2008). Mechanism of water level changes during earthquake: Near fieldversus intermediate field. *Geophysical Research Letters*, *35*(12).

Wang, C.-Y., & Manga, M. (2010). *Earthquakes and Water* (p. 225). Springer.

Wang, C.-Y., Manga, M, Dreger, D., & Wong, A. (2004). Streamflow increase due to rupturing of hydrothermal reservoirs: Evidence from the 2003 San Simeon, California, Earthquake. *Geophysical Research Letters*, *31*(10), 1-5.

Wang, C.-Y., Wang, C.-H., & Kuo, C.-H. (2004). Temporal change in groundwater level following the 1999 (Mw=7.5) Chi-Chi earthquake, Taiwan. *Geofluids*, *4*(3), 210-220.

Whitehead, R. L., Harper, R. W., & Sisco, H. G. (1985). Hydrologic Changes Associated with the October 28, 1983, Idaho Earthquake. *Pageoph*, *122*, 280-293.

TABLES

Table 1: Rainfall data at Acerno rainguge 725 m a.s.l.

	Jan	Feb	Mar	Apr	May	Jun	Jul	Aug	Sep	Oct	Nov	Dic	Tot year
1973	236.6	257.2	131.0	213.0	9.4	74.8	27.6	90.0	151.0	89.0	198.2	241.8	1719.6
1974	149.8	463.8	157.2	213.0	408.4	10.4	10.4	31.4	149.2	558.4	108.4	101.2	2433.6
1975	26.2	43.4	128.8	83.6	78.2	54.6	31.2	125.0	49.6	314.6	343.6	157.8	1436.6
1976	122.8	169.8	264.2	171.4	161.0	157.6	178.2	55.0	102.0	384.6	460.2	676.2	2903.0
1977	264.0	213.8	122.8	71.2	60.2	83.0	0.2	77.4	288.8	165.6	141.8	244.6	1733.4
1978	239.2	213.0	261.2	567.6	168.2	99.4	0.8	127.4	115.2	155.0	156.4	298.6	2402.0
1979	381.2	427.6	259.6	311.4	69.6	121.0	0.8	262.2	160.6	183.8	425.8	211.2	2814.6
1980	241.8	189.2	97.4	124.6	158.8	40.0	43.2	55.4	91.6	280.8	39.2	728.0	2090.0
1981	32.2	68.2	320.6	48.2	52.0	7.8	17.0	48.0	37.0	52.6	212.8	609.4	1505.8
1982	56.8	278.0	112.0	123.6	92.2	112.6	16.6	91.2	63.2	153.0	152.0	173.8	1425.0
1983	409.0	319.4	195.0	150.6	347.6	77.4	2.6	111.0	236.2	118.0	256.4	81.4	2304.6
1984	200.4	136.6	371.0	131.6	76.0	10.2	0.0	7.8	20.6	108.8	523.0	115.2	1701.2
1985	452.0	-	-	92.8	37.8	39.4	62.6	8.8	58.4	126.2	181.4	81.2	-
1986	380.0	296.6	131.8	50.0	65.6	49.4	49.2	43.2	-	-	-	-	-
1987	275.6	162.4	157.0	143.8	93.6	113.8	6.2	19.4	184.8	165.4	182.2	190.8	1695.0
1988	3.0	146.4	181.4	259.8	43.6	86.8	67.0	-	-	282.6	201.4	270.2	-
1989	58.2	62.8	132.2	402.2	70.0	9.0	24.2	97.4	158.6	281.0	295.2	231.8	1822.6
1990	33.8	106.4	71.0	334.0	140.2	44.6	33.0	26.6	67.8	289.4	200.8	-	-
1991	-	-	-	-	-	-	-	-	-	-	-	-	-
1992	-	-	-	-	-	-	-	-	229.4	207.0	333.6	444.8	-
1993	297.4	120.0	0.2	331.4	90.4	96.4	140.0	30.8	79.4	82.6	172.4	115.0	1556.0
1994	240.0	107.6	324.0	259.8	75.8	10.8	0.2	118.0	258.8	11.8	181.2	256.4	1845.0
1995	158.8	187.2	162.8	154.8	172.0	40.8	69.6	38.8	310.8	241.1	461.4	313.0	2311.1
1996	148.2	135.8	46.6	146.6	45.2	2.2	62.6	10.6	20.2	266.6	311.0	303.6	1499.2

	Jan	Feb	Mar	Apr	May	Jun	Jul	Aug	Sep	Oct	Nov	Dic	Tot year
1997	179.8	133.8	95.6	189.2	310.4	27.0	6.0	76.0	345.8	193.2	196.2	268.8	2021.8
1998	199.0	234.4	205.4	169.4	165.8	75.6	126.4	25.6	158.0	165.0	219.4	572.8	2316.8
1999	202.5	190.7	178.6	193.2	132.9	61.7	39.0	66.7	139.7	208.0	260.6	288.0	2072.0
Mean	241.8	189.2	97.4	124.6	158.8	40.0	43.2	55.4	91.6	280.8	39.2	728.0	2090.0

Table 2: Rainfall data at Montella rainguge 500 m a.s.l.

	Jan	Feb	Mar	Apr	May	Jun	Jul	Aug	Sep	Oct	Nov	Dic	Tot year
1971	290.5	195.4	141.2	94.0	45.6	34.4	91.6	11.4	68.7	99.4	612.2	116.5	1800.9
1972	212.9	124.7	120.3	211.0	125.1	7.4	83.9	94.7	340.5	163.7	201.9	63.0	1749.4
1973	160.6	215.2	164.9	133.2	12.6	40.9	11.0	76.7	183.0	59.4	102.0	213.2	1372.7
1974	128.8	323.0	78.0	153.4	227.8	13.6	25.0	63.2	101.6	370.2	97.6	98.2	1680.4
1975	33.2	53.8	125.8	79.6	86.1	56.7	32.4	74.8	39.0	262.4	344.0	164.0	1352.2
1976	104.4	80.2	202.2	224.4	114.6	119.0	103.8	26.6	108.6	234.0	403.2	348.9	2069.9
1977	224.9	166.8	63.0	46.4	24.8	65.6	0.0	70.3	215.7	72.8	101.0	163.2	1211.5
1978	249.2	182.7	187.0	385.4	137.4	64.3	0.0	17.4	176.4	240.9	160.9	265.2	2066.8
1979	261.2	254.7	145.2	245.2	64.9	138.8	6.2	152.6	101.7	222.1	327.5	112.4	2032.5
1980	238.6	67.8	162.3	59.0	145.8	47.2	0.0	61.2	3.2	347.5	517.6	169.8	1820.0
1981	151.2	116.4	30.5	171.9	70.8	59.6	21.1	32.9	102.6	115.7	38.0	519.5	1490.2
1982	23.2	59.2	154.5	51.7	36.2	33.2	20.0	8.0	57.0	253.8	230.2	368.4	1295.4
1983	29.0	267.8	68.6	91.2	74.2	62.4	11.8	66.4	85.0	241.8	163.2	281.0	1442.4
1984	309.0	285.9	175.1	127.3	152.9	39.0	0.0	126.5	158.9	132.1	197.8	106.1	1810.6
1985	228.2	155.8	252.0	121.2	62.0	29.4	0.0	10.2	20.0	93.8	405.0	37.6	1415.2
1986	257.4	333.6	151.8	63.6	56.6	37.0	63.4	0.0	56.2	54.6	120.8	22.2	1217.2
1987	329.2	205.8	118.4	22.6	63.6	46.4	49.0	75.8	29.0	75.0	227.0	120.6	1362.4
1988	194.2	173.2	204.6	92.8	71.8	36.8	0.0	22.5	119.2	39.4	164.0	159.4	1278.2
1989	17.0	206.4	77.0	135.8	41.4	78.6	71.8	13.6	49.0	171.2	259.8	-	-

	Jan	Feb	Mar	Apr	May	Jun	Jul	Aug	Sep	Oct	Nov	Dic	Tot year
1990	18.8	15.6	77.4	288.4	76.4	0.0	45.2	92.8	37.6	142.0	249.6	239.0	1282.8
1991	15.4	119.4	47.0	255.8	123.8	16.0	20.8	10.4	41.4	204.4	478.4	59.4	1392.2
1992	78.6	18.0	89.4	151.8	48.0	67.8	28.0	27.2	83.6	287.6	180.0	249.2	1309.2
1993	47.0	43.2	179.3	61.7	64.3	6.0	-	5.3	111.0	182.0	266.4	370.9	1337.1
1994	204.9	186.2	0.0	320.8	112.5	69.7	150.2	19.0	62.3	152.7	129.2	55.3	1462.8
1995	172.4	65.7	255.7	180.7	126.2	30.4	59.4	80.6	228.1	14.0	86.5	297.5	1597.2
1996	141.5	267.0	111.5	120.0	79.5	14.0	26.5	30.5	231.0	223.0	360.0	296.0	1999.5
1997	135.8	92.8	63.2	137.4	46.4	0.0	66.0	88.2	60.5	215.4	266.4	259.0	1431.1
1998	81.4	98.8	86.4	179.6	112.4	19.4	6.0	51.8	280.4	92.0	172.4	215.2	1395.8
1999	187.1	197.4	201.6	135.4	66.2	50.4	130.9	20.6	106.2	186.1	242.4	469.9	1994.2
Mean	156.1	157.7	128.8	149.7	85.2	44.3	40.1	49.4	112.3	170.7	245.0	208.6	1565.0

Table 3: Rainfall data at Senerchia rainguge 600 m a.s.l.

	Jan	Feb	Mar	Apr	May	Jun	Jul	Aug	Sep	Oct	Nov	Dic	Tot year
1970	290.0	237.2	281.0	122.0	44.6	55.6	20.6	116.4	64.8	151.8	272.0	247.0	1903.2
1971	306.4	262.2	242.8	99.6	78.4	64.2	87.8	6.6	202.8	117.0	515.0	152.4	2135.4
1972	202.0	169.4	168.0	236.6	105.8	13.8	94.8	112.8	302.4	192.2	163.6	54.6	1816.0
1973	173.2	228.3	191.0	163.8	9.4	45.6	10.8	88.8	158.0	73.2	152.8	146.6	1411.5
1974	102.0	382.8	72.4	165.8	229.2	27.2	24.8	56.2	109.4	548.8	134.0	122.6	1975.2
1975	40.2	24.6	163.8	52.8	106.8	33.8	55.4	132.0	12.6	231.4	297.2	154.8	1305.4
1976	98.4	95.6	201.6	154.6	109.4	108.4	117.0	38.8	93.0	292.4	477.6	437.0	2223.8
1977	189.8	136.0	70.2	50.0	65.8	50.2	0.0	50.4	166.2	98.8	162.0	221.2	1260.6
1978	189.8	189.2	199.0	418.4	84.0	66.6	0.8	97.8	127.2	114.4	134.2	277.4	1898.8
1979	275.8	223.0	131.8	192.0	51.4	81.0	0.6	166.4	121.8	155.8	166.8	120.2	1686.6
1980	107.2	28.8	82.2	81.6	176.6	48.6	0.6	34.0	5.4	190.6	-	-	-
1981	-	-	-	-	-	-	-	-	-	-	-	-	-

	Jan	Feb	Mar	Apr	May	Jun	Jul	Aug	Sep	Oct	Nov	Dic	Tot year
1982	18.6	55.8	261.6	46.8	32.8	37.0	14.2	15.8	63.4	173.6	126.2	465.4	1311.2
1983	37.0	323.0	77.0	119.4	84.4	63.8	30.2	76.4	36.0	198.8	104.0	249.6	1399.6
1984	366.4	218.2	229.4	163.0	239.4	46.8	1.2	102.6	177.0	105.8	289.0	66.2	2005.0
1985	164.8	138.6	241.2	156.8	51.4	29.2	0.0	5.0	21.8	107.0	496.2	99.4	1511.8
1986	382.6	404.2	206.8	103.8	28.2	35.6	91.2	13.0	88.8	120.6	152.4	48.4	1675.6
1987	337.2	222.8	104.8	23.0	88.2	57.6	37.4	43.4	39.0	81.8	215.8	207.6	1458.6
1988	374.6	190.8	253.4	214.4	79.2	57.6	1.0	13.4	211.2	85.8	174.4	178.4	1839.2
1989	11.2	199.6	177.0	212.2	34.0	90.0	32.6	108.8	135.2	280.6	204.0	195.4	1680.6
1990	36.2	63.2	107.8	359.8	51.4	3.2	25.4	66.0	63.4	255.2	268.2	253.8	1553.6
1991	13.0	86.4	47.6	295.2	139.6	37.2	42.6	27.2	35.0	211.2	465.3	83.4	1483.0
1992	104.8	20.8	132.6	161.6	35.6	67.0	37.4	26.6	78.9	217.9	171.6	206.2	1261.0
1993	21.4	43.4	143.6	81.8	63.0	42.6	0.0	8.6	162.4	182.4	308.0	328.0	1385.4
1994	230.0	91.8	0.0	360.8	67.0	53.4	175.0	1.6	44.6	85.2	128.2	86.0	1324.0
1995	190.6	191.6	298.4	204.4	97.2	43.8	72.0	93.6	273.0	15.2	124.2	262.4	1866.8
1996	159.0	228.8	139.4	133.4	136.8	27.6	102.4	22.8	272.2	201.2	474.0	350.6	2248.2
1997	165.6	116.8	45.4	105.0	40.0	2.4	108.4	27.6	19.0	234.6	298.6	290.0	1454.2
1998	186.2	151.0	102.0	163.0	165.6	22.0	10.6	67.6	276.2	153.0	209.8	209.0	1716.0
1999	157.4	199.6	214.0	171.2	115.0	2.2	69.2	27.6	102.2	108.8	255.6	467.9	1890.7
Mean	170.0	169.8	158.1	166.0	90.0	45.3	43.6	56.8	119.4	171.9	247.9	213.6	1670.4

Table 4: Rainfall data at Caposele rainguge 426 m a.s.l.

	Jan	Feb	Mar	Apr	May	Jun	Jul	Aug	Sep	Oct	Nov	Dic	Tot year
1972	161.2	107.4	87.6	186.0	88.2	7.8	86.6	68.8	240.4	124.2	98.0	59.0	1315.2
1973	140.2	194.0	128.0	116.0	15.8	46.8	20.6	51.8	141.8	36.2	94.2	121.6	1107.0
1974	65.8	251.7	51.6	156.8	160.4	21.0	33.0	123.4	77.8	403.2	107.4	107.4	1559.5
1975	24.0	37.8	103.6	58.4	109.2	48.4	25.0	84.8	8.6	196.8	313.0	173.2	1182.8

	Jan	Feb	Mar	Apr	May	Jun	Jul	Aug	Sep	Oct	Nov	Dic	Tot year
1976	121.2	68.8	164.0	133.0	121.6	127.4	72.8	15.8	45.0	186.8	383.2	341.0	1780.6
1977	165.0	101.6	57.8	61.6	47.8	79.6	2.8	34.2	133.2	61.4	93.0	168.4	1006.4
1978	226.0	171.4	187.8	366.8	97.0	46.4	1.8	198.0	163.4	104.8	127.6	213.8	1904.8
1979	143.2	99.4	119.6	196.4	39.6	116.8	1.2	156.4	1.6	158.0	219.2	45.8	1297.2
1980	118.8	55.2	162.6	50.2	128.6	44.4	1.2	34.6	0.0	135.2	214.0	101.4	1046.2
1981	148.2	117.0	82.4	92.4	65.4	48.0	17.8	37.6	73.2	123.2	59.8	343.2	1208.2
1982	19.8	64.0	219.8	32.4	56.0	73.8	63.0	26.0	38.0	185.0	142.0	314.2	1234.0
1983	31.4	244.6	64.6	68.0	64.0	52.2	66.8	31.0	35.8	180.2	96.0	218.4	1153.0
1984	218.6	181.8	166.4	116.0	148.6	51.8	0.0	66.4	126.2	95.6	186.6	38.2	1396.2
1985	138.2	110.6	216.0	109.6	44.2	44.8	0.0	12.4	16.2	110.0	319.8	46.2	1168.0
1986	217.4	282.8	128.2	60.2	60.2	31.6	55.6	19.6	38.2	32.0	110.8	18.6	1034.2
1987	292.0	220.2	65.0	14.0	48.8	36.2	53.8	35.2	21.4	52.8	146.6	88.6	1074.6
1988	168.0	100.2	191.4	114.8	55.6	37.0	0.0	10.0	126.0	56.0	116.2	89.0	1064.2
1989	12.6	125.8	82.4	89.2	44.0	85.6	38.2	38.2	103.4	146.8	145.2	79.4	998.4
1990	24.6	21.0	82.0	228.4	52.2	3.0	59.2	24.0	43.4	140.0	205.0	190.0	1072.8
1991	0.0	80.0	30.0	197.0	94.0	27.6	22.4	40.0	47.8	211.4	364.8	61.2	1176.2
1992	92.4	10.2	73.0	145.2	47.0	73.2	38.4	19.0	38.6	200.4	119.2	151.8	1008.4
1993	59.2	81.0	132.3	58.0	97.4	45.6	9.2	15.6	136.4	144.4	238.4	327.0	1344.5
1994	204.6	202.2	0.4	249.2	56.4	61.0	118.4	0.0	37.8	76.2	116.8	70.2	1193.2
1995	210.0	67.6	230.8	164.0	101.0	13.6	67.4	126.8	164.8	37.6	46.8	304.8	1536.0
1996	66.4	220.2	141.8	101.0	71.2	23.6	47.4	30.4	135.0	135.0	350.0	190.0	1513.0
1997	-	-	-	-	-	-	-	-	-	-	-	-	-
1998	106.2	113.8	51.0	165.8	139.2	9.4	6.8	79.0	195.4	136.0	194.0	157.4	1354.0
1999	166.0	160.0	150.6	116.4	82.0	21.8	89.2	45.6	98.8	194.2	230.8	409.8	1765.2
Mean	123.7	129.3	117.4	127.7	79.1	47.3	37.0	52.8	84.7	135.7	179.2	164.1	1356.0

Table 5: Rainfall data at Materdomini rainguge 551 m a.s.l.

	Jan	Feb	Mar	Apr	May	Jun	Jul	Aug	Sep	Oct	Nov	Dic	Tot year
1972	78.0	68.4	43.0	109.0	51.6	6.0	71.4	81.8	60.2	152.6	59.6	31.0	812.6
1973	-	-	-	-	-	-	-	-	-	-	-	-	-
1974	97.0	234.2	37.8	110.2	84.8	12.2	11.0	125.4	59.6	256.0	65.2	60.4	1153.8
1975	15.8	34.2	77.0	37.6	96.4	33.0	16.2	36.2	12.0	122.6	232.8	118.4	832.2
1976	94.0	22.8	116.2	104.4	117.6	99.0	59.6	17.4	35.2	166.4	319.4	205.6	1357.6
1977	101.8	58.0	28.8	48.0	40.0	69.4	0.6	25.4	94.6	40.8	50.2	128.4	686.0
1978	125.2	120.8	114.2	233.2	70.8	41.8	1.2	187.4	144.2	106.4	94.8	147.4	1387.4
1979	115.8	132.8	80.2	139.0	46.0	120.2	1.0	119.4	63.2	144.4	163.1	66.4	1191.5
1980	136.6	26.6	119.4	31.8	119.2	35.6	0.8	29.6	5.2	185.0	-	-	-
Mean	95.5	87.2	77.1	101.7	78.3	52.2	20.2	77.8	59.3	146.8	140.7	108.2	1060.2

Table 6: Rainfall data at Laceno station 1170 m a.s.l.

	Jan	Feb	Mar	Apr	May	Jun	Jul	Aug	Sep	Oct	Nov	Dic	Tot year
1974	59.0	428.6	80.8	206.8	286.0	11.8	30.0	63.0	88.8	500.8	186.0	116.8	2058.4
1975	85.4	80.2	137.4	121.0	121.0	55.0	22.0	75.2	26.0	298.2	371.0	205.2	1597.6
1976	175.2	159.0	227.8	202.8	130.6	145.0	151.0	39.0	85.0	311.0	573.0	459.0	2658.4
1977	312.0	323.6	95.4	94.0	68.0	104.0	14.0	116.0	180.6	130.2	184.0	199.0	1730.4
1978	221.4	225.2	315.8	603.4	217.4	1.6	-	24.2	174.6	173.0	213.0	269.6	2439.2
1979	242.2	312.8	291.2	249.0	78.2	216.8	3.0	233.4	157.0	235.0	295.0	194.0	2507.6
Mean	182.5	254.9	191.4	246.2	150.2	89.0	44.0	91.8	118.7	274.7	303.7	240.6	2165.3

Table 7: Rainfall data at Montemarano rainguge 821 m a.s.l.

	Jan	Feb	Mar	Apr	May	Jun	Jul	Aug	Sep	Oct	Nov	Dic	Tot year
1972	144.6	77.4	54.8	112.6	108.6	6.0	75.6	106.2	193.8	140.6	77.2	36.4	1133.8
1973	117.2	129.6	68.0	92.4	19.8	39.8	14.2	81.4	101.2	35.2	64.8	151.6	915.2
1974	60.2	170.2	29.4	79.0	135.4	9.2	18.6	64.2	118.0	231.6	75.0	14.4	1005.2
1975	25.4	27.6	89.2	73.2	102.8	30.4	19.6	74.6	25.4	242.8	303.4	120.6	1135.0
1976	61.4	26.0	136.0	148.6	120.8	112.8	63.6	32.2	43.6	165.4	309.8	232.0	1452.2
1977	164.8	101.6	43.8	61.2	28.0	62.8	5.4	50.4	91.8	58.2	119.8	97.8	885.6
1978	157.6	134.4	138.8	258.6	104.8	55.0	1.6	72.8	114.2	88.7	58.4	185.0	1396.9
1979	187.4	181.8	110.0	147.0	28.6	121.4	3.0	103.2	65.6	149.0	211.6	140.8	1449.4
1980	166.8	62.0	93.2	47.0	135.6	47.2	0.2	86.6	8.2	475.0	261.0	172.0	1554.8
1981	148.2	80.4	50.8	82.6	73.4	47.8	26.4	37.4	94.4	122.4	36.4	365.4	1165.6
1982	7.4	22.8	212.8	24.6	36.4	21.4	64.8	32.6	30.0	210.2	126.8	229.2	1019.0
1983	29.0	168.2	34.8	113.6	61.2	35.2	23.8	59.8	43.8	137.6	84.4	131.2	922.6
1984	134.0	189.2	114.4	122.4	104.4	41.8	1.2	92.6	107.2	96.6	154.8	60.0	1218.6
Mean	108.0	105.5	90.5	104.8	81.5	48.5	24.5	68.8	79.8	165.6	144.9	149.0	1176.3

Table 8: Rainfall data at Cassano Irpino rainguge 584 m a.s.l.

	Jan	Feb	Mar	Apr	May	Jun	Jul	Aug	Sep	Oct	Nov	Dic	Tot year
1972	187.6	112.4	110.8	193.8	43.8	8.8	38.8	62.2	287.2	142.2	106.4	50.8	1344.8
1973	120.4	132.2	92.6	88.6	8.0	44.8	8.8	93.0	118.0	41.0	91.2	168.2	1006.8
1974	74.2	282.8	70.8	152.8	171.8	26.0	21.2	75.6	144.0	338.6	73.0	46.2	1477.0
1975	21.2	27.4	104.6	58.6	55.4	52.2	35.6	71.8	35.2	256.0	311.4	160.0	1189.4
1976	58.4	94.0	165.0	195.8	107.2	114.6	126.2	10.8	72.4	188.4	294.6	370.0	1798.2
1977	264.0	177.8	69.6	56.2	13.0	58.8	0.2	43.0	195.8	56.2	154.8	132.0	1221.4
1978	241.6	168.2	180.2	339.4	117.0	53.6	1.4	17.6	164.6	213.0	112.8	256.2	1838.8

1979	265.8	238.2	144.4	223.8	7.6	151.8	9.0	107.4	90.0	222.4	301.0	179.0	1940.4
1980	158.8	76.2	149.0	46.6	118.8	32.8	0.0	63.0	4.4	370.4	437.8	174.4	1632.2
1981	145.0	50.4	73.4	123.6	55.6	49.0	20.0	31.4	96.2	114.6	28.2	409.8	1197.2
1982	18.2	42.8	222.8	24.8	35.8	15.2	25.4	7.6	36.2	200.0	176.0	293.6	1098.4
1983	20.4	279.8	48.6	107.2	63.4	36.6	6.8	79.0	46.2	258.4	79.2	190.8	1216.4
1984	254.8	260.4	148.2	121.4	125.8	35.2	0.0	123.6	142.0	120.4	305.2	66.2	1703.2
Mean	140.8	149.4	121.5	133.3	71.0	52.3	22.6	60.5	110.2	194.0	190.1	192.1	1439.9

Table 9: Rainfall data at Montevergine rainguge 1.287 m a.s.l.

	Jan	**Feb**	**Mar**	**Apr**	**May**	**Jun**	**Jul**	**Aug**	**Sep**	**Oct**	**Nov**	**Dic**	**Tot year**
1969	375.6	341.2	398.2	129.4	265.4	126.4	137.8	206.2	276.2	15.4	321.6	449.4	3043.4
1970	491.4	300.8	342.4	121.6	146.8	109.4	29.8	146.0	103.4	277.8	220.2	363.6	2653.2
1971	410.4	195.8	313.2	231.6	92.2	126.4	101.6	54.2	165	131.4	795.8	182.6	2800.2
1972	332.4	323.6	237.4	303.0	164.8	1.0	119.8	94.6	439.2	292.2	115.8	221.0	2644.8
1973	422.8	266.0	145.6	178.4	28.4	101.2	49.6	99.4	157.0	70.4	88.8	389.0	1996.6
1974	10.0	17.0	7.0	22.0	10.0	2.0	1.0	8.0	8.0	19.0	12.0	10.0	1918
1975	26.6	31.7	134.2	88.0	125.8	18.6	25.6	145.0	40.6	287.2	281.6	127.6	1332.2
1976	92.6	102.0	174.4	142.6	82.2	117.4	132.0	64.2	129.4	255.6	397.6	271.2	1961.2
1977	241.6	150.6	101.8	81.4	52.4	83.8	0.0	109.0	156.4	74.8	124.2	78.8	1254.8
1978	255.6	162.8	197.6	408.6	161.0	83.2	12.8	27.8	159.6	123.4	146.2	232.6	1971.2
1979	251.6	365.0	150.6	206.2	53.0	166.2	19.0	119.0	69.6	163.4	206.0	211.2	1971.8
1980	193.6	145.0	181.0	66.0	290.2	49.0	5.6	60.2	22.4	280.6	507.2	242.0	2042.8
1981	117.8	145.8	110.0	103.0	113.8	87.4	27.2	41.8	168.0	233.6	51.4	475.4	1675.2
1982	26.0	76.4	214.6	39.4	66.6	14.4	33.8	43.4	130.0	264.8	163.2	396.2	1468.8
1983	66.0	270.0	118.0	86.0	130.4	86.2	21.4	163.0	39.0	109.4	142.0	184.8	1416.2
1984	192.8	279.4	152.2	171.0	228.0	55.2	3.4	107.0	199.0	170.0	355.0	139.8	2052.8
1985	227.8	71.8	352.8	57.2	112.0	34.6	0.0	22.6	44.0	173.4	499.4	90.0	1685.6

1986	355.4	381.6	202.4	97.6	67.0	44.0	123.2	3.8	99.8	54.6	198.8	97.0	1725.2
1987	256.4	212.0	88.0	44.6	101.8	67.0	16.8	25.0	100.8	124.4	304.4	142.4	1483.6
1988	175.2	201.6	114.2	112.6	138.4	84.6	2.2	17.8	121.0	67.4	245.6	285.0	1565.6
1989	8.2	169.4	72.8	176.4	96.0	196.2	72.0	61.4	70.2	125.4	321.4	121.2	1490.6
1990	28.2	51.4	85.0	196.6	91.2	6.4	7.2	59.8	59.6	230.6	217.4	181.5	1214.9
1991	36.6	167.0	73.6	244.4	110.4	35.2	25.0	31.2	53.6	217.6	513.6	104.2	1612.4
1992	79.0	33.4	130.4	121.0	55.8	93.8	95.6	66.6	69.0	346.0	234.8	194.2	1519.6
1993	59.2	68.0	218.0	89.0	85.8	86.6	5.6	22.8	194.0	175.6	338.0	412.8	1755.4
1994	285.6	137.2	1.8	331.4	56.0	60.8	205.6	16.4	78.4	77.0	108.4	101.4	1460
1995	235.8	138.6	258.6	230.6	130.2	71.2	8.2	227.6	234.4	18.4	101.6	386.2	2041.4
1996	170.0	237.2	201.4	159.8	180.8	102.6	49.8	11.6	298.8	204.4	349.0	330.4	2295.6
1997	215.4	142.0	60.6	183.7	37.8	1.4	53.8	45.0	4.6	223.8	480.4	344.2	1792.7
1998	110.4	85.6	227.2	259.8	335.6	30.8	1.2	149.4	274.4	100.2	227.2	186.6	1988.4
1999	258.6	311.4	201.0	219.4	150.8	54.0	59.6	44.0	146.6	151.4	280.8	364.6	2242.2
Mean	193.8	180.0	169.9	158.1	121.3	70.9	46.7	74.0	132.6	163.2	269.3	236.0	1881.5

Table 10: Caposele spring historic data – Data sheet 1 (manuale e linee guida ISPRA 84/2013)

Data sheet 1: data tecnical-admistrative	
data	**value**
Series title	Mean daily discharge - Caposele spring
Hydrological magnitude	Mean daily discharge
Unit	m^3/s
symbol	Q_d
Responsible Corporation / data source	Acquedotto Pugliese S.p.A. / Alto Calore Servizi S.p.A.
Availability	Private supply

Table 11: Caposele spring historic data – Data sheet 2 (manuale e linee guida ISPRA 84/2013)

Data sheet 2: geographical data	
data	**value**
Station Name	Caposele Spring
Municipality	Caposele
Province	Avellino
Region	Campania
Coordinate	
Datum (ellipsoid)	WGS84
Projection	GEO
Long/X	02°46'03"
Lat/Y	40°48'56"
Altitude (m. a.s.l.)	420
River basin	Sele River
River basin magnitude (Km^2)	833

Table 12: Caposele spring quantitative data – Data sheet B (manuale e linee guida ISPRA 84/2013)

Data sheet B: statistic description	
characteristic	**value**
Frequency (maximum data value/year)	365
Year's number	79
First data moment	01/01/1920 00.00
Last data moment	31/12/1999 00.00

Maximum value (m^3/s)	7,2
Minimum value (m^3/s)	2,9

Table 13: Hydraulic Conductivity of selected lithology – Unconsolidated Sedimentary Materials

Unconsolidated Sedimentary Materials	
Material	**Hydraulic Conductivity (m/sec)**
Gravel	$3x10^{-4}$ to $3x10^{-2}$
Coarse sand	$9x10^{-7}$ to $6x10^{-3}$
Medium sand	$9x10^{-7}$ to $5x10^{-4}$
Fine sand	$2x10^{-7}$ to $2x10^{-4}$
Silt, loess	$1x10^{-9}$ to $2x10^{-5}$
Till	$1x10^{-12}$ to $2x10^{-6}$
Clay	$1x10^{-11}$ to $4.7x10^{-9}$
Unweathered marine clay	$8x10^{-13}$ to $2x10^{-9}$

Table 14: Hydraulic Conductivity of selected lithology – Sedimentary Rocks

Sedimentary Rocks	
Rock Type	**Hydraulic Conductivity (m/sec)**
Karst and reef limestone	$1x10^{-6}$ to $2x10^{-2}$
Limestone, dolomite	$1x10^{-9}$ to $6x10^{-6}$
Sandstone	$3x10^{-10}$ to $6x10^{-6}$
Siltstone	$1x10^{-11}$ to $1.4x10^{-8}$
Salt	$1x10^{-12}$ to $1x10^{-10}$
Anhydrite	$4x10^{-13}$ to $2x10^{-8}$
Shale	$1x10^{-13}$ to $2x10^{-9}$

Table 15: Hydraulic Conductivity of selected lithology – Crystalline Rocks

Crystalline Rocks	
Rock Type	**Hydraulic Conductivity (m/sec)**
Permeable basalt	$4x10^{-7}$ to $2x10^{-2}$
Fractured igneous and metamorphic rock	$8x10^{-9}$ to $3x10^{-4}$
Weathered granite	$3.3x10^{-6}$ to $5.2x10^{-5}$
Weathered gabbro	$5.5x10^{-7}$ to $3.8x10^{-6}$

Crystalline Rocks	
Rock Type	**Hydraulic Conductivity (m/sec)**
Basalt	$2x10^{-11}$ to $4.2x10^{-7}$
Unfractured igneous and metamorphic rock	$3x10^{-14}$ to $2x10^{-10}$

Table 16: horizontal and vertical hydraulic conductivities for selected rock types

Material	**Horizontal Hydraulic Conductivity (m/sec)**	**Vertical Hydraulic Conductivity (m/sec)**
Anhydrite	10^{-14} to 10^{-12}	10^{-15} to 10^{-13}
Chalk	10^{-10} to 10^{-8}	$5x10^{-11}$ to $5x10^{-9}$
Limestone, dolomite	10^{-9} to 10^{-7}	$5x10^{-10}$ to $5x10^{-8}$
Sandstone	$5x10^{-13}$ to 10^{-10}	$2.5x10^{-13}$ to $5x10^{-11}$
Shale	10^{-14} to 10^{-12}	10^{-15} to 10^{-13}
Salt	10^{-14}	10^{-14}

Table 17: Specific Storage for different lithology

Material	**Specific Sorage (m^{-1})**
Plastic clay	$2,5x10^{-3}$ to $2,3x10^{-3}$
Stiff clay	$1,28x10^{-3}$ to $2,56x10^{-3}$
Medium hard clay	$9,19x10^{-4}$ to $1,28x10^{-3}$
Loose sand	$3,44x10^{-2}$ to $1,02x10^{-3}$
Dense sand	$1,28x10^{-4}$ to $2,03x10^{-4}$
Dense sandy gravel	$4,92x10^{-5}$ to $1,02x10^{-4}$
Rock, fissured	$3,28x10^{-6}$ to $6,89x10^{-5}$
Rock, sound	$<3,28x10^{-6}$ to

Table 18: Specific Yeld for different lithology

Material	**Specific Yield (%)**
Gravel, coarse	21
Gravel, medium	24
Gravel, fine	28
Sand, coarse	30
Sand, medium	32
Sand, fine	33

Material	Specific Yield (%)
Silt	20
Clay	6
Sandstone, fine grained	21
Sandstone, medium grained	27
Limestone	14
Dune sand	38
Loess	18
Peat	44
Schist	26
Siltstone	12
Till, predominantly silt	6
Till, predominantly sand	16
Till, predominantly gravel	16
Tuff	21

Table 19: Porosity for Sedimentary Rocks

Sedimentary Rocks	
Material	**Porosity (%)**
Sandstone	14 - 49
Siltstone	21 - 41
Claystone	41 - 45
Shale	1 - 10
Limestone	7 - 56
Dolomite	19 - 33

Table 20: Comparison between annual rainfall (Laceno raingouge) and annual discharge at Caposele spring (W_0)

Year	W_0 $W_0=Q_{max}*86400/\alpha$	Rain/infiltration on total aquifer area	Wo comparing with rain
	m^3/year	m^3/year	%
1974	290.371.201,1	289.320.000	100,36
1975	-	-	-
1976	337.068.549,3	280.728.000	120,07
1977	243.200.186,9	296.880.000	81,92
1978	286.571.955,1	274.176.000	104,52
1979	245.604.718,1	264.252.000	92,94

Table 21: Numerical model simulation time steps

Period	Start (days)	Stop (days)
1	0	31
2	31	59
3	59	90
4	90	120
5	120	151
6	151	181
7	181	212
8	212	243
9	243	273
10	273	304
11	304	334
12	334	365

Table 22: Observed and simulated data comparison

Observation name	Observed value	Simulated value Drain cells	Total out	Observed mean value	Simulated value	Simulated value total	Difference with drain cells	Difference with drain cells	Difference with tot flow	Difference with tot flow
	(m^3/year)	(m^3/year)	(m^3/year)	(m^3/sec)	(m^3/sec)	(m^3/sec)	(m^3/year)	(m^3/sec)	(m^3/sec)	(m^3/sec)
Caposele spring mean data	148.849.920	134.441.600	140.960.700	4,72	4,26	4,47	14.408.320	0,46	7.889.220	0,25
Caposele spring 1980 data	155.252.937	134.219.700	145.050.800	4,92	4,26	4,60	21.033.237	0,67	10.202.137	0,32
Caposele spring 1981 data	175.926.038	125.831.100	136.815.600	5,58	3,99	4,34	50.094.938	1,59	39.110.438	1,24